Universidad del Valle

De Kondo a Anderson: transporte cuántico dependiente del tiempo en un punto cuántico interactuante en el formalismo de teoría de campo de Schwinger-Keldysh

From Kondo to Anderson: time-dependent quantum transport through an interacting quantum dot within the Schwinger-Keldysh field theory formalism

Presentado por
Jhoan Alexis Fernandez Sanchez

Dirigido por
Dr. RER. NAT Karem Rodríguez Ramírez

Facultad de Ciencias Naturales y Exactas
Departamento de Física - 3146

2024

Resumen

Este trabajo profundiza en la teoría de electrones interactuantes y la formación de momentos locales, modelada por el modelo de impureza única de Anderson (SIAM) y el efecto Kondo, en el marco de las teorías de transporte cuántico a nanoescala. Se explora la conexión entre estos modelos a través de la transformación de Schrieffer-Wolff (SWT) y se estudia el transporte cuántico dependiente del tiempo a través de un punto cuántico interactuante, que sirve como puente entre los sistemas de transporte cuántico prácticos y el modelo Kondo. Utilizando la técnica de funciones de Green fuera del equilibrio de Schwinger-Keldysh (NEGF), se investiga la respuesta del sistema a un voltaje de polarización aplicado a conductores metálicos, analizando la corriente de carga de Jauho-Meir-Wingreen (JMW) dentro de las aproximaciones de estado estacionario y límite de banda ancha (WBL). Aplicando la aproximación no canónica de Hubbard-I al término de interacción electrón-electrón, se deriva expresiones analíticas para la corriente de carga dependiente del tiempo y la ocupación de espín del electrón a través del punto cuántico para distintas magnitudes de la interacción de Coulomb entre los electrones. Los resultados obtenidos muestran excelente coincidencia con la literatura previamente reportada y revelan efectos de correlación de campo medio mejorados en la dinámica de carga, mientras se evalúa la capacidad para describir los efectos Kondo en los fenómenos de transporte. Este estudio sienta las bases para modelos más realistas y abre el camino para enfoques teóricos y computacionales avanzados en la unidad de transporte cuántico del grupo de física teórica del estado sólido en la Universidad del Valle.

Palabras clave: Funciones de Green, puntos cuanticos, trasnporte cuantico, electrones interactuantes.

Abstract

This work delves into the theory of interacting electrons and local moment formation, modeled by the single impurity Anderson model (SIAM) and the Kondo effect, under the framework of nanoscale quantum transport theories. We explore the connection between these models through the Schrieffer-Wolff transformation (SWT) and study time-dependent quantum transport through an interacting quantum dot, serving as a bridge between practical quantum transport systems and the Kondo model. Using the intricate Schwinger-Keldysh nonequilibrium Green's functions (NEGF) technique, we investigate the system's response to a bias voltage applied to metallic leads, analyzing the Jauho-Meir-Wingreen (JMW) charge current within stationary and wide-band limit (WBL) approximations. Applying the non-canonical Hubbard-I approximation to the electron-electron interaction term, we derived analytical expressions for the time-dependent charge current and electron spin occupation through the quantum dot for different Coulomb interaction strengths between electrons. The results obtained align well with previously reported literature and reveal enhanced mean-field correlation effects on the charge dynamics while assessing the model's capacity to describe Kondo effects in transport phenomena. This study lays the groundwork for more realistic models and paves the way for advanced theoretical and computational approaches in the quantum transport unit of the theoretical solid-state physics group at Universidad del Valle.

Keywords: Green's functions, quantum dots, quantum transport, interacting electrons.

Agradecimientos

Agradezco y dedico este logro por completo a mis padres, Frank Alexis Fernández y Aminta Sánchez. Muchas gracias por inculcarme valores como la disciplina y la dedicación. Agradezco infinitamente su esfuerzo y sacrificio que nos permitieron, a mi hermano y a mí, acceder a una excelente educación. También agradezco a Juan José Hernández, mi mejor amigo y segundo hermano, por su apoyo incondicional durante el desarrollo de este proyecto.

Quiero expresar mi profundo agradecimiento al Prof. Juan David Velázquez por introducirme al mundo del transporte cuántico y por su contribución fundamental a mi formación como físico e investigador. Especialmente agradezco a la Prof. Karem Rodríguez por asumir la dirección de este proyecto, por sus aportes vitales, su constante apoyo y paciencia en los momentos más complicados.

Asimismo, agradezco especialmente a mis compañeros de física del semestre 2017-2 por su apoyo en los momentos de discusión y ocio. Reconozco al Prof. Ignacio Franco por su respaldo en mi formación como investigador y por motivarme continuamente a concluir mi trabajo de grado. También agradezco a todos mis compañeros de Rochester por las innumerables discusiones sobre física.

Finalmente, quiero expresar mi profundo agradecimiento a mi alma mater, la Universidad del Valle, por brindarme acceso a la educación pública, por las experiencias vividas, las grandes lecciones aprendidas y la estructura final que adquirí como científico. Pero sobre todo, por haberme puesto en el camino a maravillosos docentes que han fortalecido mi amor por la física.

Contents

1 Introduction **1**

2 Building our system **5**
2.1 Interacting electrons in solids . . . 5
2.1.1 The Hubbard Model . . . 6
2.1.2 The Kondo and Anderson models . . . 15
2.1.3 The Schrieffer–Wolff transformation . . . 20
2.2 Quantum dots & single-electron transport . . . 22
2.2.1 The interacting quantum dot system . . . 28
2.2.2 The Coulomb blockade effect in QDs . . . 29

3 TDNEGF for quantum transport **31**
3.1 Why nonequilibrium Green's functions? . . . 31
3.1.1 Many and single-particle Green's functions . . . 32
3.1.2 The Schwinger-Keldysh contour . . . 36
3.1.3 Many-body perturbation theory . . . 38
3.2 Theoretical open systems aspects of the IQDS . . . 39
3.3 Building the Jauho, Meir & Wingreen formalism . . . 41
3.3.1 Time-independent case: stationary limit . . . 45
3.3.2 Time-dependent case: wide-band limit approximation . . . 48

4 Quantum transport with TDNEGF **50**
4.1 Closing the equations of motion . . . 50
4.1.1 Non-canonical Hubbard-I approximation . . . 52
4.1.2 Hubbard bands . . . 55
4.2 Analytical expression of the JMW current . . . 55
4.2.1 Time-independent case: stationary limit . . . 56
4.2.2 Time-dependent case: WBL approximation . . . 58
4.3 Analysis of the JMW current . . . 59
4.3.1 Time-independent case: current *VS* voltage curves . . . 60

4.3.2 Time-dependent case: pulse-like & harmonic modulation 62

5 Conclusions **67**
5.1 Conclusions 67
5.2 Perspectives 69

6 Appendices **70**

A Green's function of a degenerated Fermi liquid **71**

B Langreth Rules of Analytical Continuation **73**

C Details of many-body perturbation theory **75**

D General quantum transport set up **78**
D.1 The embedding approach 79

E Stationary form of the JMW current **82**

F Detailed calculations of the implementation of TDNEGF and JMW formalism in the quantum dot system **84**

G Hubbard sub-bands procedure **92**

H Numerical Implementation of the time-dependent JMW current **94**

1 Introduction

The intrinsic many-body character of quantum systems, posed great difficulty and complexity for the pioneering quantum physicists attempting to describe the behavior of many interacting particles or quantum systems with many degrees of freedom [1, 2]. The emergence of relevant and diverse physics at different scales and collective phenomena due to strong interactions challenge the reductionist approach of describing these systems solely through fundamental forces and the standard model, as pointed out by Philip Anderson [3]. This approach to physics becomes limited in the description of novel many-body phenomena and emergent collective behavior, calling for the need to develop new theoretical tools for a better complete understanding of nature [4–8].

One captivating field of research lies at the intersection of many-body phenomena: *quantum transport theory*, which explores the dynamics of energy and charge in quantum systems. This field has broad implications across various disciplines and experimental setups [9–14]. These systems operate far from thermodynamic equilibrium, defying quick relaxation to stable states. The advent of nanotechnology [15], marked by landmark techniques like the scanning tunneling microscope (STM) and the atomic force microscope (AFM) [16, 17], has propelled quantum transport to the forefront of both experimental and theoretical research [18–20]. However, as we venture deeper into the nanoscale, challenges emerge. Quantum effects such as direct electron tunneling and complex scattering mechanisms pose obstacles in reliably fabricating devices below $20\,nm$ [21]. These challenges intensify as transport measurements reach atomic-scale processes with sub-picosecond temporal resolutions. Here, the intricate interplay of multiscale many-body electronic correlations tests our understanding of nanoscopic systems [22–25].

One of the most prominent examples of such quantum many-body phenomena persisted in the study of the formation of localized magnetic moments (LMMs) in metals: the famous Kondo effect [26], essentially a low-temperate phenomenon. In 1934, experiments in the Kamerlingh Onnes Laboratory at Leiden University discovered the existence of a resistance minimum in the resistivity of non-magnetic metals doped with a dilute small concentration of magnetic impurities (as to avoid any exchange interactions between them) coming from the spin of electrons in localized partially filled $4f$ rare-earth or $3d$ transition element orbitals [27]. While conventional transport theory of nonmagnetic metals shows a low-temperature dependence of the resistivity such that $\rho(T) =$

$\rho_0 [1 + AT^5 + ...]$ (ρ_0 being a saturated value due to defects considered in realistic metal, and the term $\propto T^5$ coming from lattice vibration effects), the increase of resistance with low temperatures was an uncanny behavior. This phenomenon remained a mystery for more than 30 years until the explanation by Japanese physicist Jun Kondo in 1964 based on earlier experiments performed with better purity control techniques in 1962 [28]. The strong interaction of a magnetic impurity with the spin of electrons in the conducting sea of a metal, particularly at low temperatures, results in antiferromagnetic coupling, as extensively studied by physicist Philip Anderson [29]. This coupling, mediated by a parameter J, favors the formation of a singlet state that effectively scatters electrons near the Fermi level, which causes the resistance to unexpectedly increase (see Figure 1.1). Kondo's original approach to the problem yielded a contribution to the resistivity that diverged at a characteristic temperature known as the Kondo temperature T_K. This temperature delineates the scale at which the Kondo effect becomes prominent. The divergence famously termed the "Kondo problem," necessitated the development of the vital renormalization group approach by K.G. Wilson in 1974 [30], along with additional analytical insights in the 1980s, exploiting the integrability of the Kondo model and its exact diagonalization through the Bethe ansatz method [31–34]. The well-defined rich physics of the Kondo problem has served as a fundamental framework for both experimentalists and theoreticians in investigating strongly interacting materials, such as heavy-fermion systems and high-temperature superconductors [4, 35].

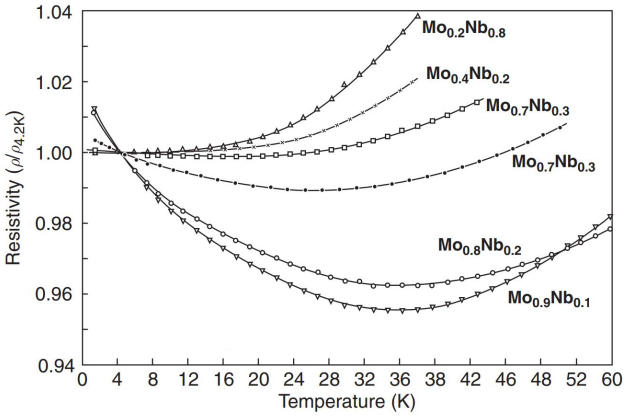

Figure 1.1: Resistance minimum in Mo_xNb_{1-x}. Here, "x" is the concentration of Mo. Once it exceeds 40%, the diluted iron atoms become magnetic, and the resistance minimum is observed: this is the Kondo effect. (Figure from Ref. [4])

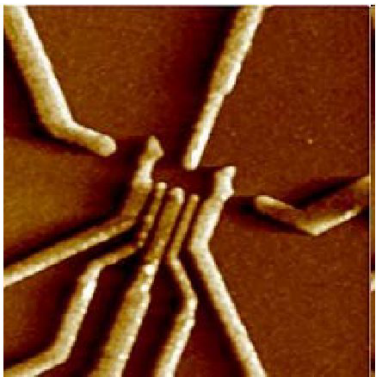

Figure 1.2: AFM image of two laterally coupled quantum dots confined by metallic gates. The leads are used to control the gate voltages to direct and detect currents through the dots via quantum point contacts. (Picture from Ref. [36])

In the era of Anderson and Kondo, physicists Schrieffer and Wolff proposed a unitary transformation rooted in second-order perturbation theory: the Schrieffer-Wolf transformation (SWT). This approach projects high-energy excitations of a given Hamiltonian out of the Hilbert space to derive a low-energy model. When applied to the Anderson Hamiltonian, this transformation yields the Kondo Hamiltonian, linking the Anderson and Kondo models [37]. However, the s-d or Kondo

model presupposes the existence of a local moment of spin S coupled with the conducting sea of electrons in the metal, treating the LMM as a separate entity. Conversely, the single impurity Anderson model (SIAM) treats the LMM as the spin of another electron that can be exchanged for other electrons in the conducting sea. Thus, we favor the more realistic Anderson model [38]. Recognizing this advantage, the *first objective of this work* is to employ the SWT as a bridge between Kondo-like models and the Anderson model. This approach allows us to leverage the Anderson model as a more realistic and comprehensive framework for investigating the interacting quantum dot system, which serves as the primary focus of this study.

In 2024, the Noble Prize in chemistry was given to Moungi G. Bawendi, Louis E. Brus and Aleksey Yekimov [39] "for the discovery and synthesis" of one the most important systems in nanophysics that can be model with the SIAM: quantum dots (QDs). Quantum dot systems are artificial man-made structures containing up to several thousand electrons (see Fig. 1.2). These present quantum confinement to the nanoscale in all three dimensions, leading to engineered discrete electronic structure and size-dependent energy levels [40]. This is why they are referred to as artificial atoms. The ease with which QDs can be controlled offers a variety of possible applications for the design of nanomaterials with tunable chemical, physical, and optical properties [41], the design of realistic quantum computing platforms [42], and materials with widely spin-dependent properties (spintronics) [43]. In addition, the sensibility of QDs to the additional presence of individual electrons can dramatically affect its transport properties as Coulumb interactions become relevant, extending the possibility of single-electron transport [44]. Thus, quantum confinement and many-body electronic correlations can lead to the interplay of interesting effects, such as the Coulomb blockade phenomena (conductance through these structures present oscillatory behavior), and more importantly, the manifestation of the Kondo effect with QDs serving as impurities [35, 45–47]. In this context, the SIAM, with an additional metallic contact, constitutes the system of focus of this work: the interacting quantum dot system (IQDS).

The theoretical description of such complex many-body systems often relies on powerful techniques, such as density renormalization group (DMRG) and tensor Networks (TNs) calculations [48–50], dynamical mean field theory (DMFT) [51], quantum master equations (QME) [52], path integral methods [53, 54], hierarchical equations of motion (HEOM) [55], density functional theory (DFT) [56], and semiclassical methods [57–59]. One widely used approach is the Schwinger-Keldysh nonequilibrium Green's functions (NEGF) technique [7, 60–63]. Pioneered by Julian Schwinger and Leonid Keldysh in their seminal works in the 1960s [64–66], NEGF provides a versatile framework to study quantum transport in open systems, accounting for both electron-electron and electron-phonon interactions, and accurately capturing nonequilibrium dynamics [67]. Its application has yielded crucial insights into transport properties of interacting systems, making it an indispensable tool for elucidating the intricacies of quantum transport in nanoscale systems driven far from equilibrium [68–71]. For our work, the most relevant insight of this technique on interacting quantum transport problems is the Jauho-Meir-Wingreen (JMW) current formalism [72], introduced in 1994 and more general than Landauer-Buttiker theory for transport in nanoscopic systems. This formalism builds a recipe for the calculation of nonequilibrium transport quantities such as the

charge current passing through a general central nanoscopic region, while including many-body correlations effects via the NEGF structure. It reproduces Landauer's theory in a certain limit, assumes no electronic interactions in the environment of reservoir Hamiltonians, and implements the wide-band limit (WBL) for the interaction of the central region with the environment that conveniently yields analytical results in the noninteracting case (see Chapter 3).

As a beautiful aspect of the technique, NEGF has a forward perturbative structure proper of quantum field theory methods [2, 73] that we can make use of to treat the electronic correlations and their effects in quantum transport systems. To outline the procedure, NEGF main concern is the calculation of the interacting many-body self-energy Σ_{MB} in Dyson's equation (see Eq. (3.26)) given by an infinite sum of terms represented by an infinite sum of Feynman diagrams [7]. Several approximations are considered for the self-energy [74], where the physics of the specific problem determines the approximation chosen for the study of correlation effects, and different approximations lead to particular results for the transport features [75]. This procedure defines the many many-body perturbation theory (MBPT) methods for the study of complex many-body phenomena. Here, we focus on the non-canonical Hubbard-I approximation (HIA) [76] for electron-electron correlations as a preliminary study of correlation effects in transport systems that lead to analytical results within the WBL. Thereby, the *second objective* of this work is to study the NEGF approach to elucidate the physics of the JMW current formalism for transport in the WBL in the IQDS within the HIA. The analytical expressions obtained are very complicated to elucidate without a numerical method to evaluate them. Hence, the *third objective* of this work is to implement a numerical calculation for the JMW current to analyze the quantum transport through the IQDS for different system parameters such as on-site energies, system-bath coupling strengths, temperature, and chemical potentials, and different bias voltages driving the system out of equilibrium. This work aims to provide a gentle introduction for students interested in quantum transport and many-body perturbation theory.

This work is organized as follows: in Ch. 2 we explore the physics of interacting electrons in solids with the relevant Hubbard model. Then, we study the Kondo and Anderson models and explore their connection through the Schrieffer-Wolf transformation. Next, the basics of quantum dots and single-electron transport in nanoscale systems are introduced. Finally, by adding two metallic reservoirs to the Hubbard mode the interacting quantum dot system is constructed and the important Coulomb blockade and Kondo effects in quantum dots are studied. In Ch. 3, we introduce the time-dependent nonequilibrium Green's function formalism (TDNEGF) as the fundamental quantum theoretical method to approach the problem, we describe relevant open system aspects of transport problems, and we introduce the Jauho-Meir-Wingreen current formalism for the study of quantum transport features. The calculation of this quantity for interacting the quantum dot system is treated in detail in Ch. 4, where we derive analytical expressions for both the stationary and time-dependent situations within the HIA. Subsequent numerical implementations are performed to elucidate the transport features of the problem. Finally, in Ch. 5 we give overall conclusions of our work and discuss brief perspectives relevant to the analysis of our central system.

2 Building our system

The theoretical model employed to approach the system focus of this work, namely, the interacting quantum dot system (IQDS), consists of the Hubbard model with two additional tunneling Hamiltonians to metallics reservoirs forming a quantum junction. In this chapter, we discuss the main ingredients for its construction. First, the relevant Hubbard model is discussed as an approach to interacting electrons in solids. Then, we discuss the physics of the Kondo and Anderson models from a historical perspective to reveal their ultimate connection through the Schrieffer-Wolf transformation (SWT). Next, we delve into the fundamentals of QDs and single-electron transport. Finally, by adding two metallic reservoirs to the Hubbard model, we build the IQDS and discuss a phenomenon in this system: the Coulomb blockade effect of QDs.

2.1 Interacting electrons in solids

The physical description of solids has evolved over the years. A first perspective considers solids as made from several units called atoms that interact among them and are found at different average distances (hence relating to the ideas of gas, solid, and liquid) [77]. Physicists require a statistical description of particles to determine the properties of systems with many degrees of freedom [78]. However, the atomic nature of the units conforming solids and the many interactions between electrons, ions, and nuclei imposed several problems in the theoretical treatment of such many-particle systems, where quantum effects inevitably arise. These studies focused on the magnetic and electrical properties of different materials, and phenomenological approximations based on intuitive physical arguments were proposed to explain experimental results. One of the first phenomenological models for solids at this intersection is Drude's simple yet powerful model [79, 80], which roughly treats electrons as free and independent entities colliding with immovable core ions (nuclei) in the solid; no electron-electron interactions are considered and the solid would not pertain a complex band structure. From Boltzmann to Drude, and from Sommerfeld to Jellium, passing through Debye, Einstein, and many others [80] the modern picture of solids has suffered dramatic changes with the advent of first-principles quantum descriptions [81, 82].

In this context, the study of magnetism of materials constituted one of the main focus of

theoretical efforts. Here, we define magnetic ions, as the building blocks of materials where the partially filled outer shells present unpaired electrons that give rise to magnetic properties. Among many attempts to describe magnetism in such materials, we find the Heisenberg model for materials with localized magnetism, which proposes the existence and energetic prevail of permanent spin degrees of freedom forming magnetic moments in the material and are incredibly useful to describe localized magnetism such as in magnetic insulator materials and certain classes of ferro-, ferri- or antiferromagnets [83]. The fundamental insight came from 1928 Heinsenberg's seminal paper [84], where types of exchange interactions between electrons due to Coulomb repulsion were the driving force of quantum magnetism, and electrons were assumed to be tightly localized at each magnetic ion orbital yielding a negligible contribution from their kinetic energy. When electrons were not localized at the materials, models by Edmund Stoner and John Slater were developed in the 1930s for itinerant magnetism, where magnetism is carried by delocalized conducting electrons conforming to a self-consistent phenomenological exchange, and collective novel magnetic properties emerge that explain ferromagnetic formation. Typical limitations of the Heisenberg model arose when considering materials with highly localized partially filled $4f$ or $3d$ orbitals, corresponding to some rare-earth metals, transition metals, and magnetic dilute alloys. The same electron group is responsible for magnetism and conduction in such materials as the electrons in for example $3d$ orbitals giving rise to spin magnetic moments form a band. Hence, kinetic energy contributions of the electrons compete against electronic correlations, and treating such electrons simply as localized magnetic moments (LLMs) becomes inadequate [4, 79, 81, 85]. This is *band magnetism* and it seemed to develop in the narrow energy bands of incomplete shells of transition and rare-earth metals. Attempts to construct a theory for magnetism in such materials led to the S-D model of magnetism by Frohlich and Nabarro [86], later considered by Zener [87] to account for magnetism in iron-group materials. Later on, the RKKY (Ruderman, Kittel, Kasuya, Yosida) interaction was developed as an indirect exchange interaction between localized spins mediated by the surrounding conducting electrons in the incomplete $4f$ orbitals [88–90]. Additionally, the 1930s stoner theory lacks a microscopic first-principles deduction for the origin of itinerant magnetism, for example in the explicit consideration of electron-electron interactions.

The solution to the issues presented above came from John Hubbard in his seminal paper of 1963 [91], where the **Hubbard model** was proposed as one of the first microscopic first-principle constructions of interacting electrons in the narrow energy bands of certain solids. As depicted in later sections, the one-site Hubbard model is the central ingredient for constructing the IQDS.

2.1.1 The Hubbard Model

We derive the Hubbard model starting from the modern picture of solids [80, 81]. A solid can be seen as a collection of many constituent parts such as atoms or molecules which form positive charge nuclei and negatively charged electron shells. Some electrons are tightly bound to the nuclei forming fully occupied shells, the *core electrons*. In contrast, *conduction electrons* are weakly bound to the nuclei and have more degrees of freedom that contribute dominantly to the properties of

the solid. In this way, we can see a solid as a combination of ions in a lattice (formed by nuclei and core electrons) and conduction electrons, with a Hamiltonian given by

$$\hat{H} = \hat{H}_e + \hat{H}_i + \hat{H}_{ei}, \tag{2.1}$$

each Hamiltonian term is given by:

$$\hat{H}_e = \hat{T}_e + \hat{V}_{ee} = \sum_{i=1}^{N_e} \frac{\hat{\mathbf{p}}_i^2}{2m} + \frac{1}{2}\sum_{i,j}^{i\neq j} \frac{e^2}{4\pi\varepsilon_0 \left|\hat{\mathbf{r}}_i - \hat{\mathbf{r}}_j\right|}, \tag{2.2}$$

$$\hat{H}_i = \hat{T}_i + \hat{V}_{ii} = \sum_{\alpha=1}^{N_i} \frac{\hat{\mathbf{P}}_\alpha^2}{2M_\alpha} + \frac{1}{2}\sum_{\alpha,\beta}^{\alpha\neq\beta} \frac{Z_\alpha Z_\beta e^2}{4\pi\varepsilon_0 \left|\hat{\mathbf{R}}_\alpha - \hat{\mathbf{R}}_\beta\right|}, \tag{2.3}$$

$$\hat{H}_{ei} = -\sum_{i=1}^{N_e}\sum_{\alpha=1}^{N_i} \frac{Z_\alpha e^2}{4\pi\varepsilon_0 \left|\hat{\mathbf{r}}_i - \hat{\mathbf{R}}_\alpha\right|} = \hat{V}_{ei}^{(0)} + \hat{V}_{ep}, \tag{2.4}$$

where Eq. (2.2) describes the electrons in the solid with the usual position and momentum operators $\hat{\mathbf{r}}_i$ and $\hat{\mathbf{p}}_i$ for the i^{th} electron out of the N_e; Eq. (2.3) describes the ionic part, where the ion α out of the N_i is described by position and momentum operators $\hat{\mathbf{R}}_\alpha$ and $\hat{\mathbf{P}}_\alpha$; Eq. (2.4) describes the interaction between ions and electrons. In first principles theories of nuclear effects, it is customary to write the position of the ions as $\hat{\mathbf{R}}_\alpha = \hat{\mathbf{R}}_\alpha^{(0)} + \hat{\mathbf{u}}_\alpha$, where $\hat{\mathbf{u}}_\alpha$ determines the actual displacement from the equilibrium stationary position $\hat{\mathbf{R}}_\alpha^{(0)}$ of the ions in the lattice of the solid [92]. With this in mind, Eq. (2.4) can be split as a sum between $\hat{V}_{ei}^{(0)}$ which denotes the periodic potential emerging from the lattice periodic structure of the solid given by

$$\hat{V}_{ei}^{(0)} = -\sum_{i=1}^{N_e}\sum_{a=1}^{N_i} \frac{Z_\alpha e^2}{4\pi\varepsilon_0} \frac{1}{\left|\hat{\mathbf{r}}_i - \mathbf{R}_\alpha^{(0)}\right|}, \tag{2.5}$$

and $\hat{V}_{ep}$ corresponding to the electron-phonon interaction term[1]. Along these lines, it is found that $\hat{V}_{ii}$ for the interaction between ions can be split into two parts: $\hat{V}_{ii} = \hat{V}_{ii}^{(0)} + \hat{V}_{ep}$. The first term is susceptible to the Bohr-Oppenheimer approximation [80] and represents the rigid lattice $\mathbf{R}_\alpha^{(0)}$[2], while the second accounts for the lattice dynamics or collective vibrations described by phonons. Finally, Z_α is the atomic number of ion α, ϵ_0 is the electric permittivity of free space, m accounts for the electron mass, and M_α for the ion's mass.

The Hubbard model emerges from the first-principles Hamiltonian (2.1) after several simplifications relevant to the objective of describing band magnetism, as first deduced by Hubbard [91].

[1]The "phonons" described by $\hat{V}_{ep}$ are the quanta for the collective vibrations traveling through the solid's period lattice [73]. The indication of the exact form of this term, $\hat{V}_{ii}^{(0)}$ and $\hat{V}_p$ is beyond the scope of this thesis and can be further explored in references [82, 92].

[2]In principle, all operators present a complex time-dependence, but not for the rigid $\mathbf{R}_\alpha^{(0)}$.

The starting point is a series of experimental and intuitive observations about the nature of solids [81, 83, 85, 93]:

1. Contrary to the electron gas picture of solids, in the case of rare-earth and transition compounds the partially filled electrons in localized d- or f-bands facilitate the sense of referring to electrons being on a particular atom site, giving rise to an atomistic view of the solid where electron correlations may become important. The key insight however is better viewed in the words of Hubbard [91]:

   > *"A theory of correlation effects in narrow energy bands is inevitably somewhat different from a theory of correlation effects in the free electron gas. The electron charge density in a d-band is concentrated near the nuclei of the solid and sparse between the atoms, making it possible to speak with some meaning of an electron being "on" a particular atom. This circumstance gives rise to the possibility of an atomic description of the d-band despite its considerable bandwidth. It is, in fact, found experimentally that the d-electrons of transition metals exhibit behavior characteristic of both the ordinary band model and the atomic model."*

   Hence, the d-electrons' somewhat mixed localized and itinerant nature renders the possibility of the same groups of electrons to account for conduction and magnetic properties (band magnetism as described at the beginning of section 2.1): band ferromagnetism is experimentally observed to be produced by electrons in relatively narrow energy bands of d-electrons. Explicitly, from the argument that when the Fermi surface lies within a single conduction band we may assume that the coupling between bands is negligible as they present far away from the Fermi energy. *This is the most important assumption of the essentially single-band Hubbard model.* It is important to note that based on the localized picture by Heitler and London [94], the highly localized electrons in f-orbitals allow for a purely atomistic picture to capture the essential localized behavior of rare-earth compounds qualitatively. In reality, the single-band simplification is rather unjustified in the rare-earth compounds; despite the high localization of f-electrons, the electron interactions are larger than the small inter-band splitting[3], thereby producing additional charge fluctuation effects caused by the interplay between f-levels and delocalized s- and p-band electrons [83]. For such systems, multiband models or Anderson/Kondo models (see section 2.1.2) result in better descriptions.

2. Imagine you have a positively charged ion surrounded by a cloud of electrons. If an additional electron is introduced, the existing electron cloud will rearrange itself to partially cancel out the added electron's charge. This rearrangement diminishes the extra electron's ability to "see" the full charge of the ion and the other electrons, effectively reducing the strength of the electrostatic forces. This is the *screening effect*. In delocalized s- or p-bands, electrons can move relatively freely and respond quickly to changes in charge distribution. As they effectively hybridize with states of the d-band electrons, this rapid response tends to "screen"

[3] This interband splitting is defined as the energy difference between the highest occupied state in one band and the lowest unoccupied state in a different band, which we refer to as simply the "energy separation" for the bands.

or dampen the electrostatic effects that one electron would otherwise feel from another or the positively charged ions. This requires a certain renormalization for the model parameters where such effects may be considered only through a self-consistent Hartree-Fock field.

3. Phonon dynamics may play important roles in the properties of solids [82]. In the case of band magnetism and the context of the Hubbard model, it appears that effects coming from lattice dynamics are negligible ($\hat{V}_{ep} \to 0$). However, the formation of bands requires the periodic lattice structure ($\hat{V}_{ei}$) to play an important role.

By applying all previous assumptions to the Hamiltonian in Eq. (2.1), we obtain the Hamiltonian

$$\hat{H} \approx \hat{H}_0 + \hat{H}_1, \tag{2.6}$$

where we have restricted ourselves to d-band electrons in a nondynamical rigid ion lattice. Here, $\hat{H}_0 = \hat{T}_e^d + \hat{V}_{ei}^{(0,d)}$ is the single-particle part, conforming the kinetic energy of d-electrons (first term) and their interaction with the ion lattice periodic potential, and $\hat{H}_1$ is the two-body Coulomb interactions between d-band electrons. In Figure 2.1 we observe the narrow energy band structure from the localized d-orbitals at each lattice ion site.

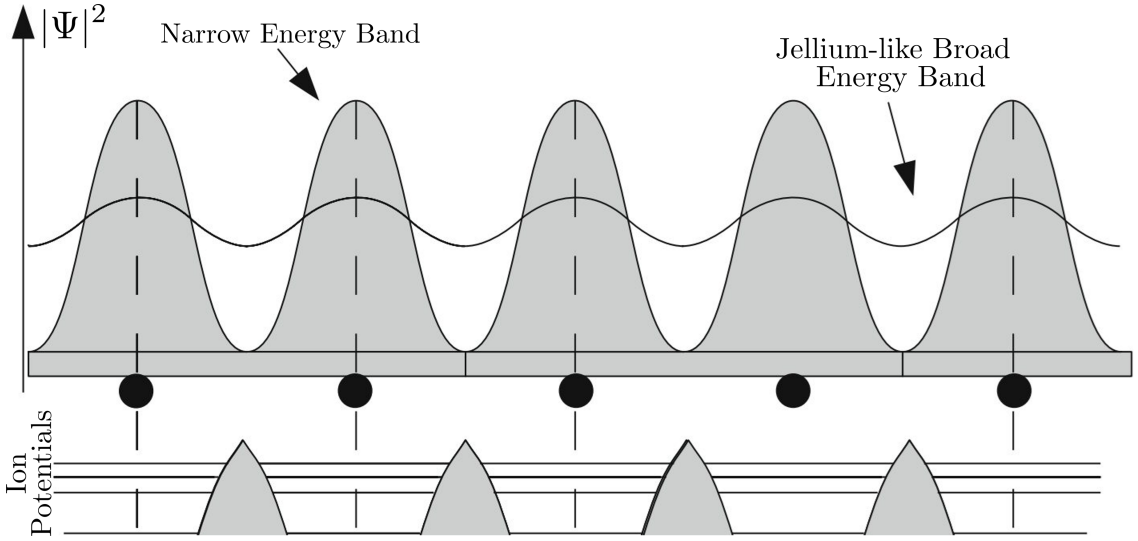

Figure 2.1: Diagram of the lattice potential structure and narrow band formation due to the d-electrons in the solid. (Figure taken from [81])

With this picture in mind, electrons yield a strong reference to the atomic structure and are still itinerant due to the nonnegligible hybridization of lattice sites. We proceed with the usual second quantization process [61] of the model by considering the atomic wavefunction complete

base (in the subspace of the d-band states) in position basis $\varphi_{\mu\sigma}(\mathbf{r}-\mathbf{R}_i) = \left\langle \mathbf{r} \mid \varphi_{\mu\sigma}^{(i)} \right\rangle$, with:

$$|\varphi_{\mu\sigma}(\mathbf{k})\rangle = \frac{1}{\sqrt{N_i}} \sum_{j=1}^{N_i} e^{i\mathbf{k}\cdot\mathbf{R}_j} \left|\varphi_{\mu\sigma}^{(j)}\right\rangle, \tag{2.7}$$

where μ denotes the d-orbitals degeneracy determining the number of sub-bands, $\mathbf{R}_i$ is the position of the ion site, and σ denotes the spin degree of freedom. The second quantized version of the $\hat{H}_0$ Hamiltonian is:

$$\hat{H}_0 = \sum_{ij\sigma} \sum_{\mu\nu} T_{ij}^{\mu\nu} \hat{c}_{i\mu\sigma}^{\dagger} \hat{c}_{j\nu\sigma}, \tag{2.8}$$

where the hopping integrals T_{ij} are given by:

$$T_{ij}^{\mu\nu} = \int d^3 r \varphi_{\mu\sigma}^{*}(\mathbf{r}-\mathbf{R}_i) \left(-\frac{\hbar^2}{2m}\Delta + V_{ei}^{(0,d)}\right) \varphi_{\nu\sigma}(\mathbf{r}-\mathbf{R}_j). \tag{2.9}$$

As a relevant note, we can transform the single-particle Hamiltonian of the kinetic energy contribution to momentum space using a Fourier transform[4]. This yields its eigenvalue problem

$$\hat{T}_{\mathbf{k}} |u_{m\mathbf{k}\sigma}\rangle = \varepsilon_m(\mathbf{k}) |u_{m\mathbf{k}\sigma}\rangle, \tag{2.10}$$

where the eigenstates $|u_{m\mathbf{k}\sigma}\rangle$ relate electron states in the m sub-bands whose number is the same as the number of atomic orbitals employed for the degeneracy of the d-orbitals. We can use them to build the matrix $U_{\mathbf{k}\sigma}^{m\mu} = \langle u_{m\mathbf{k}\sigma} \mid \varphi_{\mu\sigma}(\mathbf{k})\rangle$ that diagonalizes $\hat{T}_{\mathbf{k}}$:

$$\hat{U}_{\mathbf{k}\sigma} \hat{T}_{\mathbf{k}} \hat{U}_{\mathbf{k}\sigma}^{\dagger} = \begin{pmatrix} \varepsilon_1(\mathbf{k}) & 0 & \cdots & 0 & 0 \\ 0 & \varepsilon_2(\mathbf{k}) & \cdots & 0 & 0 \\ & \cdots & \cdots & 0 & \\ 0 & 0 & \cdots & 0 & \varepsilon_{2l+1}(\mathbf{k}) \end{pmatrix}. \tag{2.11}$$

With this, we write:

$$\hat{H}_0 = \sum_{\mathbf{k}m\sigma} \varepsilon_m(\mathbf{k}) \hat{c}_{\mathbf{k}m\sigma}^{\dagger} \hat{c}_{\mathbf{k}m\sigma}, \tag{2.12}$$

and in close analogy to the second quantization form of a gas of noninteracting fermions in a periodic potential (like for a macroscopic metal whose kinetic energy predominates correlations, typical of fermionic reservoirs representations) $\varepsilon_m(\mathbf{k})$ are the bloch energies determining the band structure of the solid [79]. This Hamiltonian is frequently employed for the representation of the "open" part of the IQDS, as we discuss in Ch 3.

We follow the same procedure for the two-body interacting part ($\hat{H}_1$), whose interacting diagram is depicted in Figure 2.2. This leads to:

$$\hat{H}_1 = \frac{1}{2} \sum_{ijkl} \sum_{\mu\mu'\nu\nu'} \sum_{\sigma\sigma'} v(i\mu, j\nu; l\mu', k\nu') \hat{c}_{i\mu\sigma}^{\dagger} \hat{c}_{j\nu\sigma'}^{\dagger} \hat{c}_{k\nu'\sigma'} \hat{c}_{l\mu'\sigma}, \tag{2.13}$$

[4] Explicitly given by $T_{\mathbf{k}}^{\mu\nu} = \frac{1}{N_i} \sum_{i,j} T_{ij}^{\mu\nu} e^{-i\mathbf{k}\cdot(\mathbf{R}_i - \mathbf{R}_j)}$.

where interacting parameters $v\left(i\mu,j\nu;l\mu',k\nu'\right)=\left\langle i^{\mu}j^{\nu}|\hat{H}_1|l^{\mu'}k^{\nu'}\right\rangle$ are given by the overlapping integral:

$$v\left(i\mu,j\nu;l\mu',k\nu'\right)=\iint d^3rd^3r'\varphi^*_{\mu\sigma}\left(\mathbf{r}-\mathbf{R}_i\right)\varphi^*_{\nu\sigma'}\left(\mathbf{r}'-\mathbf{R}_j\right)\frac{e^2}{4\pi\varepsilon_0\left|\mathbf{r}-\mathbf{r}'\right|}\varphi_{\mu'\sigma}\left(\mathbf{r}-\mathbf{R}_l\right)\varphi_{\nu'\sigma'}\left(\mathbf{r}'-\mathbf{R}_k\right). \tag{2.14}$$

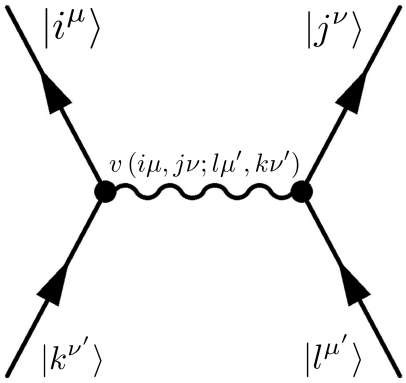

Figure 2.2: Two-body interaction diagram for the $\hat{H}_1$ Hamiltonian.

We note the spin independence of the Hamiltonian (no magnetic fields or other sources of spin dependency [95]) so we write

$$v\left(i\mu\sigma_1,j\nu\sigma_2;l\mu'\sigma_4,k\nu'\sigma_3\right)=\delta_{\sigma_1\sigma_4}\delta_{\sigma_2\sigma_3}v\left(i\mu,j\nu;l\mu',k\nu'\right). \tag{2.15}$$

The next *fundamental assumption* of the model is the consideration that the parameters in (2.14) can be approximated by the matrix element integrals $v\left(\mu\nu;\mu'\nu'\right)=v\left(i\mu,i\nu;i\mu',i\nu'\right)$, i.e., it is assumed from the locality of the atomic basis that the **inter**-atomic electronic correlation effects become negligible against the **intra**-atomic ones. Interacting electrons always belong to the same site, and we can write:

$$\hat{H}_1=\frac{1}{2}\sum_{i\sigma\sigma'}\sum_{\mu\mu'\nu\nu'}v\left(\mu\nu;\mu'\nu'\right)\hat{c}^{\dagger}_{i\mu\sigma}\hat{c}^{\dagger}_{i\nu\sigma'}\hat{c}_{i\nu'\sigma'}\hat{c}_{i\mu'\sigma}. \tag{2.16}$$

Using atomic *Ni* (nickel) wavefunctions (while also ignoring *d*-orbital degeneracy with possible sub-band structure −we drop μ and ν−), Hubbard justified the previous fundamental assumption by calculating some values of the interacting parameters, such as $v(ii;ii)\approx 20eV$, $v(ij;ij)\approx 6eV$, $v(ii;ij)\approx 0.5\text{eV}$, $v(ij;ik)\approx 0.1\text{eV}$, and $v(ii;jj)\approx 0.025\text{eV}$. We note how the intra-atomic interactions have a larger contribution. As noticed by both Hubbard and Assa Auerbach, even though we still are not fully justified in neglecting the inter-atomic parameters $v(ij;ij)$ due to the coupled charge fluctuations at different sites, the resulting effective model emerging from such considerations is otherwise not so poor as a starting point for a theory of correlations.

Typically, only two types of terms in (2.16) are particularly important (we drop any other index combination terms because of their negligible magnitude and contribution to the material's magnetic properties [81]): the **direct terms** giving rise to the Coulomb repulsion $U_{\mu\nu} \equiv v(\mu\nu;\mu\nu)$, corresponding to the case $\mu = \mu'/\nu = \nu'$, and the **exchange terms** (with no classical analog) originating from the statistical nature of Fermi-particles[5] $J_{\mu\nu} \equiv v(\mu\nu;\nu\mu)$, corresponding to the case $\mu = \nu'/\nu = \mu'$:

$$\hat{H}_1 = \frac{1}{2}\sum_{i\sigma\sigma'}\sum_{\mu\nu}\left[\left(1-\left(\delta_{\mu\nu}\delta_{\sigma\sigma'}\right)U_{\mu\nu}\hat{n}_{i\mu\sigma}\hat{n}_{i\nu\sigma'} + \left(1-\delta_{\mu\nu}\right)J_{\mu\nu}\hat{c}^{\dagger}_{i\mu\sigma}\hat{c}^{\dagger}_{i\nu\sigma'}\hat{c}_{i\mu\sigma'}\hat{c}_{i\nu\sigma}\right]. \tag{2.17}$$

Finally, we neglect the d-orbital degeneracy to get a single effective band model ($\mu = \nu = 1$) akin to a model for a s-band solid and arrive at the Hamiltonian:

$$\hat{H} = \sum_{ij\sigma} T_{ij}\hat{c}^{\dagger}_{i\sigma}\hat{c}_{j\sigma} + \frac{U}{2}\sum_{i\sigma}\hat{n}_{i\sigma}\hat{n}_{i\bar{\sigma}} = \sum_{ij\sigma} T_{ij}\hat{c}^{\dagger}_{i\sigma}\hat{c}_{j\sigma} + U\sum_{i}\hat{n}_{i\uparrow}\hat{n}_{i\downarrow}, \tag{2.18}$$

where $T_{ii} = \varepsilon_i$ (on-site "coupling") is understood as the lattice energy required for an electron to occupy the lattice site[6], and U is the on-site interaction strength of the single-band electrons. An important parameter of this model is the electron occupation $n = \sum_{i\sigma}\langle n_{i\sigma}\rangle\,; 0 \leq n \leq 2$. Each site is degenerate in spin with the possibility of containing two electrons of opposite spin ($n = 2$). This notation is employed in this work for the case of a single-site Hubbard model ($\varepsilon_i \to \varepsilon_0$). The Hamiltonian in Eq. (2.18) is the famous **Hubbard model** that John Hubbard deduced in his seminal work [91]. Before we move on to the Anderson and Kondo models, we describe two important limiting cases of this Hamiltonian to build some intuition of its physics: the **band limit** and the **atomic limit** (or infinitely narrow band limit) with its variant consisting of the **strong-coupling limit**.

1. The band limit: If we set $U = 0$, no electronic correlation effects are taken into account in the study of the solid. In this scenario, we arrive at the description given by the Hamiltonian of Eq. (2.8), which can be diagonalized to determine the band structure $\varepsilon_m(\mathbf{k})$ of the solid. The spectral properties are then completely determined by the band structure energy dispersion relation and this is why this situation is referred to as the band limit. This is one of the few scenarios where the Hubbard model can be fully solved analytically, as demonstrated in section 3.3.1. In the case of a solid in the mesoscopic scale, this limit constitutes a model perfect for an infinite periodic metal as an unlimited supply of electrons: a fermionic reservoir, with which quantum systems of finite sizes and myriad complexities can exchange energy and electrons. As seen in section 2.2, this is the scenario of relevant quantum transport setups.

[5] A consequence of the exchange principle of quantum mechanics and Heisenberg noted these terms were responsible for ferromagnetism in materials with localized magnetism [84].

[6] If we consider the hopping between nearest neighboring sites only we arrive at the tight-binding approximation, where electrons only hop to the nearest next neighbor sites in virtue of the small hybridization between second-neighbors. It is denoted by the subscript $\langle i,j\rangle$, which indicates summation over i and j for nearest neighbors only. This approximation is compatible with descriptions of solids with narrow energy bands.

2. The atomic limit: sometimes referred to as the infinitely narrow band model. It assumes that the coupling between lattice sites is negligible compared to the on-site Coulomb repulsion U (with $|U| > 0$), hence resembling a band structure with vanishing dispersion (or infinitely narrow band), analogous but not exactly as if the solid were a collection of isolated atoms. It must be emphasized that this limiting case is reached because of the competition between hopping processes among sites and the formation of doubly, singly or empty states energetically more expensive due to the Coulomb repulsion and onsite lattice energies. In this limit, the model emphasizes the local (on-site) interactions over the kinetic energy of the electrons moving between sites. We let each energy site to be same, $T_{ij} = \varepsilon_0 \delta_{ij}$, and hence the band structure resembles $\varepsilon(\mathbf{k}) \to \varepsilon_0$, $\forall\, \mathbf{k}$.

   We can proceed by analyzing the spectral features of the Hubbard model in the atomic limit. This can be done (as considered by Hubbard) with the so-called equation of motion techniques, depicted in Ch. 3 and employed in Ch. 4. Here, we outline the procedure and note that it follows as a limiting case of the general situation depicted in section 4.2.1. We follow reference [81] and start by obtaining an equation of motion for the expectation value of the operator $-i\theta(t-t')\left\{\hat{c}_{i\sigma}(t), \hat{c}^{\dagger}_{j\sigma}(t')\right\}$ (the retarded single-particle Green's function) in time domain. This equation can be translated to the energy domain in the stationary situation where the equation for the expectation value can be effectively solved by taking advantage of the limiting scenario. As customary in the theory of Green's functions (see Ch 3.1), this expectation value can be used to compute the spectral density $\rho_\sigma(E)$, giving as a result:

$$\rho_\sigma(E) = (1 - n_{\bar{\sigma}})\, \delta\left(E - \varepsilon_0\right) + n_{\bar{\sigma}} \delta\left(E - \varepsilon_0 - U\right), \tag{2.19}$$

   where $n_{\bar{\sigma}} = n_\sigma = \left\langle \hat{n}_\sigma \right\rangle$ (both spin occupation are symmetrically the same) is the expectation value of the electron number operator or the occupation of the system, and we note the appearance of two possible energy excitations at $E_1 = \varepsilon_0$ and $E_2 = \varepsilon_0 + U$ with spectral weights $1 - n_{\bar{\sigma}}$ and $n_{\bar{\sigma}}$, respectively. The fundamental feature of the Coulomb interaction in the spectral properties of the system manifests in the appearance of an energetically inconvenient energy state associated with the double occupancy of a single lattice site degenerated in spin. In the infinitely narrow band limit, the Bloch band of the solid (which in this case becomes a degenerate level with energy ε_0) is split into two sorts of discrete (or infinitely narrow) quasiparticle energies defining two sub-bands at energies E_1 and E_2. Their associated spectral weights represent the probabilities for an electron of spin σ to occupy an empty energy level at the lattice site $(1 - n_{\bar{\sigma}})$ or to encounter one electron of opposite spin there $(n_{\bar{\sigma}})$, for which an energy cost of U must be paid. This is intuitively seen if you assume $n_{\bar{\sigma}} = 0$ (empty lattice site), for which the energetic cost for an electron to transfer to this level would be ε_0 ($\rho_\sigma(E) = \delta\left(E - \varepsilon_0\right)$). These are the **Hubbard bands**, first discussed by Hubbard in his seminal work [91] and they are relevant for the study of this Thesis as discussed in section 4.1.2. We refer to the band centered at $E_2(E_1)$ as the higher(lower) sub-band. Electrons moving in the higher sub-band are more likely to hop to lattice sites with existing electrons of opposite spin, and electrons in the lower sub-band have energies

favoring the hopping to empty lattice sites. This distinction is the landmark feature of such a quasiparticle band structure [81].

If we now assume nonzero bandwidth in the band structure ($T_{ij} \neq 0$) such that the dominant energy is the Coulomb repulsion energy $U \gg T_{ij}$, the system presents yet another regime known as the strong-coupling limit. The non-vanishing hopping parameters T_{ij} produce a nonnegligible contribution of electrons' kinetic energy, which now hop between sites. Such processes (with their additional non-diagonal terms with respect to the atomic limit Hubbard Hamiltonian) change the eigenstates of the atomic limit case by allowing electrons to hop to neighboring sites and back. In some cases, electrons can temporarily hop to sites with one electron of opposite spin (with an unfavorable energetic cost of U) and then tunnel back to its original site. Furthermore, the initial electron could exchange spin with the electron at the neighboring site and hop back to its initial site with the opposite spin. These are the so-called **virtual hopping processes** [4]. In the strong-coupling limit, they are especially relevant if we imagine a total occupation of $n = 1$, i.e., one electron per site at each lattice site of the solid. This is the **half-filling** situation and is important for the study of ferromagnetic properties of metals presenting localized magnetism, where double occupations are very costly energy states. An effective low-energy Hamiltonian can be deduced from the half-filling situation in the strong-coupling limit of the Hubbard model: the **Heisenberg Hamiltonian**, which describes the resulting favorable antiferromagnetic alignment of neighboring electrons (now seen as localized spins due to the half-filling situation). It is behind the virtual hopping processes affecting the energy state of the system through the so-called superexchange mechanism [83].

From the discussion above, the kinetic energy is expected to lift the degeneracy of states with energies E_1 and E_2 present in the atomic limit. The new energies group around them smearing out the previously discrete energies and developing a peak structure at energies associated with changing double occupations: for a two-site Hubbard model, we could have an additional peak at energy $\varepsilon_0 + 2U$ corresponding to the cost of two double occupations (two electrons with opposite spins per site). In general, satellite peaks at $\varepsilon_0 + pU;\ p = -1, -2... ; p = 2, 3...$ emerge due to multiple of such processes whose associated spectral weights are very small as they constitute relatively improbable processes in the strong-coupling situation (see Figure 2.3). Finally, the role of temperature is also important in this widening of the spectral energies due to the introduction of thermal fluctuations: higher energies produce wider spectral peaks and electrons presenting stronger delocalization about the lattice sites.

In the weak coupling regime where U is comparable with the hybridization among levels, the first option to explore the physics of the Hubbard model is the **mean-field** approximation. In this approach, the quartic term in Eq. (2.18) is replaced using the expectation value (hence mean field) of the spin occupation operators: $\hat{n}_{i\sigma}\hat{n}_{i\bar{\sigma}} \to \langle \hat{n}_{i\sigma} \rangle \hat{n}_{i\bar{\sigma}} + \hat{n}_{i\sigma} \langle \hat{n}_{i\bar{\sigma}} \rangle$, leading to the Hamiltonian $\hat{H} \to \hat{H}_S = \sum_{ij\sigma} \left(T_{ij} + U \langle \hat{n}_{i\bar{\sigma}} \rangle \delta_{ij} \right) \hat{c}^{\dagger}_{i\sigma} \hat{c}_{j\sigma}$, where we note a renormalization or shifting of the site energies $E_{i\uparrow} = \varepsilon_0 + U\langle \hat{n}_{i\downarrow} \rangle$ and $E_{i\downarrow} = \varepsilon_0 + U\langle \hat{n}_{i\uparrow} \rangle$ (for $T_{ij} = \varepsilon_0 \delta_{ij}$), hinting to a self-consistent procedure for the calculation of the mean-field values of the operators [96]. A better outline of this procedure is studied in the next section for the Anderson model.

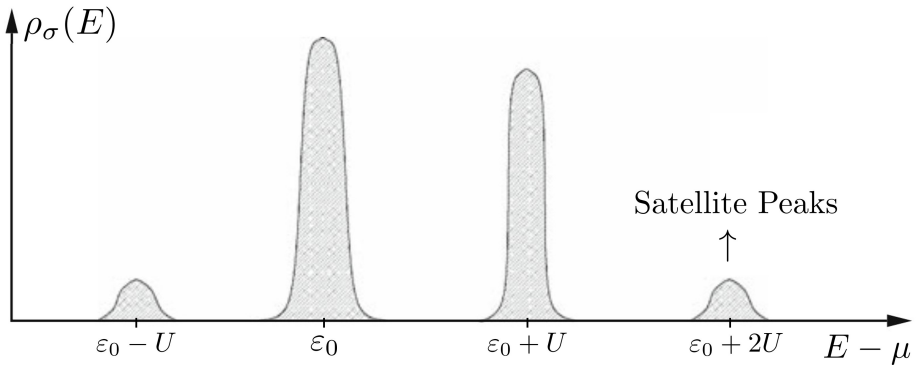

Figure 2.3: Spectral density of the strong-coupling limit. The smearing out of the degenerate energies can be depicted. (Figure taken from [81])

Beyond mean-field methods lies the realm of perturbation theory with Feynman diagrams thoroughly discussed in Ch 3. The essence of this method is to capture the electronic correlations of interacting problems from an infinite sum of terms, each higher order containing more correlation effects leading to modified perturbation treatments that include even more many-body effects and reveal additional aspects of Hubbard systems (relevant to the purpose of this work) such as the Kondo effect, and the appearance of a Kondo resonance in the electronic density of states of the system [4], briefly discussed in the consequent sections. However, the physics of the approximation employed in this work to study the Coulomb interaction is not enough to account for such strong correlation effects in transport [76]. This is one of the reasons to highlight the Schrieffer-Wolf transformation of section 2.1.3 as a bridge to study only Anderson physics as a starting point.

2.1.2 The Kondo and Anderson models

Neither of the models discussed in the previous section explained the origins of local magnetic moment (LMM) formation in magnetic alloys with impurities that tended to preserve or lose localized spins, thereby not always forming LMMs [85]. In addition, as mentioned in Ch 1, some materials with certain magnetic impurity concentrations developed a resistance minimum as a function of temperature that puzzled solid-state physicists in the 1930s [27]. This section details the path followed to resolve these issues, conforming to the fundamental ideas behind LLM formation, asymptotic freedom, and Kondo physics.

Building on the ideas of virtual bound-state resonance employed to describe the interaction of electrons with the d-orbitals of magnetic ions developed by Andre Blandin and Jacques Friedel [97], Phillip Anderson built the single impurity Anderson model (SIAM) to explain LMM formation in 1961 [29]. The physical situation is that of an impurity atom with incomplete localized d' or f-orbitals interacting with the continuum of states in a noninteracting metal with a determined band structure described by Eq. (2.12). For simplicity, let us assume a simple band structure with no sub-bands (the degeneracy of the orbitals is neglected). Then, the Hamiltonian for the metal

(a fermionic reservoir denoted by the subscript "M") is written as

$$\hat{H}_M = \sum_{\mathbf{k}\sigma} \varepsilon_{\mathbf{k}} \hat{c}^\dagger_{\mathbf{k}\sigma} \hat{c}_{\mathbf{k}\sigma}. \tag{2.20}$$

The Hamiltonian for the impurity is the single-site version of the Hubbard model Hamiltonian in Eq. (2.18) (we now use "d" to differentiate from the second quantization operators of electrons in the metal):

$$\hat{H}_D = \varepsilon_0 \sum_{\sigma} \hat{d}^\dagger_\sigma \hat{d}_\sigma + U \hat{n}_\uparrow \hat{n}_\downarrow, \tag{2.21}$$

where the subscript "D" for the Hamiltonian stands for the "device" or system of interest,[7] in this case the impurity atom. The fundamental addition in the paradigm of the Anderson model is the Hamiltonian $\hat{H}_T$ for the interaction between the metal and the impurity atom. We use a basis of localized atomic wave functions $|\phi^d_\sigma\rangle$ for the impurity and a basis of Bloch states denoted by $|\mathbf{k}\sigma\rangle$. In the derivation of the diagonalized Hamiltonian in Eq. (2.12), the band structure is deduced from the change from position to momentum basis in the description of the solid. The original atomic basis functions are now written in momentum and replaced by Bloch functions $\psi_{\mathbf{k}\sigma}(\mathbf{r}) = \langle \mathbf{r}|\mathbf{k}\sigma\rangle$. In this way, it seems natural to think of the product state basis as a complete basis for the full system description, where the change to momentum space and subsequent diagonalization is performed in a subspace of the lattice. In general, this is valid under the assumption that the tunneling processes associated with purely single-electron energies, and the chosen basis be correctly localized to avoid higher-order hybridization contributions [13][8]. Hence, the non-diagonal terms of the matrix representation of the full Hamiltonian in the chosen basis constitute the interaction between the conducting sea and the impurity atom:

$$\hat{H} = \sum_{k\sigma} \varepsilon_{\mathbf{k}\sigma} |\mathbf{k}\sigma\rangle\langle\mathbf{k}\sigma| + \sum_{\sigma} \varepsilon_0 |\phi^d_\sigma\rangle\langle\phi^d_\sigma| + \sum_{\mathbf{k}\sigma} V_{\mathbf{k}\sigma} |\phi^d_\sigma\rangle\langle\mathbf{k}\sigma| + V^*_{\mathbf{k}\sigma} |k\rangle\langle\phi^d_\sigma|, \tag{2.22}$$

or in second quantization form:

$$\hat{H} = \hat{H}_D + \hat{H}_M + \hat{H}_T, \quad \hat{H}_T = \sum_{\mathbf{k}\sigma} V_{\mathbf{k}\sigma} \hat{d}^\dagger_\sigma \hat{c}_{\mathbf{k}\sigma} + V^*_{\mathbf{k}\sigma} \hat{c}^\dagger_{\mathbf{k}\sigma} \hat{d}_\sigma, \tag{2.23}$$

where the tunneling (or hybridization) coefficients $V_{\mathbf{k}\sigma} = \langle \mathbf{k}\sigma|\hat{H}_T|\phi^d_\sigma\rangle$ are given by:

$$V_{\mathbf{k}\sigma} = \int \mathrm{d}\mathbf{r}\, \psi_{\mathbf{k}\sigma}(\mathbf{r}) V_T(\mathbf{r}) \phi^d_\sigma(\mathbf{r}). \tag{2.24}$$

The potential $V_T(\mathbf{r})$ is responsible for the actual transfer of electrons between the parts of the system as a consequence of the interaction of the impurity atom with the ionic lattice potential

[7] We are paving the way towards the paradigm we use from section 2.2.2 to the rest of this work.

[8] The tight-binding approach is clearly compatible with these assumptions and it is often imposed in the definition of the Hubbard model [93].

$V_{ion}(\mathbf{r})$ of the metal. The full deduction for the Hamiltonian stems from a model for this first-principles potential. The seminal work by Anderson [29] deduces the following expression for the tunneling coefficients:

$$V_{\mathbf{k}\sigma} = \int d\mathbf{r}\, e^{-i\mathbf{k}\cdot\mathbf{r}} V_{ion}(\mathbf{r})\phi^d_\sigma(\mathbf{r}), \tag{2.25}$$

which is obtained with the "muffin-tin" potential model [4]. The muffin-tin potential is a theoretical model used to simplify the complex potential landscape in a crystal, making it particularly useful for deriving the Anderson model from first principles. In this model, the potential is divided into two regions: one inside the muffin-tin sphere of radius R_0 centered around each atom, where the potential is given by the sum of the ionic potential, $V_{\text{ion}}(r)$, and a constant term, W. In the interstitial region outside the sphere, the potential is considered constant, which is set to zero here for simplicity:

$$V(r) = \left(V_{\text{ion}}\left(r\right) + W\right)\theta\left(R_0 - r\right). \tag{2.26}$$

The constant W is determined such that both the ionic potential inside the sphere and the potential in the interstitial region are balanced. This ensures that the muffin-tin potential provides a realistic approximation of the true potential landscape within the crystal, thereby allowing for accurate calculations of electronic properties. This potential captures the essential physics of the localized atomic states and the conduction electrons in a crystal lattice for the Anderson model after the application of first-order degenerate perturbation theory to evaluate the elements of the first-principle Hamiltonian steaming from the $\hat{V}_T(\mathbf{r})$ felt by an isolated impurity described by the atomic localized basis $|\phi^d_\sigma\rangle$. Finally, the full Anderson model is given by:

$$\hat{H}_A = \sum_{\mathbf{k}\sigma} \varepsilon_{\mathbf{k}} \hat{c}^\dagger_{\mathbf{k}\sigma}\hat{c}_{\mathbf{k}\sigma} + \varepsilon_0 \sum_\sigma \hat{d}^\dagger_\sigma \hat{d}_\sigma + U\hat{n}_\uparrow\hat{n}_\downarrow + \sum_{\mathbf{k}\sigma}\left(V_{\mathbf{k}\sigma}\hat{d}^\dagger_\sigma\hat{c}_{\mathbf{k}\sigma} + V^*_{\mathbf{k}\sigma}\hat{c}^\dagger_{\mathbf{k}\sigma}\hat{d}_\sigma\right). \tag{2.27}$$

The relevant ingredients to understand this model are **the atomic limit** and **noninteracting limit** ($U = 0$), which then facilitates the application of a mean-field treatment to elucidate the physics of this model. Here is a summary of the most important takeaway points of this model:

1. Atomic limit: As in the previous section, we only deal with the Hamiltonian (2.21). The possible quantum states are simple: we could have a single spin up or down electron with energy $E_1 = \varepsilon_0$ (magnetic), or a doubly occupied state with energy $E_2 = 2\varepsilon_0 + U$ (nonmagnetic). The energy cost to add an electron to a magnetic state is $\varepsilon_0 + U$, while the cost to remove it is $-\varepsilon_0$. This is summarized by the energy change $\Delta E = \frac{U}{2} \pm \left(E_f + \frac{U}{2}\right)$. Relative to zero (where below zero energies represent favorable low excitation states and we can assume $\varepsilon_0 < 0$), we see from that energy change that we must ensure $U > \varepsilon_0 + U/2$ if we require $\varepsilon_0 + U$ to be sufficiently greater than zero (unfavorable). But we also need $U < \varepsilon_0 + U/2$ to achieve the same. In both cases, the doubly occupied state is highly unfavorable and only the spin degrees of freedom remain. A localized moment could be formed in this situation and a half-filling condition could be satisfied.

2. $U = 0$ case: How does the conducting sea affect the spectral properties of the impurity atom? In general, there is a competition between the hybridization $V_{\mathbf{k}}$ and the interacting Coulomb constant U. The former tends to equalize up and down spin occupancy and the latter tends to unbalance them due to the energy cost of U for the double occupancy. To appreciate the interplay, we start by assuming $U = 0$ in Eq. (2.27). The impurity level is sharp and discrete previous to the interaction with the continuum. This hybridization means that the impurity state can exchange electrons with the conduction band, giving the impurity state a finite lifetime. The finite lifetime of the impurity state leads to an energy uncertainty, causing a broadening or spread in its energy level within the density of states. This produces a resonance from the interference arising from the hybridization reflecting the energy of the impurity level: a Fano resonance [98] (see Figure 2.4). In Ch. 3, it is shown how these effects can be rigorously described with the concept of the **embedded self-energy**. It is intuitive to see that this resonance increases the probability for a balanced up-and-down spin occupation from multiple hopping processes between the continuum states and the impurity atom, in contrast to the introduction of unfavorable balanced spin states steaming from the energy cost U once the Coulomb repulsion is switched on.

3. Mean-field treatment: Finally, the key for understanding the competence of the scales associated with U and $V_{\mathbf{k}\sigma}$ that unravels the principles of local moment formation is the mean-field approximation, mentioned in section 2.1.1 at the bottom of page 14, transforming the quartic Coulomb term into a single particle Hamiltonian that shifts the impurity energies such that $E_{i\uparrow} = \varepsilon_0 + U\langle\hat{n}_{i\downarrow}\rangle$ and $E_{i\downarrow} = \varepsilon_0 + U\langle\hat{n}_{i\uparrow}\rangle$. In his seminal work [29], Anderson obtained the electron spin occupations, resulting in the self-consistent expressions (ε_F is the Fermi energy of the conducting sea):

$$\langle\hat{n}_\uparrow\rangle = \frac{1}{2} + \frac{1}{\pi}\,\mathrm{arctg}\,\frac{\varepsilon_F - \varepsilon_0 - U\,\langle\hat{n}_\downarrow\rangle}{\Gamma}, \quad \langle\hat{n}_\downarrow\rangle = \frac{1}{2} + \frac{1}{\pi}\,\mathrm{arctg}\,\frac{\varepsilon_F - \varepsilon_0 - U\,\langle\hat{n}_\uparrow\rangle}{\Gamma}, \tag{2.28}$$

where Γ represents the broadening of the density of states about the energy level due to the system-bath coupling. Careful analysis of these equations leads to phase diagrams determining nonmagnetic ($\langle\hat{n}_\uparrow\rangle = \langle\hat{n}_\downarrow\rangle$) or magnetic solutions ($\langle\hat{n}_\uparrow\rangle \neq \langle\hat{n}_\downarrow\rangle$) setting the conditions for LMM formation.

The Anderson model alone did not provide a complete explanation for the observed anomalies in electrical resistivity in metals doped with magnetic impurities. One such anomaly was the resistance minimum observed at low temperatures, known as the Kondo effect [27]. In 1964, Jun Kondo tackled this problem by considering a simplified version of the Anderson model, focusing on the exchange interaction between the conduction electrons and the localized magnetic moment. This led to the formulation of the Kondo model. Anderson observed that in the limit of strong U, the hybridization term can be treated as a perturbation. Another mechanism to explain the origin of a localized moment came from the application of second-order perturbation theory in the parameters $V_{\mathbf{k}\sigma}$. This procedure is detailed in Ref. [83], where an effective model equivalent to the

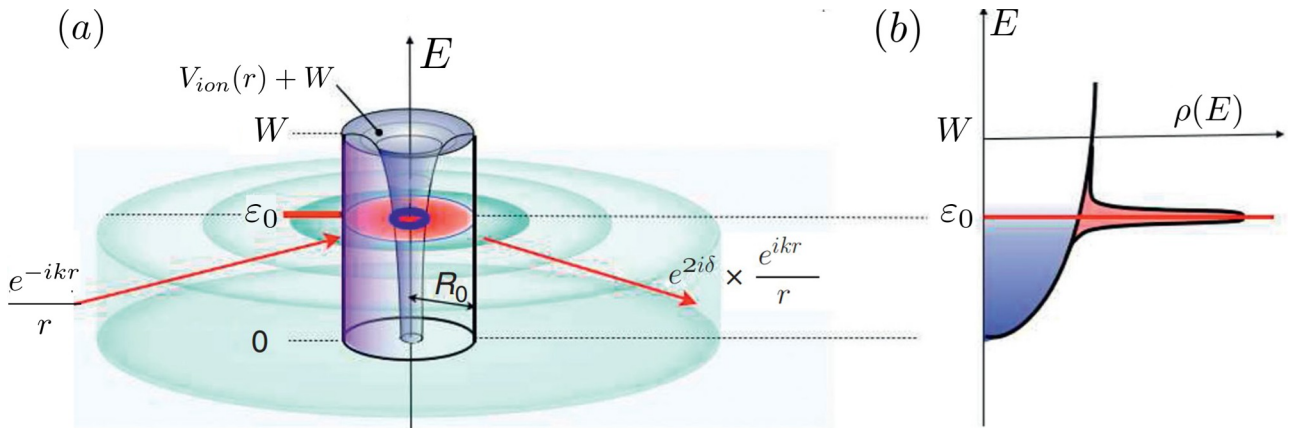

Figure 2.4: (a) Schematic representation of the muffin-tin potential (2.26) responsible for the hybridization of the degenerate conducting sea states and the localized impurity atom state. (b) The effect of the continuum to the localized level of the impurity is to produce broadening and a resonance centered at ε_0. (Figure taken from [4])

s-d model [86] emerged:

$$\hat{H}_K = \sum_{\mathbf{k}\sigma} \varepsilon_{\mathbf{k}\sigma} \hat{c}^\dagger_{\mathbf{k}\sigma} \hat{c}_{\mathbf{k}\sigma} + \sum_{\mathbf{k},\mathbf{k}'} J_{k,k'}\, \hat{c}^\dagger_{\mathbf{k}\sigma}\, \vec{\sigma}_{\sigma\bar{\sigma}}\, \hat{c}_{\mathbf{k}'\bar{\sigma}} \cdot \hat{\vec{S}}_d, \quad \hat{\vec{S}}_d \equiv \hat{d}^\dagger_\sigma \left(\frac{\vec{\sigma}_{\sigma\bar{\sigma}}}{2} \right) \hat{d}_{\bar{\sigma}}, \tag{2.29}$$

where $\vec{\sigma}_{\sigma\bar{\sigma}}$ is the vector of Pauli matrices. The s-d model describes the interaction between the conduction electrons in the s-band and localized magnetic moments arising from the d-electrons in a material. Here, the spin operator $\hat{\vec{S}}_d$ for the localized moment is produced by the spin degree of freedom in the magnetic impurity atom. The exchange coupling constant J turns out to be negative, indicating a tendency to form a singlet between the localized spin and the spin density of the surrounding conducting sea ($\hat{c}^\dagger_{\mathbf{k}\sigma}\, \vec{\sigma}_{\sigma\bar{\sigma}}\, \hat{c}_{\mathbf{k}'\bar{\sigma}}$) from an antiferromagnetic coupling. Kondo employed perturbation theory to show that the scattering of conduction electrons off the localized spin above becomes stronger at low temperatures due to higher-order spin-flip processes [99]. He performed a perturbative expansion in the exchange constant J, and observed that the second term (second-order perturbation theory) could be much larger than the first. This insight explained the resistance minimum phenomenon observed experimentally. The resistance minimum arises from the temperature-dependent scattering rate of conduction electrons off the localized magnetic moment. At high temperatures, the scattering rate is relatively constant, resulting in a normal metallic behavior where resistivity decreases as temperature decreases. However, at lower temperatures, the interaction between conduction electrons and the localized magnetic moment leads to an increased scattering rate due to spin-flip processes. This enhanced scattering causes an increase in resistivity,

$$\rho(T) = C \left[1 - 2Jn_0 \ln \frac{\Gamma}{k_B T} \right], \tag{2.30}$$

where Γ is the bandwidth induced by the conducting sea, n_0 is the density of states at the Fermi level, and J is the antiferromagnetic exchange coupling constant. The resistivity presents a minimum at a characteristic temperature, known as the Kondo temperature T_K. This is a crucial parameter in the Kondo model, representing the scale below which the Kondo effect becomes significant. It is given by :

$$T_K = \Gamma \exp\left(-\frac{1}{2Jn_0}\right).$$

More relevant to this Thesis, in terms of the Anderson model parameters T_K is given by

$$T_K = \frac{1}{2}(\Gamma U)^{1/2} \exp\left[\frac{\pi\varepsilon_0\left(\varepsilon_0 + U\right)}{\Gamma U}\right], \tag{2.31}$$

result obtained by Haldane in Ref. [100].

One of the most striking features of the Kondo effect is the appearance of the **Kondo resonance**. It originates from the interaction between conduction electrons and the localized magnetic impurity. At temperatures below the Kondo temperature T_K the strength of this interaction leads to the formation of a many-body singlet state where the localized magnetic moment is screened by the surrounding conduction electrons. This screening results in a sharp peak in the spectral density of states at the Fermi level, known as the Kondo resonance, or more historically accurately the Abrikosov–Suhl resonance [101, 102]. In bulk metals doped with impurities, the Kondo resonance enhances scattering through the localized spin, leading to increased resistivity at low temperatures. Conversely, in quantum dot structures, the Kondo resonance enhances the density of states at the Fermi level, facilitating electron tunneling through the dot and thereby increasing conductance [45]. Although this effect in quantum dots is crucial for understanding the low-temperature transport properties of correlated systems, Kondo physics is not in the scope of the approximation employed in this work to treat the Coulomb interaction. By exploiting the Anderson model's connection with the Kondo model through the famous Schrieffer–Wolff transformation, we shall focus on the more fundamental and general physics of the Anderson model as a starting point for the study of interacting systems[9]. This is the topic of the next section.

2.1.3 The Schrieffer–Wolff transformation

In the advent of the Kondo and Anderson models, obtaining the $s-d$ or Kondo Hamiltonian from applying perturbation theory in the hybridization term hinted at some effective connection of these models. Physicists Schrieffer and Wolf provided the details for such a relation through a beautiful procedure that outlines the concept of renormalization in condensed matter physics: the application of a canonical transformation that facilitated the integrating-out of higher degrees of freedom in the Anderson model. The result is a low-energy Hamiltonian resembling the Kondo Hamiltonian after the application of the now-called Schrieffer-Wolf transformation (SWT) [37].

[9] Kondo physics pertains scales and parameters in ranges already contained in the Anderson model.

The idea behind renormalization is cemented on the distinction of phenomena steaming from separated energy scales in quantum systems, as in the case of LMM formation and Kondo physics. In this sense, it is observed that the low-energy physics of effective models depends very specifically on gross features of the high-energy physics allowing for the separation of energy scales. We outline this procedure for the specific case of the Anderson model. Here, the valence fluctuations induced by the virtual charge fluctuations of the hybridization with the conducting sea are integrated out of the Anderson Hamiltonian in a sort of one-step renormalization with the application of the SWT. It is a canonical operator version of classic perturbation theory. The Hamiltonian in Eq. (2.27) is divided into two parts $\hat{H}_A = \hat{H}_0 + \hat{H}_p$, where $\hat{H}_0 = \hat{H}_D + \hat{H}_M$ is the diagonal part and $\hat{H}_p = \hat{H}_T$ as the perturbation. Generically, we can write:

$$\hat{H}_0 = \left(\begin{array}{c|c} \hat{H}_L & 0 \\ \hline 0 & \hat{H}_H \end{array} \right), \tag{2.32}$$

with $\hat{H}_L(H)$ denote the low(high) energy Hamiltonian corresponding to a single(double) occupation configuration. The term connecting both parts is:

$$\hat{H}_p = \sum_{\mathbf{k}\sigma} \left(V_{\mathbf{k}\sigma} \hat{c}^\dagger_{\mathbf{k}\sigma} \hat{d}_\sigma + V^*_{\mathbf{k}\sigma} \hat{c}^\dagger_{\mathbf{k}\sigma} \hat{d}_\sigma \right) = \left(\begin{array}{c|c} 0 & \hat{H}_p^\dagger \\ \hline \hat{H}_p & 0 \end{array} \right). \tag{2.33}$$

We aim to apply a transformation $\hat{\mathcal{U}} = e^{\hat{S}}$ defined by the anti-hermitian ($\hat{S}^\dagger = -\hat{S}$) action operator $\hat{S}$ that bring the original Hamiltonian to a diagonal form:

$$\hat{H}_{eff} = e^{\hat{S}} \hat{H}_A e^{-\hat{S}} = \hat{\mathcal{U}} \left(\begin{array}{c|c} \hat{H}_L & \hat{H}_p^\dagger \\ \hline \hat{H}_p & \hat{H}_H \end{array} \right) \hat{\mathcal{U}}^\dagger = \left(\begin{array}{c|c} \hat{H}^* & 0 \\ \hline 0 & \hat{H}' \end{array} \right), \tag{2.34}$$

which is expanded as:

$$\hat{H}_{eff} = \hat{H}_0 + i\big[\hat{S}, \hat{H}_0\big] + \hat{H}_T + i\big[\hat{S}, \hat{H}_T\big] - \frac{1}{2}\big[\hat{S}, \big[\hat{S}, \hat{H}_0\big]\big] + \cdots . \tag{2.35}$$

In their original work, Schrieffer and Wolf chose $\hat{S}$ to the first order in $V_{\mathbf{k}\sigma}$ such that we can eliminate all non-diagonal components to leading order in this relation by imposing $\big[S, \hat{H}_0\big] = i\hat{H}_T$ from which we obtain the action operator:

$$\hat{S} = \sum_{\mathbf{k}\sigma\alpha} \frac{V_{\mathbf{k}\sigma}}{\varepsilon_{\mathbf{k}\sigma} - \varepsilon_0 - U} \, n^\alpha_{\bar{\sigma}} \, \hat{c}^\dagger_{\mathbf{k}\sigma} \hat{d}_\sigma - \text{H.c.}, \tag{2.36}$$

where $n^\alpha_{\bar{\sigma}} = n_{\bar{\sigma}}$ for $\alpha = +$, and $n^\alpha_{\bar{\sigma}} = 1 - n_{\bar{\sigma}}$ for $\alpha = -$ are electron occupations akin to the spectral weights of the Hubbard band splitting. This leads to a new Hamiltonian

$$\hat{H}_{eff} = \hat{H}_0 + \frac{i}{2}\big[\hat{S}, \hat{H}_T\big], \tag{2.37}$$

which is later identified with the Kondo Hamiltonian:

$$\hat{H}_K = \sum_{\mathbf{k}\sigma} \varepsilon_{\mathbf{k}\sigma} \hat{c}^\dagger_{\mathbf{k}\sigma} \hat{c}_{\mathbf{k}\sigma} + \sum_{\mathbf{k},\mathbf{k}'} J_{k,k'}\, \hat{c}^\dagger_{\mathbf{k}\sigma}\, \vec{\sigma}_{\sigma\bar{\sigma}}\, \hat{c}_{\mathbf{k}'\bar{\sigma}} \cdot \hat{\vec{S}}_d, \quad \hat{\vec{S}}_d \equiv \hat{d}^\dagger_\sigma \left(\frac{\vec{\sigma}_{\sigma\bar{\sigma}}}{2} \right) \hat{d}_{\bar{\sigma}}. \tag{2.38}$$

With this connection in mind, we depart from the study of Kondo physics and LMMs and focus on the more fundamental Anderson model encompassing interacting physics in wider energy scales. As we see in the next section, an additional fermionic reservoir interacting with the Anderson model in a two-terminal structure conforms to the most important theoretical paradigm in quantum transport and serves as a model for the interacting quantum dot system.

2.2 Quantum dots & single-electron transport

Quantum dots (QDs) are nanoscale semiconductor particles that exhibit distinct quantum mechanical properties due to their extremely small size, typically ranging from 2 to 10 nanometers. These minute structures were first conceptualized in the 1980s, with seminal works by Ekimov and Efros, followed by significant advancements by Reed and colleagues, marking the initial discovery and development of these remarkable nanomaterials [103, 104]. QDs exhibit discrete energy levels and size-tunable electronic and optical properties, a result of the quantum confinement effect, where the dimensions of the dot are comparable to the de Broglie wavelength of the electrons within. Over the years, QDs have found a wide array of applications due to their unique properties. In optoelectronics, they are used in QD light-emitting diodes (QD-LEDs) and solar cells, providing enhanced efficiency and color purity [105]. In biomedicine, QDs serve as fluorescent probes for imaging and diagnostics, offering superior brightness and photostability compared to traditional dyes [106]. Moreover, QDs have been utilized in quantum computing and information processing, where their ability to represent qubits and facilitate coherent manipulation is invaluable [107]. A wider variety of applications is seen in Figure 2.5.

The advent of quantum dots has significantly advanced the theoretical and experimental study of single-electron transport, an essential aspect of quantum transport. Single-electron transport involves the controlled movement of individual electrons through a system, typically at low temperatures to minimize thermal fluctuations. Quantum dots, due to their discrete energy levels and Coulomb blockade effect (discussed in section 2.2.2), are ideal systems for observing and manipulating single-electron phenomena. One of the notable devices utilizing single-electron transport through QDs is the single-electron transistor (SET). The SET consists of a small conducting island (the quantum dot) connected to source and drain electrodes through tunnel junctions and capacitively coupled to a gate electrode. This configuration allows the control of electron flow one electron at a time, a capability critical for high-precision charge and quantum computing applications [108].

The discrete character of the spectrum of quantum dot structures facilitates a first-principles description based on the single-particle Hamiltonian, with the additional two-body operator for

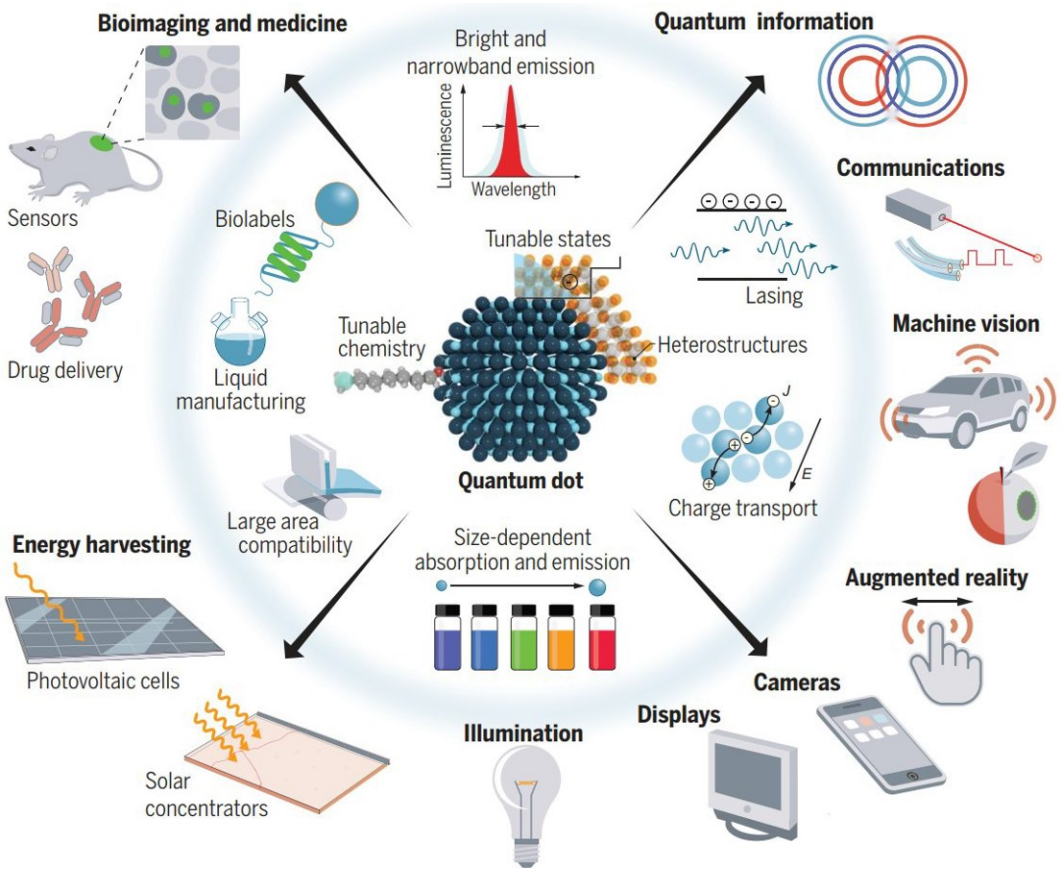

Figure 2.5: Representation of the diverse technological applications of the quantum dot interface spanning communication and information technology energy harvesting, displays, cameras, sensors, biology, and medicine. (Figure taken from [41])

the Coulomb interaction. If we choose a localized basis (an atomic orbital basis for example) for a single level QD, we can employ the Hamiltonian of Eq. (2.21) to model this system. In practical application, QDs exchange electrons with surrounding conducting materials through tunneling processes, similar to the physical situation described by the Anderson model, with a QD instead of an impurity atom.

A fundamental paradigm of quantum transport is the two-terminal configuration for transport, as it is depicted in Figure 2.6) [19, 109]. In the figure, a voltage V_{sd} is applied between a source and drain, inducing a current I through the central region or the channel. We shall refer to the central region as the device. It possesses a certain density of states $D(E)$. Both source and drain can be described by macroscopic leads serving as fermionic reservoirs. The application of V_{sd} shifts the chemical potential in both leads in such a way that $\mu_L - \mu_R = qV_{sd}$ [19] (recall that both lead's states are occupied up to a given chemical potential), where q is the electron charge. The amount qV_{sd} is referred to as the **transport window**: only the states of $D(E)$ with energies near

this zone contribute to electron flow. Whenever $V_{sd} = 0$, we have $\mu_R = \mu_L = \mu_0$ and the system is in equilibrium. We describe the electron states in both reservoirs with their Fermi-distribution functions and assume that their density of states remains unaltered by the presence of the central region, in virtue of their huge amount of degrees of freedom in comparison with the device. It is, instead, the device that is affected by its interaction with the continuum of states of the reservoirs. The bias voltage induces a non-equilibrium condition where now the left contact tends to fill out the device energy level to achieve the equilibrium situation of uniform chemical potential throughout the system. At the same time, the right contact has unoccupied states and "pulls" electrons from the device states. This process is the origin of electron flow in quantum transport setups. Electron flow would intuitively depend on $D(E)$ for energies near the bias window, or near the equilibrium chemical potential μ_0 related to the Fermi-energies of the leads. Whenever the device presents available energy states in the transport window, such states are referred to as **transport channels**. Electron flow is obviously enhanced if we have a large number of such channels at disposition.

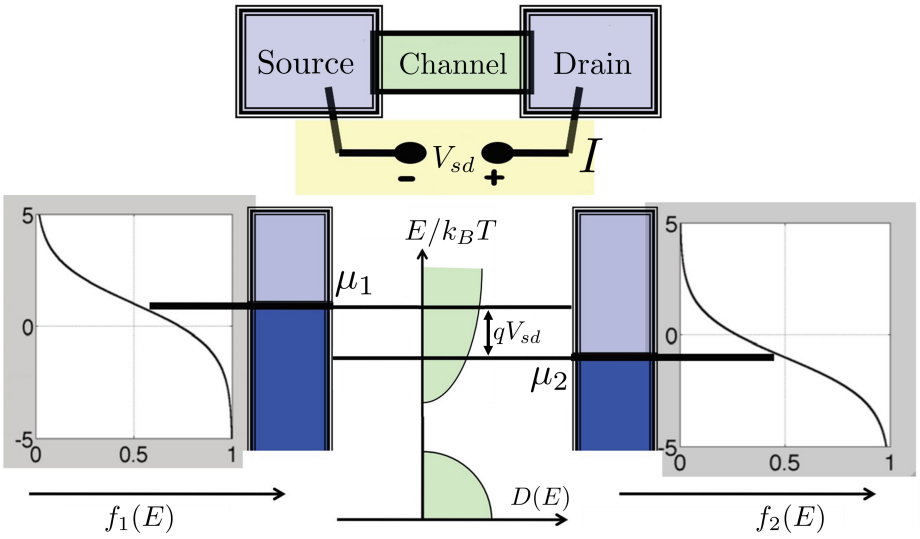

Figure 2.6: Two-terminal quantum transport set up: it consists of a source and drain (fermionic reservoirs or macroscopic nonmagnetic noninteracting metals) and a central region (channel) which could be a quantum dot structure or a bulk solid or any other quantum system susceptible to energy exchange.

The fundamental approach to this setup is widely attributed to physicist Rolf Landauer [110], whose deep physical ideas on the subject laid the foundation for understanding transport in nanoscale systems. Here we outline the fundamental ideas of his approach and provide a heuristic derivation of the Landauer current.

Based on experimental observations, Landauer began by assuming that the device behaved in a ballistic way: electrons entering the device do not give up energy to the surroundings and travel

smoothly through the channel. They change energy from one lead to the other but not inside the channel. In this picture, electron flow is taken care of by a nonzero difference between Fermi distributions and any entropy-driven process (steaming from the interaction with the reservoirs at certain temperatures) can be separated from the dynamics inside the device: from the perspective of the channels in the device, electrons are simply injected an ejected at different energies without changing their energies inside the channel. This is why Landauer referred to the device zone as the **scattering region**. Now, we assume a length L for the device and that plane waves with $+k(-k)$ momentum enter the scattering region from the left(right) lead: $\psi_{+k(-k)} = (1/\sqrt{L})e^{ikx}$ $(1/\sqrt{L}e^{-ikx})$. Despite the complicated nature of the interface between the leads and the device, experiments suggest that $+k(-k)$ states are primarily occupied by the left(right) leads with its Fermi distribution $f_{R(L)}$ [111]. The current injected from the leads is given by $I = \mathrm{Tr}(\hat{\vec{j}}\hat{\rho}_M)$, where the diagonal elements of the density matrix of the metals or contacts $\hat{\rho}_M$ are given by the Fermi distributions of the left and right leads and $\hat{\vec{j}} = (e/2)(\hat{n}\hat{\vec{v}} + \hat{\vec{v}}\hat{n})$ ($\hat{n}$ and $\hat{v}$ are the electron number and velocity operators). It can be shown that this operator applied to a wavefunction gives:

$$\vec{j}(\vec{r}) = \frac{ei\hbar}{2m}\left[\psi\left(\nabla\psi^*\right) - \psi^*(\nabla\psi)\right]. \tag{2.39}$$

We need to determine the $j_{+k(-k)}$ currents corresponding to states coming from the left(right) leads with wavefunction $\Psi_{+k(-k)}$. For simplicity, let's consider the case of a $1D$ ballistic device in the central region, the energies of incoming electron states are given by $\varepsilon_{+k} = \varepsilon_{-k} = h^2k^2/2m$. It follows that $j_{\pm k} = \pm\frac{e\hbar k}{mL}$ and then:

$$I = \mathrm{Tr}(\hat{\vec{j}}\hat{\rho}_M) = 2e\sum_{k>0}\left[j_{+k}f_{+k} + j_{-k}f_{-k}\right] = 2e\sum_{k\to 0}\frac{\hbar k}{mL}\left[f\left(\varepsilon_k - \mu_L\right) - f\left(\varepsilon_k - \mu_R\right)\right].$$

By letting $\sum_k \mapsto L/(2\pi)\int_0^\infty dk$ and $\hbar k/m = (1/\hbar)\partial\varepsilon_k/\partial k$ we obtain a simple expression known as the Landauer current formula for 1D ballistic devices:

$$I = \frac{2e}{h}\int d\varepsilon\left[f\left(\varepsilon - \mu_L\right) - f\left(\varepsilon - \mu_R\right)\right]. \tag{2.40}$$

We see how Eq.(2.40) naturally contains all previous relevant assumptions and fundamental features of the transport picture of Landauer; if $\mu_R = \mu_L = 0$, then $I = 0$, nmeaning no current flows through the device, and the system is in equilibrium. The current depends only on the difference between the Fermi functions, which reflects the imbalance of electron populations between the two reservoirs. This imbalance drives electrons to flow from the higher chemical potential to the lower one. The absence of additional terms indicates that electrons travel without scattering—maintaining coherence throughout the conductor. Thus, the flow is determined solely by the availability of electrons on either side and not hindered by resistive effects, which is the hallmark of ballistic transport. In general, a rigorous expression may be obtained for the Landauer current according to [111]:

$$I = \frac{2e}{\hbar}\int_0^\infty \mathrm{d}E\,\mathrm{Tr}\left(\hat{t}^\dagger\hat{t}\right)\left[f_{\mathrm{L}}(E) - f_{\mathrm{R}}(E)\right], \tag{2.41}$$

where it is customary to define the transmission function $T(E) = \mathrm{Tr}\left(\hat{t}^{\dagger}\hat{t}\right) = \sum_i T_i(E)$, where $\hat{t}$ is the transition operator in the non-diagonal elements of the scattering matrix operator $\hat{S}$ [111], and $T_i(E)$ are the transmission eigenvalues of the operator $\hat{t}^{\dagger}\hat{t}$ [10]. The transmission function accounts for scattering, imperfections, and resistive effects within the conductor. It modifies the Landauer current expression in Eq. (2.40) to reflect the probability that an electron at energy E successfully transmits through the device in a more realistic setup. The eigenvalues $T_i(E)$ are related to the transport channels in the scattering region (device). The value $|t_{mn}|^2$ gives the probability for an electron to transfer from channel n in lead L and transmit through the scattering region to channel m in lead R (t_{mn} are its matrix elements in some appropriate basis). If we assume a linear response regime (small bias voltage) we can rewrite the Fermi function difference as:

$$f_L(E) - f_R(E) \approx f(E) + \frac{\partial f}{\partial \mu}\mu_L - \left[f(E) + \frac{\partial f}{\partial \mu}\mu_R\right] \approx \frac{\partial f}{\partial \mu}\left(\mu_L - \mu_R\right) = \left(-\frac{\partial f}{\partial E}\right)\left(\mu_L - \mu_R\right),$$

and we can obtain an expression for the conductance [13, 40]:

$$G = \frac{I}{\left(\mu_L - \mu_R\right)/e} = \frac{2e^2}{h}\int dE \left(-\frac{\partial f}{\partial E}\right) T(E). \tag{2.42}$$

A relevant feature of Eq. (2.42) is the spread-out shape of the derivative of the Fermi function. It presents a resonance symmetric shape about the chemical potential and it multiplies the transmission function as shown in Figure 2.7. In linear response regime, the derivative determines the difference between the Fermi functions. It contributes to the conductance in the energy window defined by the chemical potential and the resonance's width $k_B T$. For energies centered at the transport channel characteristic energies (of the device), the conductance tends to develop a resonance structure with certain widths determined by the parameters of the system[11]. High temperature is detrimental to conductance since heat fluctuations increase scattering events in the scattering region and smear out transmission probabilities through the channels.

The amount $2e^2/\hbar$ in equation (2.42) is the quanta of conductance. A fundamental feature of the conductance of devices in two-terminal devices is the quantization of conductance for different values of an applied gate-voltage V_g that shifts the device's spectrum distribution. A beautiful experiment where this quantization is evidence can be found in Ref. [112] (see Figure 2.8). With this, we are now ready to build the interacting quantum dot system[12].

[10] Note how if the device is 1D ballistic device, the transmission probability approaches 1 and then $\sum_i T_i(E) = 1$, arriving at the result in Eq. (2.40)

[11] This is thoroughly discussed in section 4.3.1 and we can see this structure in Figure 2.10 of section 2.2.2.

[12] Several additional developments were considered in the theory of quantum transport all steaming from the Landauer approach. One such approach is the Jauho-Meir-Wingreen formalism for the current study in Ch. 3. For further reading, the reader is directed to

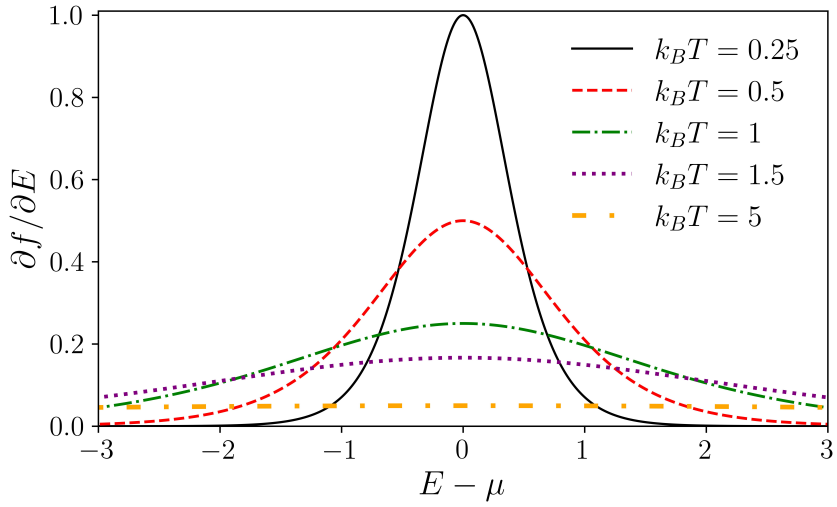

Figure 2.7: We observe $\partial f/\partial E$ vs $(E - \mu)$ for different values of k_BT. It is observed how higher temperatures smear out the resonance, thereby being detrimental to the conductance.

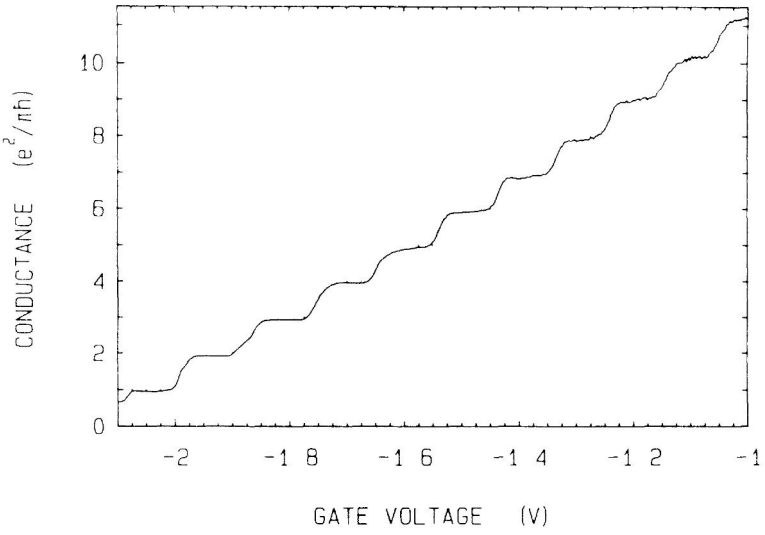

Figure 2.8: Conductance as a function of gate voltage in ballistic point contacts defined in the two-dimensional electron gas of a GaAs-AlGaAs heterostructure, with zero magnetic field [112].

2.2.1 The interacting quantum dot system

We are now ready to introduce the interacting quantum dot system (IQDS) Hamiltonian $\hat{H}_S(t) = \hat{H}_M(t) + \hat{H}_D(t) + \hat{H}_T(t)$ which consists of the Anderson model (which is the single-site Hubbard model + one fermionic reservoir) and an additional fermionic reservoir to build the typical two-terminal structure of quantum transport discussed in the previous section:

$$\hat{H}_M(t) = \sum_{k\sigma\alpha} \varepsilon_{k\alpha}(t)\hat{c}^{\dagger}_{k\alpha\sigma}\hat{c}_{k\alpha\sigma}, \quad \hat{H}_D(t) = \varepsilon_0(t)\sum_{\sigma}\hat{d}^{\dagger}_{\sigma}\hat{d}_{\sigma} + U\hat{n}_{\uparrow}\hat{n}_{\downarrow}, \quad \hat{H}_T(t) = \sum_{k\sigma\alpha} V_{k\alpha}(t)\hat{c}^{\dagger}_{k\alpha\sigma}\hat{d}_{\sigma} + h.c. \ , \tag{2.43}$$

where, $\alpha = R, L$ denotes the right and left fermionic reservoirs or metallic leads (in principle indistinguishable from each other), and the rest of the terms were previously defined. However, $\hat{H}_D$ now describes the localized discrete energy level of an artificial single-site quantum dot degenerated in spin with the intra-site Coulomb interaction U between electrons of opposite spin, characteristic of single-electron transistor devices [113]. Figure 2.9 depicts a schematic representation of the situation.

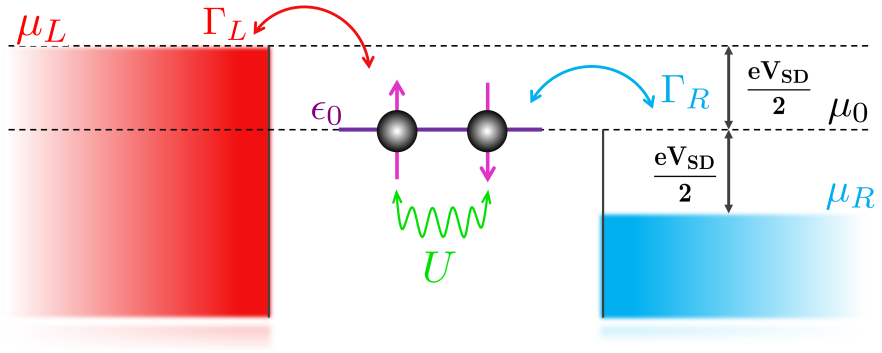

Figure 2.9: Schematic representation of the interacting quantum dot open system with a symmetric protocol of bias voltage application.

In Figure 2.9, each lead sustains a chemical potential μ_α, and the parameters Γ_α associated (see section 3.3) with the level broadening induced by the interaction of the discrete level with the continuum of the metallic leads. The application of a bias voltage $V_{SD} = \mu_L - \mu_R$ in a symmetric protocol set up typical of these systems [109] induces a non-equilibrium situation by shifting the chemical potential and differentiating the Fermi distribution functions of the leads, hence inducing charge transport in the system. The bias voltage is applied relative to the potential barrier between the quantum dot and the leads, so that $V_{sd} = 0 \rightarrow \mu_R = \mu_L = \mu_0 \approx \varepsilon_0 \approx \varepsilon_F$, where ε_{DF} is the Fermi energy of both leads. [72]. This voltage determines the transport window of the problem, effectively centered on the discrete energy level of the quantum dot.

2.2.2 The Coulomb blockade effect in QDs

As discussed in section 2.2, technological advances have made possible single-electron transport in nanostructures [113]. The ability to control electron flow one at a time in small devices makes it impossible to neglect electron correlations caused by the Coulomb interaction. The addition of electrons in structures with certain discrete energy levels (such as quantum dots) comes at an energetic cost determined by the Coulomb parameter U, which affects the conduction of electrons through the device and ultimately its quantum transport properties. This is the essence of the Coulomb blockade effect, relevant to the discussion of the IQDS.

To elucidate the Coulomb blockade effect, consider a multilevel quantum dot as a device under the application of a gate voltage $V_g(t)$ whose effect is to shift the energy spectrum in the device by an amount determined by eV_g:

$$\hat{H}_D(t) = \sum_{\alpha\sigma}(\varepsilon_\alpha + eV_g(t))\hat{d}^\dagger_{\alpha\sigma}\hat{d}_{\alpha\sigma} + U\sum_\alpha \hat{n}_{\alpha\uparrow}\hat{n}_{\alpha\downarrow}. \tag{2.44}$$

It is easy to see that the energy difference between having n and $n+1$ electrons in the dot states is given by $E(n+1) - E(n) = nU + \epsilon_{\lambda_n} - |e|V_g$, where λ_n denotes the associated single-particle state where we add the electron. Now, the levels at the quantum dot are filled by electrons sequentially as the energy state is lower to approach the Fermi energy of the leads due to the gate voltage. Clearly, at $|e|V_g = nU + \epsilon_{\lambda_n}$, the n-th level allows for a double occupation by becoming degenerate with the Fermi sea of the leads. Coherent tunneling of electrons to the quantum dot is more likely to occur at this point, giving rise to a periodic resonance structure of the conductance which ideally tends to reach a value near the quanta of conductance. We note how increasing temperature smears out the resonances and the structure is coherent with Eq. (2.42) according to the form of $\partial f/\partial E$ in Figure 2.7. Thus, the Coulomb blockade restricts the transmission of electrons to the quantum dot due to the unfavorable associated energy cost U of adding electrons to the levels of the quantum dot, until the cost is met through V_g.

We have constructed the system of interest for this work, described by the Hamiltonian (2.43) and depicted in Figure 2.9. We thoroughly discussed the physics of the fundamental Hubbard model, the connection between the Anderson and Kondo models, the concepts and ideas of single-electron transport, and the two-terminal transport setup, which are the main ingredients for the study of the IQDS. We are now ready to study the time-dependent nonequilibrium Green's functions approach to elucidate the relevant properties of the IQDS.

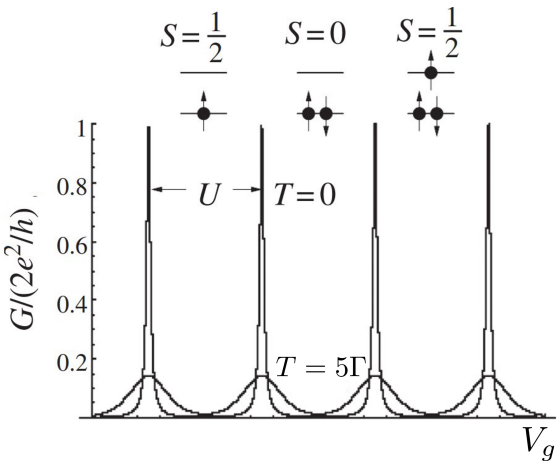

Figure 2.10: Behavior of the conductance as a function of the gate voltage in a quantum dot. The Coulomb blockade effects manifest in the zero conductance valleys for certain values of V_g, which is caused by the unmet energy cost U of adding an electron to the system. (Figure taken from [4])

3

Time-dependent nonequilibrium Green's functions for quantum transport

In this chapter, we establish the theoretical framework necessary to address the physical system introduced in the preceding chapter. Our primary tool in this endeavor is the time-dependent nonequilibrium Green's functions (TDNEGF). We provide a comprehensive explanation of TDNEGF and delve into their capabilities in accurately describing quantum transport phenomena in open systems. To commence, we present the rationale behind our choice of the TDNEGF approach and subsequently explore their definition in the Keldysh-Schwinger contour. This foundational understanding naturally leads us to the application of these objects within the context of the state-of-the-art general quantum transport setup. This application sets the stage for the utilization of the Jauho, Meir, and Wingreen formalism, crucial in studying the time-dependent response of the system when subjected to time-dependent external perturbations that drive the system far from equilibrium, particularly in terms of the produced physical charge current flowing through the system.

3.1 Why nonequilibrium Green's functions?

In the introductory chapter of this thesis, we placed an important emphasis on the intricacies of the analysis of quantum transport systems in the context of nanoscale devices such as molecular junctions or mesoscopic systems with complex materials, and we highlighted several theoretical approaches to time-resolved quantum transport, each with its constraints and limitations. Simulating the quantum dynamics of such devices, characterized by a complex interplay of strong correlations, non-equilibrium behavior, and external perturbations, is an intricate task. In principle, the solution of the time-dependent Schrödinger equation should be enough to describe the dynamical evolution of general quantum systems. However, in practice, the sheer number of equations makes this unattainable in the context of *ab initio* prescriptions (see DFT review by [114]),

even with the most powerful supercomputers available to this date. As mentioned earlier, this fact calls for new theoretical tools in the search for a practical yet complete description of many-body complex quantum systems. Fortunately, many experimentally observed properties involve only a few number of particles (such as densities and current), making it possible to evaluate these quantities from a reduced theoretical standpoint [10, 11].

The critical question is: What constitutes an appropriate reduced quantity for this purpose? The field of quantum transport has evolved, yielding various theoretical methodologies constructed around distinct reduced quantities, like the reduced single electron density matrix (RSDM) [115]. Our focus here is on one of the most versatile approaches: the time-dependent non-equilibrium Green's function (TDNEGF) formalism. NEGF stands out for its ability to treat multiple facets equally, including interparticle interactions, external perturbations, far-from-equilibrium scenarios, and arbitrary coupling to baths with an infinite amount of degrees of freedom. It provides transparent connections to other theoretical methods employed to simulate quantum transport, even reducing gracefully to established quantum transport formulae in limiting cases [5, 20].

The NEGF approach offers an ab initio method adaptable to various scenarios. It accommodates both bosonic and fermionic systems [116], regardless of dimensionality, perturbation strength, temperature, or transient versus stationary state by pertaining a hierarchical structure, inspired by Martin and Schwinger [64, 117], that governs the evolution of the Green's function, employing a self-energy kernel as an effective medium or scattering potential accounting for many-body effects [62]. The NEGF method aligns with macroscopic conservation laws, systematically truncating the hierarchy, which allows for a natural perturbative prescription of interactions. In its simplest form, the so-called Kadanoff–Baym equations govern the single-particle Green's function's motion and contain all many-body effects. The versatility of NEGF extends beyond quantum transport, encompassing diverse domains from photo-induced phenomena to quantum thermodynamics, among which several applications can be found [118–122]. Its capacity to seamlessly handle interactions, external perturbations, nonequilibrium dynamics, and arbitrary system-bath interactions in open systems, without imposing constraints on any of the aforementioned aspects, renders it ideal for our investigation.

In the following sections, together with appendices B and E, we delve deeper into the application of NEGF, unraveling the complexities of quantum transport and revealing the secrets concealed within nanoscale systems driven far from equilibrium.

3.1.1 Many and single-particle Green's functions

Green's functions are compelling tools and fundamental blocks of any quantum field theory [7] that emerge in several contexts in physics [14, 123]. However, in quantum mechanics, they can be seen as a time-ordered response to a certain physical event that dictates the probability amplitude for that event to happen. Imagine we are studying the transition from a certain initial quantum state to another which we call the final state. This transition occurs as a response to a certain event that produced the change in the quantum state, and according to the elementary rules of quantum

mechanics [124], the transition is associated with a certain transition probability amplitude that measures the probability of occurrence of the event. Green's functions naturally contain the causal and anti-causal information of such transition, thereby yielding the characteristic time and energy scales related to the transition processes in the physical system. To visualize these transitions, let us write:

$$|\Psi(t)\rangle = \hat{U}\left(t, t_0\right)|\Psi\left(t_0\right)\rangle \quad \rightarrow \quad \langle x \mid \psi, t\rangle = \int \mathrm{d}x' \langle x|T \exp\left[-\frac{i}{\hbar}\int_{t_0}^{t} dt' \hat{H}\left(t'\right)\right]|x'\rangle\langle x' \mid \psi, t_0\rangle,$$

$$\psi(x,t) = \int \mathrm{d}x' K\left(x,t,x',0\right)\psi\left(x',0\right), \tag{3.1}$$

where $\hat{U}(t,t_0)$ is the evolution operator in the Schrodinger picture of a certain system with Hamiltonian $\hat{H}(t)$ and we have a certain initial state $|\Psi\left(t_0\right)\rangle$ at time t_0 evolving to a final state $|\Psi\left(t\right)\rangle$ at time t. In equation (3.1), we then have the evolution process of the wave function. Note that

$$K\left(x,t,x',0\right) = \langle x|T \exp\left[-\frac{i}{\hbar}\int_{t_0}^{t} dt' \hat{H}\left(t'\right)\right]|x'\rangle = \langle x|\hat{U}(t,t_0)|x'\rangle = \langle x,t|x',t_0\rangle, \tag{3.2}$$

is the probability amplitude for the particle to go from a space-time point $(x', t = 0)$ (state $|\Psi, t = 0\rangle$) to (x,t) ($|\Psi, t\rangle$). We refer to $K\left(x,t,x',0\right)$ as a **transition amplitude**.

It can be shown [124] that this object is the solution response of the Schrodinger equation, such that

$$\left[-\left(\frac{\hbar^2}{2m}\right)\nabla''^2 + V\left(\mathbf{x}''\right) - i\hbar\frac{\partial}{\partial t}\right] K\left(\mathbf{x}'', t; \mathbf{x}', t_0\right) = -i\hbar\delta^3\left(\mathbf{x}'' - \mathbf{x}'\right)\delta\left(t - t_0\right), \tag{3.3}$$

where we can now see the transparent interpretation of K as a transition probability amplitude, or in the language of QFT, a one-particle propagator. Once there is a certain time-ordered in the time arguments of K, e.g., by allowing the event at time t to be a causal response of the initial one, i.e., by imposing $t > t_0$ we can define a sort of "causal" Green's functions as $G_{\mathrm{r}}\left(x,t,x',t_0\right) = K\left(x,t,x',t_0\right)\Theta(t - t_0)$.

In general, we define the many-body Green's function to describe state transitions of many-body systems as [4, 125]

$$G\left(1,2,\ldots n;1',2',\ldots n'\right) = (-i)^n \left\langle \phi \left| \mathcal{T}\psi(1)\psi(2)\cdots\psi(n)\psi^{\dagger}\left(n'\right)\cdots\psi^{\dagger}\left(1'\right)\right| \phi \right\rangle, \tag{3.4}$$

where we have a $n-$particle system undergoing a transition between a certain initial and final state, and we introduced a field operator $\hat{\psi}(N)$ for the particles in the Heisenberg picture, with the short-hand notation $N = (\mathbf{x}_N, t)$, so that $\hat{\psi}(N)$ $(\hat{\psi}^{\dagger}(N))$ annihilates (creates) a particle at position $\mathbf{x}_N$ and time t and an average over the ground state $|\phi\rangle$. The symbol $\mathcal{T}$ is the usual time-ordering operator of quantum mechanics: it orders products of operators such that the ones occurring later are placed to the left. For reasons that we explore in section 3.1.3, it turns out

that the dynamical (or static) content of any QFT theory is contained within the single-particle Green's function (SPGF) plus a many-body self-energy accounting for more than one-body effects. This provides a way to study the contents of general many-body correlators as those found in Eq. (3.4). We define the SPGF as:

$$\begin{aligned} G_{\alpha\alpha'}\left(\mathbf{x},t;\mathbf{x}',t'\right) &= -i\left\langle \mathcal{T}\hat{\psi}_{\alpha}(\mathbf{x},t)\hat{\psi}^{\dagger}_{\alpha'}\left(\mathbf{x}',t'\right)\right\rangle \\ &= -i\left\langle \hat{\psi}_{\alpha}(\mathbf{x},t)\hat{\psi}^{\dagger}_{\alpha'}\left(\mathbf{x}',t'\right)\right\rangle \Theta\left(t-t'\right) \mp i\left\langle \hat{\psi}^{\dagger}_{\alpha'}\left(\mathbf{x}',t'\right)\hat{\psi}_{\alpha}(\mathbf{x},t)\right\rangle \Theta\left(t'-t\right), \end{aligned} \tag{3.5}$$

where we can also have a spin degree of freedom denoted by α. Note how the SPGF contains both the causal ($t-t'>0$) and anti-causal ($t-t'<0$) response of the system. The $\pm$ symbol denotes the quantum statistical nature of the field operators: the $(-)$ sign for fermionic operators, and $(+)$ for bosonic operators.

Since Green's functions are strongly related to expectation values of products of field operators, and we can in principle build any observable using field operators, the determination of the SPGF provides a complete description of the system's relevant observables [8]. As a first example, we follow Ref. [4] to calculate the Green's function of a degenerate Fermi liquid of non-interacting fermions in its ground state. The details can be found in appendix A. We obtain:

$$G(\mathbf{k},\omega) = \frac{1}{\omega - \varepsilon_{\mathbf{k}} + i\delta_{\mathbf{k}}}. \tag{3.6}$$

We observe how Green's function contains the spectral information of the Fermi liquid at its poles given by $\varepsilon_{\mathbf{k}} = \omega - i\delta_{\mathbf{k}}$, where ω is the energy at which we calculate the GF, and $\delta_{\mathbf{k}} = \delta\,\mathrm{sgn}\left(k-k_F\right)$ with sgn() equal to one if its argument is positive, -1 if it is negative, and zero if it is zero, and δ is an infinitesimal real number serving as a convergence factor (see Appendix A). In the process of obtaining the GFs of the problem a Fourier transform from time to energy domain was applied. This procedure imposes a causal or anticausal structure on the GFs, manifested in the appearance of complex poles in either the lower or upper complex plane in the energy domain, depending on the sign of the imaginary part in the denominator of Eq. (3.6). As we explore in the next section, this has to do with the retarded and advanced components of the Green's functions in a time contour. Once we obtain the GF of the problem, we can use it to calculate any observable such as the particle density current (see appendix A).

An important aspect of GF theory is that it allows a natural transition to the most general nonequilibrium scenario in a quantum system, relevant to the context of quantum transport. For example, consider the case of statistical equilibrium. We start with the calculation of an observable such as

$$O = \langle \mathrm{GS}|\hat{\mathcal{O}}|\mathrm{GS}\rangle = \langle 0|\hat{U}_{-\infty,t}\hat{\mathcal{O}}\hat{U}_{t,-\infty}|0\rangle, \tag{3.7}$$

where $\hat{U}_{-\infty,t} = \hat{U}(t,-\infty)$. In the Schrodinger picture, we have $|\mathrm{GS}\rangle = \hat{U}_{t,-\infty}|0\rangle$, where $|GS\rangle$ is the ground state of an interacting zero temperature system (extension to finite temperature through the Matsubara formalism is possible [126]), $|0\rangle$ is the ground state of the non-interacting part. A

special trick is the equilibrium assumption that the evolution of the non-interacting ground state upon adiabatic switching on of the interactions and subsequent adiabatic switching them off brings the system back into the state $|0\rangle$, up to a phase factor e^{iL} [8]. Closely related to this assumption is the Gell-Mann-Low theorem [4]. Then $\hat{U}_{+\infty,-\infty}|0\rangle = e^{iL}|0\rangle$ and it follows that $e^{iL} = \langle 0|\hat{U}_{+\infty,-\infty}|0\rangle$ (upon imposing normalization for $|0\rangle$). With the previous considerations, we may write:

$$\begin{aligned}\langle \mathrm{GS}|\hat{\mathcal{O}}|\mathrm{GS}\rangle &= \langle 0|\hat{U}_{-\infty,t}\hat{\mathcal{O}}\hat{U}_{t,-\infty}|0\rangle = e^{-iL}\langle 0|e^{iL}\hat{U}_{-\infty,t}\hat{\mathcal{O}}\hat{U}_{t,-\infty}|0\rangle \\ &= e^{-iL}\langle 0|\hat{U}_{+\infty,-\infty}\hat{U}_{-\infty,t}\hat{\mathcal{O}}\hat{U}_{t,-\infty}|0\rangle = \frac{\langle 0|\hat{U}_{+\infty,t}\hat{\mathcal{O}}\hat{U}_{t,-\infty} \mid 0\rangle}{\langle 0|\hat{U}_{+\infty,-\infty}|0\rangle}.\end{aligned} \tag{3.8}$$

We then consider only the forward-time evolution with an additional cost of the denominator $\langle 0|\hat{U}_{+\infty,-\infty}|0\rangle$, relevant in the diagrammatic formulation of perturbation theory. In general, the equilibrium assumption fails, as we can not always bring the system to the same equilibrium state in the distant future when general external perturbation drives the system far from equilibrium. This calls for a better formulation of the theory in the search for computing expectation values.

In terms of the SPGF, we can derive eq. (3.8) following the same idea to obtain

$$iG\left(\mathbf{x},t;\mathbf{x}',t'\right) = \frac{\left\langle \Phi_0 \left| T\left[S(\infty,-\infty)\hat{\psi}(\mathbf{x},t)\hat{\psi}^{\dagger}\left(\mathbf{x}',t'\right)\right] \right| \Phi_0 \right\rangle}{\langle \Phi_0|S(\infty,-\infty)|\Phi_0\rangle}, \tag{3.9}$$

where S is the scattering matrix, typical of equilibrium perturbation theory [73] and defined by

$$S(\infty,-\infty) = T\exp\left(-i\int_{-\infty}^{\infty} dt_1 \hat{H}_I\left(t_1\right)\right), \tag{3.10}$$

where H_I is the interacting part (every non-quadratic term) of the Hamiltonian.

Following the tools of quantum statistical mechanics [127], expectation values are computed from the state operator $\hat{\rho}(t)$ of the system, such that

$$\langle\hat{\mathcal{O}}\rangle(t) \equiv \frac{\mathrm{Tr}\{\hat{\mathcal{O}}\hat{\rho}(t)\}}{\mathrm{Tr}\{\hat{\rho}(t)\}} = \frac{1}{\mathrm{Tr}\{\hat{\rho}(t)\}}\,\mathrm{Tr}\left\{\hat{U}_{-\infty,t}\hat{\mathcal{O}}\hat{U}_{t,-\infty}\hat{\rho}(-\infty)\right\}. \tag{3.11}$$

In the equation above, we wrote $\hat{\rho}$ in the Schrodinger picture and defined it as a known quantity in the distant past, where at time $t = -\infty$ the system's Hamiltonian was a noninteracting one. It could be, for instance, the equilibrium density matrix in the grand-canonical ensemble. Let us assume that interactions are adiabatically switched on and off before the application of an external time-dependent perturbation at time $t > 0$, where the system is driven out of equilibrium. In this general nonequilibrium scenario, eq. (3.11) defines a forward and backward evolution that can not be eliminated by using the aforementioned equilibrium assumption trick; the system is now in an unknown superposition of excited states once we evolve it according to $\hat{U}_{\infty,-\infty}$.

As it was noted by Keldysh in his seminal work [66], Eq. (3.11) defining the expectation value of the operator $\hat{\mathcal{O}}$ turns out to have a one-to-one correspondence between the forward and backward time evolutions, and the parametrization of the observable in a complex two-branch contour. This is the so-called Schwinger-Keldysh contour and it is the subject of the next subsection.

3.1.2 The Schwinger-Keldysh contour

The forward and backward evolution in the calculation of expectation values of observables is directly related to the parametrization of the expectation value in a complex two-branch contour, the Schwinger-Keldysh shown in the figure 3.1.

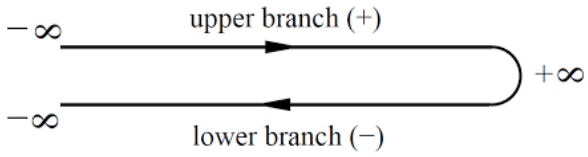

Figure 3.1: Keldysh Contour introduces two branches, where the upper branch is a progressive contour between times, and the lower branch is a regressive one (Figure from Ref. [8]).

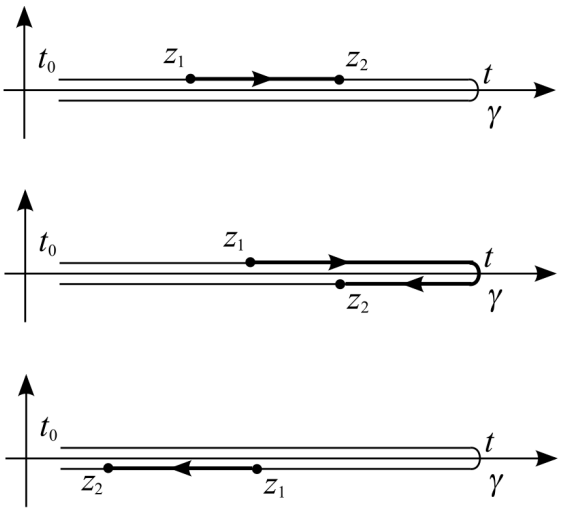

Figure 3.2: Different orders for arguments in the contour (Figure from Ref. [60]).

The contour is defined as $\gamma \equiv \underbrace{(t_0, t)}_{\gamma_+} \oplus \underbrace{(t, t_0)}_{\gamma_-}$ and we denote by $z' = t'_-$ the point of γ lying on the forward or upper branch γ_- with value t' and by $z' = t'_+$ the point of γ lying on the backwards or lower branch γ_+ with value t'. With this in mind, operators are defined in the contour according to

$$\hat{A}(z') \equiv \begin{cases} \hat{A}_+(t') & \text{if } z' = t'_+ \\ \hat{A}_-(t') & \text{if } z' = t'_- \end{cases}. \tag{3.12}$$

According to complex analysis, parametrization over the contour immediately sets an order of its arguments. Some ways in which arguments in the contour can be arranged are shown in figure 3.2. Points in the backward branch could have a smaller projection to the real-time axis (see third diagram) but they are still considered as being after any point in the forward branch. Analogous to the time-ordering operator, a contour-ordering operator can be defined such that

$$\mathcal{T}\left\{\hat{A}(z_1)\,\hat{B}(z_2)\right\} = \begin{cases} T\left\{\hat{A}_+(t_1)\,\hat{B}_+(t_2)\right\} & \text{if } z_1 = t_{1+} \text{ and } z_2 = t_{2+} \\ \hat{A}_-(t_1)\,\hat{B}_+(t_2) & \text{if } z_1 = t_{1-} \text{ and } z_2 = t_{2+} \\ \hat{B}_-(t_2)\,\hat{A}_+(t_1) & \text{if } z_1 = t_{1+} \text{ and } z_2 = t_{2-} \\ \bar{T}\left\{\hat{A}_-(t_1)\,\hat{B}_-(t_2)\right\} & \text{if } z_1 = t_{1-} \text{ and } z_2 = t_{2-} \end{cases}. \tag{3.13}$$

Using the Schwinger-Keldysh contour, different propagators can be defined according to how the first and second-time arguments are placed in the contour. Defined the contour-ordered Green's function as:

$$G_C(1,1') \equiv \begin{pmatrix} G_{11}(1,1') & G_{12}(1,1') \\ G_{21}(1,1') & G_{22}(1,1') \end{pmatrix}, \tag{3.14}$$

where the notation G_{12} indicates that the first time-argument is in the forward branch and the second in the backward branch. In this way, "i" as a subindex in the first position of G_{ij} indicates the position of the first argument in either the forward branch ($i = 1$) or the backward branch ($i = 2$), and j indicates the position of the second argument in one of the branches ($j = 1, 2$ as well). Changing a bit the notation, we can define

$$G_{11}(1,1') = G(1,1') = -i\left\langle \mathcal{T}\left(\psi(1)\psi^{\dagger}(1')\right)\right\rangle, \tag{3.15}$$

as the causal or time-ordered GF,

$$G_{22}(1,1') = \tilde{G}(1,1') = -i\left\langle \tilde{\mathcal{T}}\left(\psi(1)\psi^{\dagger}(1')\right)\right\rangle, \tag{3.16}$$

as the anti-causal or anti-ordered GF ($\tilde{\mathcal{T}}$ orders products of operators in increasing times, opposite to $\mathcal{T}$),

$$G_{21}(1,1') = G^{>}(1,1') = -i\left\langle \psi(1)\psi^{\dagger}(1')\right\rangle, \tag{3.17}$$

as the greater GF (as obviously $1' > 1$), and

$$G_{12}(1,1') = G^{<}(1,1') = \mp i\left\langle \psi^{\dagger}(1')\,\psi(1)\right\rangle, \tag{3.18}$$

as the lesser GF. Keldysh noted that the four GFs defined in the complex contour were redundant, as it can be easily shown that

$$0 = G_{11}(1,1') - G_{12}(1,1') - G_{21}(1,1') + G_{22}(1,1'). \tag{3.19}$$

In this way, there is one linearly dependent and redundant propagator. By applying the transformation $G_C \to LG_CL^{\dagger}$ with

$$L = \frac{1}{\sqrt{2}}\begin{pmatrix} 1 & -1 \\ 1 & 1 \end{pmatrix}, \tag{3.20}$$

which we refer to as Keldysh rotation, we can construct the following tridiagonal matrix in Keldysh space for the contour-ordered GFs:

$$\begin{pmatrix} G & G^{<} \\ G^{>} & \hat{\tilde{G}} \end{pmatrix} \to \begin{pmatrix} 0 & G^{\mathrm{A}} \\ G^{\mathrm{R}} & G^{\mathrm{K}} \end{pmatrix}, \tag{3.21}$$

where we define the retarded (advanced) Green's function $G^{R(A)}$ and the Keldysh Green's function G^{K} such that:

$$G^{R(A)} = \theta(\pm(t-t'))(G^{>(<)} - G^{<(>)}), \tag{3.22}$$

$$G^K = G^> + G^<. \tag{3.23}$$

In the scope of this thesis, we will not have to deal with G^K, which is related to the equilibrium limit of the theory at hand as it provides a natural regularization in the path integral formulation of nonequilibrium theories [8]. Note that $G^R = (G^A)^\dagger$ and $[G^{<(>)}]^\dagger = -G^{<(>)}$. A beautiful feature of the theory is noted here, as we only need the retarded (advanced) and lesser (greater) Green's functions for a complete description of the nonequilibrium dynamics.

When dealing with contour-ordered GFs, it is desirable to project to the real-time axis to do calculations. The final projected form of propagators in the real-time axis is referred to as real-time formalism. The key ingredient for this is the set of rules developed by Langreth and Wilkins [128] (see Appendix B for details). In general, we encounter contour-ordered objects of the form

$$C\left(z_1, z_{1'}\right) = \int_\gamma d\tau \; A\left(z_1, \tau\right) B\left(\tau, z_{1'}\right), \tag{3.24}$$

and when projecting these objects onto the real-time axis, results from the application of Langreth's rules lead to:

$$C^R\left(t, t'\right) = \int_{-\infty}^{\infty} A^R\left(t, \tau\right) B^R\left(\tau, t'\right) d\tau, \quad \hat{c}^<\left(t, t'\right) = \int_{-\infty}^{\infty} \left[A^R\left(t, \tau\right) B^<\left(\tau, t'\right) + A^<\left(t, \tau\right) B^A\left(\tau, t'\right)\right] d\tau. \tag{3.25}$$

As a note about notation, double subindices are employed to describe contour-ordered Green's functions with complex arguments in Keldysh contour as opposed to real-time Green's functions with real arguments. As we can always translate from a complex Keldysh argument to real-time arguments as noted in the definition in (3.12) and from the above discussion, we drop the messy contour notation from now on and stick to real arguments. With this freedom, subindices may be used to describe the expectation values of operators living in similar or different subspaces of the total Hilbert space (see Eq. (3.27) in the next section).

3.1.3 Many-body perturbation theory

Many-body perturbation theory (MBPT) provides an excellent methodology for unraveling many-body correlation effects in quantum transport phenomena. It can be entirely deduced in the language of the NEGF formalism. Here, we outline the procedure of MBPT; additional details can be found in appendix C. Analogous to the BBGKY hierarchy in classical statistical mechanics [78], Martin and Schwinger developed a hierarchy for the Green's function propagators [64], starting from the contour-ordered SPGF: $G\left(1, 1'\right) = -\mathrm{i}\left\langle \mathrm{T}_\gamma\left[\hat{\psi}_{\mathrm{H}}(1)\hat{\psi}^\dagger_{\mathrm{H}}\left(1'\right)\right]\right\rangle$. This process constitutes an infinite hierarchy in terms of higher-order propagators. The solution to the hierarchy is the Dyson equation

$$G\left(1, 1'\right) = G_0\left(1, 1'\right) + \int \mathrm{d}\overline{1}\; \mathrm{d}\overline{2} G_0(1, \overline{1})\Sigma_{\mathrm{MB}}(\overline{1}, \overline{2})G\left(\overline{2}, 1'\right), \tag{3.26}$$

where the term Σ_{MB} is the many-body self-energy functional containing all many-body effects from the interacting part of the quantum theory. We do not employ a double subindex notation here

as we are not referring to time arguments ordered in Keldysh contour. Systematic construction of the infinite terms in the self-energy functional in terms of Feynman diagrams leads to the regular MBPT formulation of quantum field theories [129]. Among many approximations for the self-energy [74], the second-order expansion for electron-electron interactions constitutes the important second Born self-energy, whose equation and Feynman diagram representation can be found in appendix C.

Another way to visualize the origin of higher-order terms leading to different many-body effects in the self-energy functional is by differentiating the SPGF in its different components. We can also use the resulting self-consistent differential equations with a suitable approximation for the interacting terms to attempt to close the system of equations. This process is referred to as the **equation of motion method**. For example, for the retarded component in Eq. (3.22) we obtain

$$\frac{\partial}{\partial t}G^R_{\alpha\beta}(t-t') = -i\langle\left[[\hat{H},\hat{\psi}_\alpha(t)],\hat{\psi}^\dagger_\beta(t')\right]\rangle - i\langle[\hat{\psi}^\dagger_\alpha(t),\hat{\psi}^\dagger_\beta(t')]\rangle\delta(t-t'), \tag{3.27}$$

where the double subindex $\alpha\beta$ implies that the expectation value underlying the Green's function definition is taken between operators belonging to equal or different subspaces of the total Hilbert space, such as $\hat{\psi}_\alpha(t)$ or $\hat{\psi}_\beta(t)$. The relevant part is the commutator $[\hat{H},\hat{\psi}_\alpha(t)]$, responsible for the emergence of higher-order propagators. Any self-energy approximation of electron correlation effects should lead to an equivalent ruling out of terms in this commutator. In this thesis, we focus on the mean-field Hubbard-I approximation (HIA) to the e-e interactions, which consists of neglecting fluctuations (influence of strong external fields or high temperatures), opposite-spin correlations in the leads, and all other higher-order terms are approximated at the Hartree-Fock level [13, 76, 91, 95, 130]. Thus, we close the system of equations for the Green's function components of the quantum dot system (section 4.1). This approximation scheme is equivalent to neglecting all terms without coinciding quantum numbers for at least two fermionic operators in the commutator of the Hubbard term. The non-canonical aspect and further details of the HIA are explained in chapter 4.

3.2 Theoretical open systems aspects of the IQDS

The realization of quantum transport models involves an open system paradigm. Quantum systems must be regarded as open systems when treating any realistic system subjected to coupling to an uncontrollable environment that influences it in a non-negligible way, e.g., in the measurement process. In quantum transport setups, we often deal with an environment (heat baths) in which the system of interest exchanges energy and particles, as depicted in figure 3.3. Each part of the total system is described by its own density matrix, where the total density matrix $\hat{\rho}_T(t) = \hat{\rho}_S(t)\otimes\hat{\rho}_B(t)$ evolves unitarily according to the Von-Neumann equation, where $\hat{\rho}_S(t)$ is the density matrix for the central region, and $\hat{\rho}_B(t)$ the density matrix for the baths or full environment. However, our interest lies in the reduced dynamics of the system described by $\hat{\rho}_S(t)$, and usual procedures in the theory of open system involve tracing over the bath degrees of freedom [131]. Something

worth mentioning is the fact that the reduced single electron density matrix often denoted by $\sigma(t)$, defined as the expectation value of single-particle operators of the underlying field theory is intimately connected with the SPGF through the straightforward relation $\sigma(t) = -iG^<(t,t)$. This connects the TDNEGF theory with the theory of open quantum systems from master equation approaches [131]. In this section, we discuss some general aspects of transport in the context of open systems. See appendix D for additional details.

We start from a system such as the one in Figure 3.3, consisting of a metallic junction with a multilevel central device. This region, in turn, is coupled locally with the metallic reservoirs: only at the boundary of the reservoirs and the central device do we perceive hybridization allowing tunneling processes. Crucially, the interacting quantum dot system (IQDS) resembles such a boundary-driven configuration (see section 2.2.1). Recalling the Hamiltonian in Eq. (2.43), the metallic leads are given by:

$$\hat{H}_M = \sum_{k\alpha\sigma} \varepsilon_{k\alpha\sigma}(t)\hat{c}^\dagger_{k\alpha\sigma}\hat{c}_{k\alpha\sigma}, \tag{3.28}$$

where $\alpha = L, R$ for the left and right leads respectively, and $\varepsilon_{k\alpha\sigma}(t) = \varepsilon^0_{k\alpha\sigma} + \Delta_\alpha(t)$, $\varepsilon^0_{k\alpha}$ is the band structure of the leads and $\Delta_\alpha(t)$ shifts the energy levels due to a time-dependent applied voltage. In a real situation, this applied voltage is established in the tunneling structure by accumulation and charge depletion near the lead-system interface's barrier [72]. For the case of a multilevel system with spin-dependent parameters (a straightforward generalization of the IQDS of section 2.2.1), the coupling Hamiltonian also assumes time-dependent parameters, such that the precise form of the time dependence is determined by the geometry and by the self-consistent response of charge produced by the external driving. It is given by

$$\hat{H}_T = \sum_{k\alpha m\sigma} V_{k\alpha m\sigma}(t)\hat{c}^\dagger_{k\alpha\sigma}\hat{d}_{m\sigma} + h.c.\ . \tag{3.29}$$

Here, the central region can be modeled by non-interacting time-dependent energy levels

$$\hat{H}_D = \sum_{m\sigma} \varepsilon_{m\sigma}(t)\hat{d}^\dagger_{m\sigma}\hat{d}_{m\sigma} + \sum_m U_m \hat{n}_{m\uparrow}\hat{n}_{m\downarrow}, \tag{3.30}$$

where the $\hat{d}^\dagger_{m\sigma}(\hat{d}_{m\sigma})$ creates(annihilates) an electron in the energy level m (with a total of M levels), and $\varepsilon_{m\sigma}(t)$ has a time-dependence produced by the application of some time-dependent bias voltage shifting the levels of the system (we refer to the voltage affecting the levels as the gate voltage), and we have several Coulumb integrals U_m for the on-site interaction at each energy level.

We now outline the most important aspect of the system in Figure 3.3: *the embedding approach* (Further details and notation specifications can be found in appendix D). Consider that by choosing a single particle basis, we can divide the matrix representation of the total Hamiltonian by sub-system blocks [67, 75] for each part of the system. We write the matrix representation of operators such that $\hat{H}_D \to (\mathbf{H}_D)_{ij} = \langle i,\sigma|\hat{H}_D|j,\sigma\rangle$, where $|i,\sigma\rangle$ is a ket state of the basis. Using

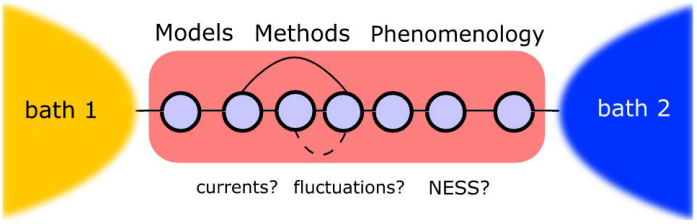

Figure 3.3: Quantum transport setup of interest as a boundary-driven system: the central device D couples locally to the leads at their boundaries in a junction-like setup for transport in nanodevices.

this representation for Green's function and Hamiltonians, it is possible to write an EOM in the Schwinger-Keldysh contour for the Green's function $\mathbf{G}_D$ of the device only, such that[1]:

$$\Big[i\partial_z \mathbf{1} - \mathbf{H}_D(z)\Big]\mathbf{G}_D\left(z,z'\right) = \delta\left(z,z'\right)\mathbf{1} + \int d\bar{z}\ \mathbf{\Sigma}_D(z,\bar{z})\mathbf{G}_D\left(\bar{z},z'\right), \tag{3.31}$$

where the full many-body self-energy $\mathbf{\Sigma}_D = \mathbf{\Sigma}_{\text{em}} + \mathbf{\Sigma}_{\text{MB},D}$: the many-body self-energy $\mathbf{\Sigma}_{\text{MB,D}}$ contains any interactions coming from the device degrees of freedom only. The information regarding the influence of the leads on the system is physically contained in the embedding self-energy $\mathbf{\Sigma}_{\text{em}}$ (written in terms of the leads GFs and the tunneling amplitudes $V_{\alpha\mu m}$) for which is very customary to apply the Wide-Band Limit (WBL) that captures the main physics in the macroscopic lead-central device interplay. This approximation neglects the exact form of the leads' density of states making the coupling constants $V_{\alpha\mu i}(t,\varepsilon)$ time-independent and the energy shift (real part of the embedding self-energy) zero, as we see in the next section. Note how this beautiful approach exposes the open system character of our model in a natural way from the Green's function structure. In particular, the fermionic leads constitute the dissipative environment of our problem.

3.3 Building the Jauho, Meir & Wingreen formalism

In this section, we build the general Jauho, Meir, and Wingreen (JMW) charge current formalism for giving the fundamentals of the quantum transport in our systems [72]. The idea is to study the change in the properties of each part of the system. We start from the Hamiltonian model $\hat{H}_S(t) = \hat{H}_M(t) + \hat{H}_T(t) + \hat{H}_D(t)$ with each term given by equations (3.28), (3.29), and (3.30). For the present case, we want to study the time evolution of the particle number in one of the leads, as this is closely related to the charge current. The number operator is given by

$$\hat{N} = \sum_{\alpha\sigma}\int \psi^\dagger_\sigma(r)\psi_\sigma(r)d^3r = \sum_{k\alpha\sigma}\hat{c}^\dagger_{k\alpha\sigma}\hat{c}_{k\alpha\sigma},$$

[1]The bold notation is employed to reference the different subsystem, as shown in Eq. D.3

and the charge current operator is defined in terms of the derivate of the particle number of one of the leads $\hat{J}_e = -e\frac{d\hat{N}}{dt}$. The mean value of this expression can be written in the following form:

$$J_e = -e\Big\langle \frac{d\hat{N}}{dt}\Big\rangle = -\frac{ie}{\hbar}\langle[\hat{H}_S, \hat{N}]\rangle = -\frac{ie}{\hbar}\langle[\hat{H}_S, \sum_{k\alpha\sigma}\hat{c}^\dagger_{k\alpha\sigma}\hat{c}_{k\alpha\sigma}]\rangle. \tag{3.32}$$

It is easy to deduce that the particle number operator is a conserved quantity in the non-coupled system. Using that fact, we can write:

$$\begin{aligned}
[\hat{H}_M + \hat{H}_D + \hat{H}_T, \hat{N}] &= [\hat{H}_T, \hat{N}] \\
&= \Big[\sum_{k\alpha m\sigma} V_{k\alpha m\sigma}(t)\hat{c}^\dagger_{\alpha k\sigma}\hat{d}_{m\sigma} + h.c, \sum_{p\alpha\sigma'}\hat{c}^\dagger_{p\alpha\sigma'}\hat{c}_{p\alpha\sigma'}\Big] \\
&= \sum_{pk\alpha\sigma\sigma'}\Big(V_{k\alpha m\sigma}[\hat{c}^\dagger_{\alpha k\sigma}\hat{d}_{m\sigma}, \hat{c}^\dagger_{p\alpha\sigma'}\hat{c}_{p\alpha\sigma'}] + V^*_{k\alpha m\sigma}[\hat{d}^\dagger_{m\sigma}\hat{c}_{k\alpha\sigma}, \hat{c}^\dagger_{p\alpha\sigma'}\hat{c}_{p\alpha\sigma'}]\Big) \\
&= \sum_{k\alpha m\sigma}\Big(-V_{k\alpha m\sigma}\hat{c}^\dagger_{k\alpha\sigma}\hat{d}_{m\sigma} + V^*_{k\alpha m\sigma}\hat{d}^\dagger_{m\sigma}\hat{c}_{k\alpha\sigma}\Big).
\end{aligned} \tag{3.33}$$

Now we go back to Eq. (3.32) to get:

$$J_e = -\frac{ie}{\hbar}\sum_{k\alpha m\sigma}\Big\langle -V_{k\alpha m\sigma}\hat{c}^\dagger_{k\alpha\sigma}\hat{d}_{m\sigma} + V^*_{k\alpha m\sigma}\hat{d}^\dagger_{m\sigma}\hat{c}_{k\alpha\sigma}\Big| -V_{k\alpha m\sigma}\hat{c}^\dagger_{k\alpha\sigma}\hat{d}_{m\sigma} + V^*_{k\alpha m\sigma}\hat{d}^\dagger_{m\sigma}\hat{c}_{k\alpha\sigma}\Big\rangle \tag{3.34}$$

$$= e\sum_{k\alpha m\sigma} V_{k\alpha m\sigma}\underbrace{\frac{i}{\hbar}\Big\langle \hat{c}^\dagger_{k\alpha\sigma}\hat{d}_{m\sigma}\Big|\hat{c}^\dagger_{k\alpha\sigma}\hat{d}_{m\sigma}\Big\rangle}_{G^<_{k\sigma,m\sigma}} - V^*_{k\alpha m\sigma}\underbrace{\frac{i}{\hbar}\Big\langle \hat{d}^\dagger_{m\sigma}\hat{c}_{k\alpha\sigma}\Big|\hat{d}^\dagger_{m\sigma}\hat{c}_{k\alpha\sigma}\Big\rangle}_{G^<_{m\sigma,k\sigma}}, \tag{3.35}$$

where we have introduced the lesser hybrid GFs $G^<_{k\sigma,m\sigma}$. With the property $G^< = -[G^<]^\dagger$, we get (Re() denotes the real part of the argument):

$$J_e = 2e\sum_{k\alpha\sigma m}\mathrm{Re}(V_{k\alpha m\sigma}(t)G^<_{m\sigma,k\sigma}(t,t')). \tag{3.36}$$

Next, we try to find an expression for the hybrid GFs in terms of the individual Green's functions of the leads and the system. For this purpose, it is useful to find the equation of motion of the Greens functions and to use Langreth rules. Let's proceed with the former first:

$$\begin{aligned}
\frac{dG_{m\sigma(t,t')}}{dt'} &= \frac{d}{dt'}\left(-\frac{i}{\hbar}\Big\langle \hat{d}_{m\sigma}(t)\hat{c}^\dagger_{k\alpha\sigma}\Big\rangle\theta(t-t') + \frac{i}{\hbar}\Big\langle \hat{c}^\dagger_{k\alpha\sigma}(t')\,\hat{d}_{m\sigma}(t)\Big\rangle\theta(t'-t)\right) \\
&= -\frac{i}{\hbar}\left\langle T\hat{d}_{m\sigma}(t)\frac{\partial\hat{c}^\dagger_{k\alpha\sigma}(t')}{dt'}\right\rangle + \frac{i}{\hbar}\Big\langle\Big\{\hat{d}_{m\sigma}(t), \hat{c}^\dagger_{k\alpha\sigma}(t)\Big\}\Big\rangle\delta(t-t') \\
&= -\frac{i}{\hbar}\Big\langle T\hat{d}_{m\sigma}(t)\Big[\hat{c}^\dagger_{k\alpha\sigma}, \hat{H}\Big]\Big\rangle.
\end{aligned} \tag{3.37}$$

The commutator $[\hat{c}_{k\alpha\sigma}, \hat{H}]$ is given by

$$\begin{aligned}
[\hat{c}_{k\alpha\sigma}, \hat{H}_S] &= [\hat{c}_{k\alpha\sigma}, \hat{H}_M + \hat{H}_T] && (3.38)\\
&= [\hat{c}^\dagger_{k\alpha\sigma}, \sum_{q\alpha\sigma} \varepsilon_{q\alpha\sigma'} \hat{c}^\dagger_{q\alpha\sigma'} \hat{c}_{q\alpha\sigma'}] + [\hat{c}^\dagger_{k\alpha\sigma}, \sum_{q\alpha\sigma' m} V^*_{q\alpha\sigma' m} \hat{d}^\dagger_{m\sigma'} \hat{c}_{q\alpha\sigma'}] && (3.39)\\
&= -\varepsilon_{k\alpha\sigma} \hat{c}^\dagger_{k\alpha\sigma} - \sum_{\alpha m'} V^*_{k\alpha\sigma m'} \hat{d}^\dagger_{m'\sigma}. && (3.40)
\end{aligned}$$

Then, replacing in the equation of motion we obtain

$$i\hbar \frac{dG_{m\sigma,k\sigma(t,t')}}{dt'} = -\varepsilon_{k\alpha\sigma} \underbrace{\left(-\frac{i}{\hbar}\left\langle T\hat{d}_{m\sigma}(t)\hat{c}^\dagger_{k\alpha\sigma}(t')\right\rangle\right)}_{G_{m\sigma,k\sigma}(t,t')} - \sum_{\alpha m'} V_{k\alpha\sigma m'} \underbrace{\left(-\frac{i}{\hbar}\left\langle T\hat{d}_{m\sigma}(t)\hat{d}^\dagger_{m'\sigma}(t')\right\rangle\right)}_{G_{mm'\sigma}(t,t')}, \quad (3.41)$$

$$\underbrace{\left(-i\hbar\frac{\partial}{\partial t} - \varepsilon_{k\alpha\sigma}\right)}_{\mathcal{D}} G_{m\sigma,k\sigma}(t,t') = \sum_{\alpha n} V^*_{k\alpha\sigma n} G_{mn\sigma}(t,t'). \quad (3.42)$$

The bare green function of the lead is given by $\mathcal{G}_{k\alpha\sigma}(t,t') = -\frac{i}{\hbar}\langle T\hat{c}_{k\alpha\sigma}(t)\hat{c}^\dagger_{k\alpha\sigma}(t')\rangle$ and it satisfies $\mathcal{D}\mathcal{G}_{k\alpha\sigma}(t,t') = \delta(t,t')$, where $\mathcal{D} = (i\hbar\frac{\partial}{\partial t} - \epsilon_{k\alpha\sigma})$ denotes a differential operator which is the inverse of the bare Green's function in Fourier space. Similar to the embedding approach section, by multiplying the equation of motion by $\mathcal{G}_{k\alpha\sigma}(\tau,t')$ and integrating for τ, we obtain

$$\begin{aligned}
\underbrace{\int \overbrace{d\tau \mathcal{G}_{k\alpha\sigma}(\tau,t')\mathcal{D}}^{\delta(\tau-t')} G_{m\sigma,k\sigma}(t,\tau)}_{G_{m\sigma,k\sigma}(t,t')} &= \sum_n \int d\tau V^*_{k\alpha\sigma n}(\tau) G_{mn\sigma}(t,\tau)\mathcal{G}_{k\alpha\sigma}(\tau,t') && (3.43)\\
G_{m\sigma,k\sigma}(t,t') &= \sum_n \int d\tau V^*_{k\alpha\sigma n} G_{mn\sigma}(t,\tau)\mathcal{G}_{k\alpha\sigma}(\tau,t'), && (3.44)
\end{aligned}$$

where in the first line, we have used the integration by parts to make $\mathcal{D}$ act on $\mathcal{G}$, and used the fact that $\mathcal{G}$ satisfies the bare equation of motion. Now we apply the Langreth rules to the last term and we obtain $G^<$ in terms of the individual Green's function in the Keldysh contour, i.e.:

$$G^<_{m\sigma,k\sigma}(t,t') = \sum_n \int d\tau V^*_{k\alpha\sigma n}\Big(G^R_{mn\sigma}(t,\tau)\mathcal{G}^<_{k\alpha\sigma} + G^<_{mn\sigma}(t,\tau)\mathcal{G}^A_{k\alpha\sigma}(\tau,t')\Big). \quad (3.45)$$

Before going back to eq. (3.36), let's find the form of the retarded and advanced bare Green's functions for the leads. Using the Heisenberg equation of motion is easy to see that the explicit dependence of the time for the operators takes into account a phase that includes the time dependence of the band structure, that is:

$$\hat{c}_{k\alpha\sigma}(t) = \hat{c}_{k\alpha\sigma} e^{-\frac{i}{\hbar}\int_{-\infty}^{t} \varepsilon_{k\alpha\sigma}(\tau)d\tau}, \quad \text{and} \quad \hat{c}^\dagger_{k\alpha\sigma}(t') = \hat{c}^\dagger_{k\alpha\sigma} e^{\frac{i}{\hbar}\int_{\infty}^{t'} \varepsilon_{k\alpha\sigma}(\tau)d\tau}. \quad (3.46)$$

Using these expressions, we can write

$$\begin{aligned}\mathcal{G}^R_{k\alpha\sigma}(t,t') &= -\frac{i}{\hbar}\theta(t-t')\left\langle\left\{\hat{c}_{k\alpha\sigma}(t),\hat{c}^\dagger_{k\alpha\sigma}(t')\right\}\right\rangle = -\frac{i}{\hbar}\theta(t-t')\,e^{-\frac{i}{\hbar}\int_{t'}^{t}\varepsilon_{k\alpha\sigma}(\tau)d\tau}\left\langle\left\{\hat{c}_{k\alpha\sigma},\hat{c}^\dagger_{k\alpha\sigma}\right\}\right\rangle \\ &= -\frac{i}{\hbar}\theta(t-t')\,e^{-\frac{i}{\hbar}\int_{t'}^{t}\varepsilon_{k\alpha\sigma}(\tau)d\tau},\end{aligned} \tag{3.47}$$

for the advanced green function, we have

$$\begin{aligned}\mathcal{G}^A_{k\alpha\sigma}(t,t') &= \frac{i}{\hbar}\theta(t'-t)\left\langle\left\{\hat{c}_{k\alpha\sigma}(t),\hat{c}^\dagger_{k\alpha\sigma}(t')\right\}\right\rangle = \frac{i}{\hbar}\theta(t'-t)\,e^{-\frac{i}{\hbar}\int_{t'}^{t}\varepsilon_{k\alpha\sigma}(\tau)d\tau}\left\{\hat{c}_{k\alpha\sigma},\hat{c}^\dagger_{k\alpha\sigma}\right\} \\ &= \frac{i}{\hbar}\theta(t'-t)\,e^{-\frac{i}{\hbar}\int_{t'}^{t}\varepsilon_{k\alpha\sigma}(\tau)d\tau},\end{aligned} \tag{3.48}$$

and for $\mathcal{G}^<_{k\alpha\sigma}(t,t')$, we obtain

$$\begin{aligned}\mathcal{G}^<_{k\alpha\sigma}(t,t') &= \frac{i}{\hbar}\left\langle\hat{c}^\dagger_{k\alpha\sigma}(t')\,\hat{c}_{k\alpha\sigma}(t)\right\rangle = \frac{i}{\hbar}e^{-\frac{i}{\hbar}\int_{t'}^{t}\varepsilon_{k\alpha\sigma}(\tau)d\tau}\left\langle\hat{c}^\dagger_{k\alpha\sigma}\hat{c}_{k\alpha\sigma}\right\rangle \\ &= \frac{i}{\hbar}e^{-\frac{i}{\hbar}\int_{t'}^{t}\varepsilon_{k\alpha\sigma}(\tau)d\tau}f\left(\varepsilon^0_{k\alpha\sigma}\right),\end{aligned} \tag{3.49}$$

where $\varepsilon^0_{k\alpha\sigma}$ denotes the constant part of the time-dependent energy bands $\varepsilon_{k\alpha\sigma}(t) = \varepsilon^0_{k\alpha\sigma} + \Delta_\alpha(t)$. We can finally go back to eq. (3.36) to write

$$\begin{aligned}J_e &= 2e\sum_{k\sigma mn}\int d\tau Re\Bigg(V_{k\alpha m\sigma}(t)V^*_{k\alpha\sigma n}(\tau)\Big(G^R_{mn\sigma}(t,\tau)\frac{i}{\hbar}(t,t')f(\varepsilon^0_{k\alpha\sigma})e^{-\frac{i}{\hbar}\int_t^\tau\varepsilon_{k\alpha\sigma}(\tau')d\tau'} \\ &+ G^<_{mn\sigma}(t,\tau)\frac{i}{\hbar}\theta(t'-t)e^{-\frac{i}{\hbar}\int_t^\tau\varepsilon_{k\alpha\sigma}(\tau')d\tau'}\Big)\Bigg) \\ &= -\frac{2e}{\hbar}\sum_{k\sigma mn}\mathrm{Im}\int_{-\infty}^{t}d\tau V_{k\alpha m\sigma}(t)V^*_{k\alpha\sigma n}(\tau)e^{-\frac{i}{\hbar}\int_\tau^t\Delta_\alpha(\tau)d\tau'}e^{-\frac{i}{\hbar}\varepsilon_{k\alpha\sigma}(\tau-t)}\Big(G^R_{mn\sigma}(t,\tau)f(\varepsilon^0_{k\alpha\sigma})+G^<_{mn\sigma}(t,\tau)\Big),\end{aligned}$$

where in the second expression we have factorized a $i/\hbar$ and the phase associated with the temporal evolution, and in the third line we have separated the temporal contribution of the energy. Now, is useful to write the sum over momentum like a sum over energies, using the spectral density function, $\sum_k \to \int d\varepsilon A(\varepsilon)$ and define the linewidth function as

$$\Gamma^\alpha_{mn\sigma}(\varepsilon,t,t') = 2\pi A(\varepsilon)V_{m\alpha\sigma}(\varepsilon,t)V^*_{n\alpha\sigma}(\varepsilon,t')e^{-\frac{i}{\hbar}\int_{t'}^{t}\Delta_\alpha(\tau)d\tau'}. \tag{3.50}$$

Replacing the current and putting all in terms of the trace over spin and molecular space, we finally obtain (we dropped the e subindex and denote the current flow from lead α to the system)

$$J_\alpha(t) = -\frac{2e}{\hbar}\int\frac{d\varepsilon}{2\pi}\int_{-\infty}^{t}d\tau\ \mathrm{Im\,Tr}\Big[\Gamma^\alpha(\varepsilon,\tau,t)\big(G^R(t,\tau)f_\alpha(\varepsilon)+G^<(t,\tau)\big)e^{-\frac{i}{\hbar}\varepsilon(\tau-t)}\Big], \tag{3.51}$$

where $f_\alpha(\varepsilon)$ is the Fermi-function of lead $\alpha = L, R$ and Im denotes the imaginary part. This is the central equation for the charge current in the JMW formalism, where the current is expressed in terms of local quantities. Note how this expression is independent of the device Hamiltonian $\hat{H}_D$. This expression suggests an interpretation as the out-tunneling rate $G^<$ for the first term, and an in-tunneling rate for the second term proportional to the occupation in the leads and to the density of states in the central region. Note how the obtention of this expression was independent of the specific form of the central system (see first line of eq. (3.33)). For our interacting quantum dot, it is possible to see that the JMW current reduces to the formula employed in [76] for the left (or right if we change L for R) lead:

$$J_{\mathrm{L}}(t) = -2\frac{e}{\hbar}\int_{-\infty}^{t} \mathrm{d}t_1 \int \frac{\mathrm{d}\varepsilon}{2\pi}\,\mathrm{Im}\sum_{\sigma}\left\{\mathrm{e}^{-\mathrm{i}\varepsilon(t_1-t)}\,\Gamma^{\mathrm{L}}\left(\varepsilon, t_1, t\right)\left[G^{<}_{\sigma\sigma}\left(t,t_1\right) + f_{\mathrm{L}}(\varepsilon)G^{\mathrm{r}}_{\sigma\sigma}\left(t,t_1\right)\right]\right\}. \quad (3.52)$$

The main focus of this work is the development of the formalism for $M = 1$ energy levels. This situation corresponds to the interacting resonant level model suitable for the IQDS of Eq. 2.43 consisting of a single energy level with energy $\varepsilon_0(t)$ and on-site Coulomb repulsion U. We first focus on the case $U = 0$ as in the standard treatment by Jauho et. al. [72] (with the exception of spin-independent parameters), and the device Hamiltonian is simply given by

$$\hat{H}_D = \varepsilon_0(t)\sum_{\sigma}\hat{d}^{\dagger}_{\sigma}\hat{d}_{\sigma}, \quad (3.53)$$

where we note how the system corresponds with the noninteracting case with trivial time dependence (they commute at different times with themselves) just as the lead Hamiltonians. This aspect is important for the discussion of Ch. 4.

We highlight two relevant scenarios for the dynamics of this model; in the first, a sufficiently long time has passed for the charge current to be constant under a certain initial configuration (with a given applied bias). Thus, the system reaches a steady state situation: this is the **stationary limit**. In the second, the transient response of the initial configuration is studied in the particular case where an analytical solution exists when certain considerations are imposed by the **wide-band limit approximation** for the time-dependent scenario. In the next sections, we derive the relevant expressions in both scenarios while their physics is discussed later on in chapter 4.

3.3.1 Time-independent case: stationary limit

After a sufficiently long time, the charge current reaches a steady state situation characterized by a time-independent linewidth function $\Gamma(\varepsilon, t, t') \to \Gamma(\varepsilon)$ and expectation values have a trivial time dependence in time differences $R(t, t') = R(t - t')$, where R is any expectation value. This allows for the application of Fourier transforms (now that time-translational invariance is restored), where physics in the energy space is more practical and sufficient. As it was proven by Stefanucci and Cini [68], long-time dynamics tend to wash out initial conditions in the Keldysh formalism for the

charge current, which is the expected physical scenario. First, we define the Fourier transform:

$$G(\varepsilon) = \int_{-\infty}^{\infty} dt\, G(t) e^{i\varepsilon t}, \text{ and} \tag{3.54}$$

$$G(t) = \int \frac{d\varepsilon}{2\pi} G(\varepsilon) e^{-i\varepsilon t}. \tag{3.55}$$

In general, it can be shown that the integral over t_1 in Eq. (3.52) can be performed to give

$$J_{L(R)} = \frac{ie}{\hbar} \int \frac{d\varepsilon}{2\pi} \operatorname{Tr}\left\{ \Gamma^{L(R)}(\varepsilon) \left[G^{<}(\varepsilon) + f_{L(R)}(\varepsilon) \big(G^{r}(\varepsilon) - G^{a}(\varepsilon) \big) \right] \right\}, \tag{3.56}$$

even in the fully interacting case, where $G^{A}(\varepsilon) = [G^{r}(\varepsilon)]^{*}$, $G^{<}(\varepsilon)$ and $G^{r}(\varepsilon)$ are written as matrices and the trace is over spin space. The details of these calculations are found in Appendix E. In steady state, clearly $J_R = -J_L$ and we can symmetrize the current as $J = (J_L - J_R)/2$ to obtain:

$$J = \frac{ie}{2\hbar} \int \frac{d\varepsilon}{2\pi} \operatorname{Tr}\Big\{ \left[\Gamma^{L}(\varepsilon) - \Gamma^{R}(\varepsilon) \right] G^{<}(\varepsilon) + \left[f_L(\varepsilon)\Gamma^{L}(\varepsilon) - f_R(\varepsilon)\Gamma^{R}(\varepsilon) \right] \left[G^{r}(\varepsilon) - G^{a}(\varepsilon) \right] \Big\}. \tag{3.57}$$

Let us start with the retarded self-energy defined as

$$\Sigma^{r}(t,t') = \sum_{k\alpha} V_{k\alpha}^{*}(t) \mathcal{G}_{k\alpha}^{r}(t,t') V_{k\alpha}(t'), \tag{3.58}$$

as it was discussed in section D.1. In the steady limit $\varepsilon_{k\alpha}(t)$ and $V_{k\alpha}(t)$ are constant and if we let $\tau = t - t'$ we can write:

$$\Sigma^{r}(\tau) = \sum_{k\alpha} |V_{k\alpha}|^2 \, \mathcal{G}_{k\alpha}^{r}(\tau) \quad \text{and} \quad \mathcal{G}_{k\alpha}^{r}(\tau) = -i\theta(\tau) e^{-i\varepsilon_{k\alpha}\tau}.$$

When computing the Fourier transform, the following formula becomes very useful:

$$\int_{-\infty}^{\infty} dt \theta(t) e^{i\varepsilon t} = \frac{i}{\varepsilon + i\delta}. \tag{3.59}$$

Calculating the transform of Eq. (3.58) (using equations (3.54)-(3.55)), we have:

$$\begin{aligned} \Sigma^{r}(\varepsilon) &= \sum_{k\alpha} |V_{k\alpha}|^2 \int_{-\infty}^{\infty} \mathcal{G}_{k\alpha}^{r}(\tau) e^{i\varepsilon\tau} d\tau = \sum_{k\alpha} |V_{k\alpha}|^2 \int_{-\infty}^{\infty} -i\theta(\tau) e^{i(\varepsilon - \varepsilon_{k\alpha})\tau} d\tau \\ &= \sum_{k\alpha} |V_{k\alpha}|^2 (-i) \frac{i}{\varepsilon - \varepsilon_{k\alpha} + i\eta}, \end{aligned}$$

so that

$$\Sigma^{r(a)}(\varepsilon) = \sum_{k\alpha} \frac{|V_{k\alpha}|^2}{\varepsilon - \varepsilon_{k\alpha} \pm i\eta}. \tag{3.60}$$

Note that the Fourier transform of bare retarded or advanced propagators, relevant in the stationary limit, is given by:

$$\mathcal{G}^{r(a)}_{k\alpha}(\varepsilon) = \int_{-\infty}^{\infty} \mathcal{G}^{r(a)}_{k\alpha}(\tau) e^{i\varepsilon\tau} d\tau = \frac{1}{\varepsilon - \varepsilon_{k\alpha} \pm i\eta}. \tag{3.61}$$

Rewriting Eq. (3.60) in a more convenient form leads to:

$$\Sigma^{r(a)}(\varepsilon) = \sum_{k\alpha} \frac{|V_{k\alpha}|^2}{\varepsilon - \varepsilon_{k\alpha} \pm i\eta} \cdot \frac{\varepsilon - \varepsilon_{k\alpha} \mp i\eta}{\varepsilon - \varepsilon_{k\alpha} \mp i\eta} = \sum_{k\alpha} \frac{|V_{k\alpha}|^2 (\varepsilon - \varepsilon_{k\alpha})}{(\varepsilon - \varepsilon_{k\alpha})^2 + \eta^2} \mp \frac{i}{2} \frac{2|V_{k\alpha}|^2 \eta}{(\varepsilon - \varepsilon_{k\alpha})^2 + \eta^2} = \Lambda(\varepsilon) \mp \frac{i}{2}\Gamma(\varepsilon),$$

such that

$$\Sigma^{r(a)}(\varepsilon) = \Lambda(\varepsilon) \mp \frac{i}{2}\Gamma(\varepsilon), \tag{3.62}$$

where we have $\Lambda(\varepsilon) = \sum_\alpha \Lambda^\alpha(\varepsilon)$ and $\Gamma(\varepsilon) = \sum_\alpha \Gamma(\varepsilon)^\alpha$ as the level-shift and level-width functions respectively. The function $\Lambda(\varepsilon)$ is the real part of the self-energy and it carries the information about the quantum dot level energy shift caused by the coupling to the reservoirs. Similarly, we obtain the lesser component of the self-energy function in the stationary limit as:

$$\Sigma^<(\varepsilon) = \sum_{k\alpha} |V_{k\alpha}|^2 \mathcal{G}^<_{k\alpha}(\varepsilon) = i \sum_\alpha \Gamma^\alpha(\varepsilon) f_\alpha(\varepsilon). \tag{3.63}$$

The Dyson equations for the molecular Green's functions are now products (due to the time convolution theorem [61]) in energy space and the retarded Green's functions can be obtained by solving Eq. (D.12) in energy space for the noninteracting case. That is:

$$G^<(\varepsilon) = G^r(\varepsilon)\Sigma^<(\varepsilon)G^a(\varepsilon), \qquad G^{r(a)}(\varepsilon) = \frac{1}{\left[\mathcal{G}^{r(a)}(\varepsilon)\right]^{-1} - \Sigma^{r(a)}(\varepsilon)}, \tag{3.64}$$

where $\mathcal{G}^{r(a)}(\varepsilon)$ is the retarded(advanced) component of the bare Green's function for the isolated system. It follows straightforwardly from its equation of motion in energy space (η is an infinitesimal real number):

$$\mathcal{G}(\varepsilon)^{r(a)} = \frac{1}{\varepsilon - \varepsilon_0 \pm i\eta}. \tag{3.65}$$

From the equations in (3.64) we can easily obtain the retarded and advanced propagators, and the lesser propagator in energy space as:

$$G^{r(a)}_{\sigma\sigma}(\varepsilon) = \frac{1}{\varepsilon - \varepsilon_{0(U)} - \Lambda(\varepsilon) \pm \frac{i}{2}\Gamma(\varepsilon)}, \quad \text{and} \quad G^<(\varepsilon) = i\frac{\Gamma^L(\varepsilon)f_L(\varepsilon) + \Gamma^R(\varepsilon)f_R(\varepsilon)}{[\varepsilon - \varepsilon_0 - \Lambda(\varepsilon)]^2 + [\Gamma(\varepsilon)/2]^2}. \tag{3.66}$$

Finally, the charge current in Eq. (3.57) is given by

$$J = \frac{e}{\hbar}\int \frac{d\varepsilon}{2\pi} \frac{\Gamma^L(\varepsilon)\,\Gamma^R(\varepsilon)}{[\varepsilon - \varepsilon_0 - \Lambda(\varepsilon)]^2 + [\Gamma(\varepsilon)/2]^2} \left[f_L(\varepsilon) - f_R(\varepsilon)\right]. \tag{3.67}$$

3.3.2 Time-dependent case: wide-band limit approximation

The wide-band limit approximation consists of assuming that the leads' density of states remains constant. This is valid as long as the leads are large enough (macroscopic) that their properties are unaffected by the presence of the resonant level. This is precisely a way to define a non-strong system-bath coupling regime, where the system does not affect the bath physics. Experimentally, we can set the resonant level to lay within a broad, flat region of the leads' density of states [72]. This justifies the application of the WBL to our model. As a consequence, the environment affects the central system without a memory in an adiabatic fashion. This implies considering a delta function for the retarded embedding self-energy, neglecting the level-shift $\Lambda(\varepsilon)$, and considering energy-independent constant linewidth functions such that $\Gamma(t) = \Gamma^L(t) + \Gamma^R(t)$, where $\Gamma_{L/R}(t) = \Gamma^{L/R}(t,t) = \Gamma^{L/R}\left|u_{L/R}(t)\right|^2$. Then

$$\Sigma^r(t,t') = -\frac{i}{2}\Gamma(t)\delta(t-t'), \tag{3.68}$$

and with this self-energy it is straightforward to see that

$$G^{r,a}(t,t') = \mathcal{G}^{r,a}(t,t')\exp\left\{\mp\int_{t'}^{t} dt_1 \frac{1}{2}\Gamma(t_1)\right\}, \quad \mathcal{G}^{r,a}(t,t') = \mp i\theta(\pm t \mp t')\exp\left[-i\int_{t'}^{t} dt_1 \varepsilon_0(t_1)\right], \tag{3.69}$$

where we can see the great advantage of this approximation: it yields explicit analytical results. By denoting $\mathrm{Im}\, G^<(t,t) = n(t)$, where $n(t)$ is the occupation of the resonant level, we go back to Eq. (3.51)

$$J_\alpha(t) = -\frac{e}{\hbar}\left[\Gamma^\alpha(t)n(t) + \int \frac{d\varepsilon}{\pi} f_\alpha(\varepsilon)\int_{-\infty}^{t} dt_1\, \Gamma^\alpha(t_1,t)\,\mathrm{Im}\left\{e^{-i\varepsilon(t_1-t)}G^r(t,t_1)\right\}\right]. \tag{3.70}$$

We find a solution for the lesser Green's function by using Keldysh equation (C.9). If we use the equations in (3.69), simple algebra leads to:

$$n(t) = \sum_\alpha \Gamma^\alpha \int \frac{d\varepsilon}{2\pi} f_\alpha(\varepsilon)\left|A_\alpha(\varepsilon,t)\right|^2, \tag{3.71}$$

where the function $A_\alpha(\varepsilon,t)$ is defined for compactness as:

$$A_{L/R}(\varepsilon,t) = \int dt_1 u_{L/R}(t_1)\, G^r(t,t_1)\exp\left[i\varepsilon(t-t_1) - i\int_t^{t_1} dt_2 \Delta_{L/R}(t_2)\right] \tag{3.72}$$

Following Ref. [72], we write the current in Eq. (3.70) as a sum of outgoing and in-going current contributions from the right or left lead to the central region:

$$J_\alpha(t) = J_\alpha^{\mathrm{out}}(t) + J_\alpha^{\mathrm{in}}(t), \tag{3.73}$$

$$J_\alpha^{\text{out}}(t) = -\frac{e}{\hbar}\Gamma^\alpha(t)n(t), \tag{3.74}$$

$$J_\alpha^{\text{in}}(t) = -\frac{e}{\hbar}\Gamma^\alpha u_\alpha(t)\int \frac{d\varepsilon}{\pi} f_\alpha(\varepsilon)\,\text{Im}\left\{A_\alpha(\varepsilon,t)\right\}. \tag{3.75}$$

Finally, the relevant quantity is the total current flowing through the region as quantified by the symmetrized current $J(t) = [J_L(t) - J_R(t)]/2$.

We have discussed relevant aspects of the interacting quantum dot system and outlined the theoretical formalism for characterizing its transport features, including the JMW current. Additionally, we reproduced the standard treatment by Juaho et al. [72] for the noninteracting case ($U = 0$) and single-level ($M = 1$) configuration. This involved calculating relevant expressions for two key scenarios: the stationary limit and the time-dependent Wide-Band Limit (WBL) situation, which are the focus of the remainder of this work. Implementing numerical methods is crucial for visualizing and analyzing the current's time-dependent behavior. In Chapter 4, we explore the broader interacting case in both scenarios, analyze the stationary and noninteracting cases for the time-dependent current (consistent with the noninteracting case $U = 0$ as per [72]), and implement numerical methods to elucidate the JWM current.

4 Quantum transport with TDNEGF

With the foundational theoretical elements introduced for examining the interacting quantum dot system (IQDS), our focus now shifts toward the central objective of this study: evaluating the quantum transport properties of the system in terms of the charge current generated under various bias voltages. Employing the equation of motion approach within NEGF framework for the interacting problem, we discern that the closure and resolution of the resulting equations are feasible only within the Hubbard-I approximation (HIA) for electron-electron interactions within the one-level quantum dot. Then, we derive an analytical expression for the charge current as a function of time and assess it under different initial configurations, using Julia programming language. This procedure is the basis for our subsequent analysis of quantum transport properties.

4.1 Closing the equations of motion

We focus on the system depicted in Figure 2.9: the IQDS. We employ the equation (3.27) for the Hamiltonian model $\hat{H}_S(t) = \hat{H}_M(t) + \hat{H}_D(t) + \hat{H}_T(t)$, specified in equation (2.43) and section 3.2. For simplicity, we consider spin-independent parameters $V_{k\alpha\sigma} = V_{k\alpha}$, $\varepsilon_{k\alpha\sigma} = \varepsilon_{k\alpha}$ and $\varepsilon_{0\sigma} = \varepsilon_0$. We define the relevant lesser and retarded GFs in the Keldysh-Schwinger contour for the QD as:

$$G^{<}_{\sigma\sigma}(t,t') = i\left\langle \hat{d}^{\dagger}_{\sigma}(t')\,\hat{d}_{\sigma}(t)\right\rangle, \qquad G^{r}_{\sigma\sigma}(t,t') = -i\theta(t-t')\left\langle \left\{\hat{d}_{\sigma}(t), \hat{d}^{\dagger}_{\sigma}(t')\right\}\right\rangle. \tag{4.1}$$

For the retarded propagator (using Eq. (3.27)) we get

$$i\partial_t G^{r}_{\sigma\sigma}(t,t') = \delta(t-t') + i\theta(t-t')\left\langle \left\{\left[\hat{H}_S(t), \hat{d}_{\sigma}(t)\right], \hat{d}^{\dagger}_{\sigma}(t')\right\}\right\rangle, \tag{4.2}$$

and we have to solve each commutator coming from $\left[\hat{H}_S(t), \hat{d}_{\sigma}(t)\right] = \left[\hat{H}_M, \hat{d}_{\sigma}\right] + \left[\hat{H}_D, \hat{d}_{\sigma}\right] + \left[\hat{H}_T, \hat{d}_{\sigma}\right]$. The details of this procedure can be found in appendix F where we develop each term to solve for $\left[\hat{H}_S(t), \hat{d}_{\sigma}(t)\right]$. This leads to the first total commutator of this section:

$$\left[\hat{H}_S(t), \hat{d}_{\sigma}(t)\right] = -\varepsilon_0\hat{d}_{\sigma} - U\hat{d}_{\sigma}\hat{n}_{\bar{\sigma}} - \sum_{k\alpha\alpha} V^{*}_{k\alpha}\hat{c}_{k\alpha\sigma}. \tag{4.3}$$

In Eq. (4.2) we identify new hybrid and higher-order Green's functions to account for high-order electron-electron interaction effects and electronic transition amplitudes from the device to the metallic reservoir and vice-versa. These functions are defined by

$$G^r_{\sigma\sigma,U}(t,t') = -i\theta(t-t')\left\langle\left\{\left(\hat{d}_\sigma\hat{n}_{\bar{\sigma}}\right)(t),\hat{d}^\dagger_\sigma(t')\right\}\right\rangle, \quad G^r_{k\alpha\sigma}(t,t') = -i\theta(t-t')\left\langle\left\{\hat{c}_{k\alpha\sigma}(t),\hat{d}^\dagger_\sigma(t')\right\}\right\rangle. \tag{4.4}$$

We rewrite the following nice-looking non-closed differential equation for the retarded Green's function:

$$i\partial_t G^r_{\sigma\sigma}(t,t') = \delta(t-t') + \varepsilon_0(t)G^r_{\sigma\sigma}(t,t') + UG^r_{\sigma\sigma,U}(t,t') + \sum_{k\alpha} V^*_{k\alpha}(t)G^r_{k\alpha\sigma}(t,t'). \tag{4.5}$$

The next step of our calculation is to find an EOM for $G^r_{k\alpha\sigma}(t,t')$. Notice how we repeatedly use the equation of motion method to obtain a differential equation for the different propagators. Such is the essence of this method. Using equation (3.27) again for this new propagator we find:

$$i\partial_t G^r_{k\alpha\sigma}(t,t') = i\theta(t-t')\left\langle\left\{\left[\hat{H}_S(t),\hat{c}_{k\alpha\sigma}(t)\right],\hat{d}^\dagger_\sigma(t')\right\}\right\rangle. \tag{4.6}$$

Now we have $\left[\hat{H}_S(t),\hat{c}_{k\alpha\sigma}(t)\right] = \left[\hat{H}_M,\hat{c}_{k\alpha\sigma}(t)\right] + \left[\hat{H}_D,\hat{c}_{k\alpha\sigma}(t)\right] + \left[\hat{H}_T,\hat{c}_{k\alpha\sigma}(t)\right]$. We skip the details of the recurring commutator calculations which can be found in detail in Appendix F. An analogous procedure leads to the second complete commutator:

$$\left[\hat{H}_S(t),\hat{c}_{k\alpha\sigma}(t)\right] = -\epsilon_{k\alpha}\hat{c}_{k\alpha\sigma} - V_{k\alpha}\hat{d}_\sigma(t). \tag{4.7}$$

With the commutator in Eq. (4.7), we return to Eq. (4.6) to get

$$\left(i\partial_t - \varepsilon_{k\alpha}(t)\right)G^r_{k\alpha\sigma}(t,t') = V_{k\alpha}(t)G^r_{\sigma\sigma}(t,t'). \tag{4.8}$$

Here comes a key consideration in this derivation. Define the Green's function for the uncoupled leads, or the bare Green's function, as the solution of:

$$\left(i\partial_t - \varepsilon_{k\alpha}(t)\right)\mathcal{G}^r_{k\alpha}(t,t') = \delta(t-t') \longrightarrow \mathcal{G}^r_{k\alpha}(t,t') = -i\theta(t-t')\exp\left[-i\int_{t'}^{t}\varepsilon_{k\alpha}(\tau)d\pi\right]. \tag{4.9}$$

This is equivalent to defining the bare Green's function as $\mathcal{G}^{r/a}_{k\alpha} = \mp i\,\theta(\pm t \mp t')\left\langle\left\{\hat{c}_{k\alpha}(t),\hat{c}^\dagger_{k\alpha}(t')\right\}\right\rangle$. Similarly, it follows that the bare lesser Green's function for the leads is given by:

$$\mathcal{G}^<_{k\alpha}(t,t') = if\left(\epsilon^0_k\right)\exp\left[-i\int_{t'}^{t}dt_1\epsilon_{k\alpha}(t_1)\right]. \tag{4.10}$$

Based on the fact that the macroscopic leads are simply metallic ones with no interactions, we can obtain an integral equation for their Green's functions since the $\hat{H}_M$ commutes with itself at different times and presents no interacting terms. Therefore, the energy contribution from the lead

electrons is purely kinetical and encoded in the energy bands, as usually established in the theory of bands for macroscopic metals with Fermi functions $f_\alpha(\epsilon) = f(\epsilon - \mu_\alpha)$. Let $t \mapsto \pi$, multiply by $\mathcal{G}^r_{k\alpha}(t,\pi)$ and integrate over $d\tau$ in Eq. (4.8) to obtain:

$$\int \underbrace{\mathcal{G}^r_{k\alpha}(t,\tau)\left(i\partial_\tau - \varepsilon_{k\alpha}(\tau)\right)}_{\delta(t-\tau)} G^r_{k\alpha\sigma}(\tau,t')\,d\tau = \int \mathcal{G}^r_{k\alpha}(t,\tau)V_{k\alpha}(\tau)G^r_{\sigma\sigma}(\tau,t')\,d\tau.$$

Hence, we obtain the formal solution of Eq. (4.8) as[1]:

$$G^r_{k\alpha\sigma}(t,t') = \int_K \mathcal{G}^r_{k\alpha}(t,\tau)V_{k\alpha}(\tau)G^r_{\sigma\sigma}(\tau,t')\,d\tau. \tag{4.11}$$

It is convenient to define the retarded embedding self-energy, analogous to the analysis of section 3.3.1:

$$\Sigma^r(t,t') = \sum_{k\alpha} V^*_{k\alpha}(t)\mathcal{G}^r_{k\alpha}(t,t')\,V_{k\alpha}(t') = -i\theta(t-t')\sum_\alpha \int \frac{d\varepsilon}{2\pi} e^{-i\varepsilon(t-t')}\Gamma^\alpha(\varepsilon,t,t'), \tag{4.12}$$

$$\Gamma^\alpha(\varepsilon,t,t') = 2\pi\rho(\varepsilon)u_\alpha(t')\,u_\alpha(t)V_\alpha(\varepsilon)V^*_\alpha(\varepsilon)\exp\left[\mathrm{i}\int_t^{t'} d\tau\,\Delta_\alpha(\tau)\right]. \tag{4.13}$$

The last equality in Eq. (4.12) is not straightforward and we refer to Appendix F for a detailed derivation. Using equations (4.11) and (4.12) into (4.5) we get:

$$(i\partial_t - \varepsilon_0(t))\,G^r_{\sigma\sigma}(t,t') = \delta(t-t') + UG^r_{\sigma\sigma,U}(t,t') + \int \Sigma^r(t,\tau)G^r_{\sigma\sigma}(\tau,t')\,d\tau, \tag{4.14}$$

which is the EOM for the retarded QD propagator still coupled to the higher-order interacting propagator $G^r_{\sigma\sigma,U}(t,t')$.

4.1.1 Non-canonical Hubbard-I approximation

We have obtained an equation of motion for the device retarded propagator in terms of an unknown interacting propagator $G^r_{\sigma\sigma,U}(t,t')$. Let us now turn to the problem of obtaining an equation of motion for $G^r_{\sigma\sigma,U}(t,t')$ by following a similar procedure as for Eq. (4.2):

$$i\partial_t G^r_{\sigma\sigma,U}(t,t') = \delta(t-t')\left\langle\left\{\left(\hat{d}_\sigma\hat{n}_{\bar\sigma}\right)(t),\hat{d}^\dagger_\sigma(t)\right\}\right\rangle + i\theta(t-t')\left\langle\left\{\left[\hat{H}_S(t),\left(\hat{d}_\sigma\hat{n}_{\bar\sigma}\right)(t)\right],\hat{d}^\dagger_\sigma(t')\right\}\right\rangle.$$

We compute the commutator $\left[\hat{H}_S,\left(\hat{d}_\sigma\hat{n}_{\bar\sigma}\right)(t)\right]$ (see appendix F) to obtain:

$$\left[\hat{H}_S,\left(\hat{d}_\sigma\hat{n}_{\bar\sigma}\right)(t)\right] = -\left(\varepsilon_0(t)+U\right)\left(\hat{d}_\sigma\hat{n}_{\bar\sigma}\right)(t) - \sum_{k\alpha}\left(V_{k\alpha}(t)c^\dagger_{k\alpha\bar\sigma}\hat{d}_\sigma d_{\bar\sigma} + V^*_{k\alpha}(t)\hat{c}_{k\sigma\alpha}\hat{n}_{\bar\sigma} + V^*_{k\alpha}(t)\hat{d}_\sigma d^\dagger_{\bar\sigma}\hat{c}_{k\alpha\bar\sigma}\right). \tag{4.15}$$

[1] Integration of propagators is always understood with their arguments lying in the real-time branches of the Schwinger-Keldysh contour.

Crucially, we observe that this commutator plays a pivotal role in hierarchically introducing higher-order terms for the interacting Green's functions as we repeatedly formulate equations of motion for the resulting higher-order propagators. As expounded in Section 3.1.3, we circumvent this challenge by resorting to the Hubbard-I approximation (HIA)—a mean-field approximation. This method is a common practice in many-body perturbation theory (MBPT) [61] akin to the systematic neglect of specific diagrams in the self-consistent expansion of self-energy of the problem [95]. To elaborate, this approximation involves discarding terms lacking matching quantum numbers for a minimum of two fermionic operators within the commutator in Eq. (4.15). This leads to:

$$\left[\hat{H}_S, \left(\hat{d}_\sigma \hat{n}_{\bar{\sigma}}\right)(t)\right] \approx -\left(\varepsilon_0(t) + U\right)\left(\hat{d}_\sigma \hat{n}_{\bar{\sigma}}\right)(t) - \sum_{k\alpha} V^*_{k\alpha}(t)\left(\hat{c}_{k\alpha\sigma}\hat{n}_{\bar{\sigma}}\right)(t). \tag{4.16}$$

We define a hybrid higher-order Green's function as $G^r_{k\alpha\sigma,U}(t,t') = -i\theta\left(t-t'\right)\left\langle\left\{\left(\hat{c}_{k\alpha\sigma}\hat{n}_\sigma\right)(t), \hat{d}^\dagger_\sigma(t')\right\}\right\rangle$ that allows us to obtain an equation of motion for $G^r_{\sigma\sigma,U}(t,t')$:

$$\left(i\partial_t - \varepsilon_0(t) - U\right) G^r_{\sigma\sigma,U}(t,t') = \delta(t-t')\left\langle\hat{n}_{\bar{\sigma}}(t)\right\rangle + \sum_{k\alpha} V^*_{k\alpha}(t) G^r_{k\alpha\sigma,U}(t,t'). \tag{4.17}$$

The usual HIA proceeds by applying the Hartree approximation decoupling $\hat{c}_{k\alpha\sigma}\hat{n}_{\bar{\sigma}} \approx \hat{c}_{k\alpha\sigma}\left\langle\hat{n}_{\bar{\sigma}}\right\rangle$ such that the energy levels are self-consistently renormalized by the expectation value of the number operator of electrons with a given spin in the level, at each instant of time. Instead, the non-canonical aspect of our HIA consists of finding an EOM for the new hybrid propagator:

$$i\partial_t G^r_{k\alpha\sigma,U}(t,t') = i\theta(t-t')\left\langle\left\{\left[\hat{H}_S, \left(\hat{c}_{k\alpha\sigma}\hat{n}_\sigma\right)(t)\right], \hat{d}^\dagger_\sigma(t')\right\}\right\rangle.$$

By analogous procedure, we compute the commutator above (see Appendix F) and we get:

$$\left[\hat{H}_S, \left(\hat{c}_{k\alpha\sigma}\hat{n}_{\bar{\sigma}}\right)(t)\right] = -\varepsilon_{k\alpha}\hat{c}_{k\alpha\sigma}\hat{n}_{\bar{\sigma}} - V_{k\alpha}\hat{d}_\sigma\hat{n}_{\bar{\sigma}} + \sum_{q\beta}\hat{c}_{k\alpha\sigma}c^\dagger_{q\beta\sigma}d_{\bar{\sigma}} - \sum_{q\beta}V^*_{q\beta}\hat{c}_{k\alpha\sigma}d^\dagger_{\bar{\sigma}}c_{q\beta\sigma}. \tag{4.18}$$

Within the usual HIA [76, 91, 130], the previous commutator reduces to:

$$\left[\hat{H}_T, \left(\hat{c}_{k\alpha\sigma}\hat{n}_{\bar{\sigma}}\right)(t)\right] \approx -\varepsilon_{k\alpha}\hat{c}_{k\alpha\sigma}\hat{n}_{\bar{\sigma}} - V_{k\alpha}\hat{d}_\sigma\hat{n}_{\bar{\sigma}}.$$

Finally, we obtain the following EOM for the hybrid higher-order Green's function:

$$\left(i\partial_t - \varepsilon_{k\alpha}(t)\right) G^r_{k\alpha,U}(t,t') = V_{k\alpha}(t) G^r_{\sigma\sigma,U}(t,t'). \tag{4.19}$$

Due to the trivial time dependence of the Hamiltonian $\hat{H}_D(t)$, we have commutation at different times. This allows us to write all our Green's functions in integral form. With this, we can define bare propagators with trivial equations of motion such as [2]:

$$\mathcal{G}^r_0(t,t') = -i\theta(t-t')\exp\left[-i\int_{t'}^{t}\varepsilon_0(\tau)d\tau\right], \tag{4.20}$$

[2] From now on, we denote $n_{\bar{\sigma}}(t) = \langle\hat{n}_{\bar{\sigma}}(t)\rangle$.

$$\mathcal{G}_U^r(t,t') = -i\theta(t-t')\exp\left[-i\int_{t'}^{t}\varepsilon_0(\tau)d\tau\right]\exp\left[-iU(t-t')\right] = \mathcal{G}_0^r(t,t')\exp\left[-iU(t-t')\right], \tag{4.21}$$

$$\tilde{\mathcal{G}}_0^r(t,t') = \big(1-n_{\bar{\sigma}}(t')\big)\mathcal{G}_0^r(t,t'), \tag{4.22}$$

$$\tilde{\mathcal{G}}_U^r(t,t') = n_{\bar{\sigma}}(t')\,\mathcal{G}_U^r(t,t'). \tag{4.23}$$

We now proceed by writing equations (4.14), (4.17) and (4.19) in full integral form:

$$G_{\sigma\sigma}^r(t,t') = \mathcal{G}_0^r(t,t') + \int \mathcal{G}_0^r(t,\tau)\,\Sigma^r(\tau,\tau')G_{\sigma\sigma}^r(\tau',t')\;d\tau d\tau' + U\int \mathcal{G}_0^r(t,\tau)G_{\sigma\sigma,U}^r(\tau,t')\,d\tau, \tag{4.24}$$

$$G_{\sigma\sigma,U}^r(t,t') = \tilde{\mathcal{G}}_U^r(t,t') + \int d\tau\mathcal{G}_U^r(t,\tau)\sum_{k\alpha}V_{k\alpha}^*(\tau)G_{k\alpha\sigma,U}^r(\tau,t'), \tag{4.25}$$

$$G_{k\alpha\sigma,U}^r(t,t') = \int d\tau\mathcal{G}_{k\alpha}^r(t,\tau)V_{k\alpha}(\tau)G_{\sigma\sigma,U}^r(\tau,t'). \tag{4.26}$$

We eliminate $G_{k\alpha\sigma,U}^r(t,t')$ by using Eq. (4.26) into Eq. (4.25) to get:

$$G_{\sigma\sigma,U}^r(t,t') = \tilde{\mathcal{G}}_U^r(t,t') + \int \mathcal{G}_U^r(t,\tau)\Sigma^r(\tau,\tau')\,G_{\sigma\sigma,U}^r(\tau',t')\,d\tau d\tau'. \tag{4.27}$$

Finally, we use Eq. (4.27) in Eq. (4.24) and we obtain:

$$\begin{aligned} G_{\sigma\sigma}^r(t,t') = \mathcal{G}_0^r(t,t') &+ \int \mathcal{G}_0^r(t,\tau)\,\Sigma^r(\tau,\tau')G_{\sigma\sigma}^r(\tau',t')\,d\tau d\tau' + U\int \mathcal{G}_0^r(t,\tau)\tilde{\mathcal{G}}_U^r(\tau,t')\,d\tau \\ &+ U\int \mathcal{G}_0^r(t,\tau)\mathcal{G}_U^r(\tau,\tau')\,\Sigma^r(\tau',\tau'')\,G_{\sigma\sigma,U}^r(\tau'',t')\,d\tau d\tau' d\tau''. \end{aligned} \tag{4.28}$$

We direct the reader to Appendix F for further calculations of the third term in (4.28) written in purple. Additional calculations lead to:

$$\begin{aligned} G_{\sigma\sigma}^r(t,t') = \mathcal{G}_0^r(t,t') + \tilde{\mathcal{G}}_U^r(t,t') - n_{\bar{\sigma}}(t')\,\mathcal{G}_0^r(t,t') &+ \int \mathcal{G}_0^r(t,\tau)\,\Sigma^r(\tau,\tau')G_{\sigma\sigma}^r(\tau',t')\,d\tau d\tau' \\ &+ \int \big(\mathcal{G}_U^r(t,\tau) - \mathcal{G}_0^r(t,\tau)\big)\Sigma^r(\tau,\tau')\,G_{\sigma\sigma,U}^r(\tau',t')\,d\tau d\tau', \end{aligned} \tag{4.29}$$

which is the equation of motion for the unknown retarded propagator $G_{\sigma\sigma}^r(t,t')$. However, if we aim to obtain an analytical solution for this equation, an additional procedure is necessary with the consideration of the important Hubbard bands.

4.1.2 Hubbard bands

Here, we outline the key procedure that offers a simple way to obtain an analytical solution for the Green's functions from Eq. (4.29). By introducing two new Green's functions

$$\tilde{G}^r_{\sigma\sigma,0}(t,t') = \frac{G^r_{\sigma\sigma,0}(t,t')}{1-n_{\bar{\sigma}}(t')}, \qquad \tilde{G}^r_{\sigma\sigma,U}(t,t') = \frac{G^r_{\sigma\sigma,U}(t,t')}{n_{\bar{\sigma}}(t')}, \tag{4.30}$$

and splitting the GF in Eq. (4.29) in two contributions such that $G^r_{\sigma\sigma}(t,t') = G^r_{\sigma\sigma,0}(t,t') + G^r_{\sigma\sigma,U}(t,t')$, we can deduce a Dyson equation satisfied by each new GF in Eq. (4.30). Solutions to these equations are presented in Appendix G by the expressions (G.4) and (G.5) are straightforward in the wide-band limit approximation for our system. Algebraic manipulations lead to the following expression:

$$G^r_{\sigma\sigma}(t,t') = \big(1-n_{\bar{\sigma}}(t')\big)\tilde{G}^r_{\sigma\sigma,0}(t,t') + n_{\bar{\sigma}}(t')\,\tilde{G}^r_{\sigma\sigma,U}(t,t')\,. \tag{4.31}$$

Direct application of Eq. (C.9) leads to another equation from which we can obtain $n_\sigma(t) = iG^<_{\sigma\sigma}(t,t)$ after solving Eq. (G.7):

$$G^<_{\sigma\sigma}(t,t') = \big(1-n_{\bar{\sigma}}(t')\big)\tilde{G}^<_{\sigma\sigma,0}(t,t') + n_{\bar{\sigma}}(t')\,\tilde{G}^<_{\sigma\sigma,U}(t,t')\,. \tag{4.32}$$

Once again, we can obtain analytical solutions for lesser components of the new GFs by solving Eq. (G.7). As noted in section 2.1.1, the Coulomb repulsion is responsible for the emergence of a quasi-band structure formed by two bands centered at energies ε_0 and $\varepsilon_0 + U$, whose intuitive spectral weights are given by $1-n_{\bar{\sigma}}(t')$ and $n_{\bar{\sigma}}(t')$, respectively. Then, we can easily see how the Green's functions in (4.30) relate to the concept introduced by Hubbard in its seminal work [91]: the **Hubbard bands** or Hubbard excitations[3]. Therefore, we notice how the analytical treatment depicted in [76] is facilitated by the recognition of the quasi-band structure of the Hubbard terms of $\hat{H}_D$, whose contributions are closely contained by the new Green's functions defined above.

4.2 Analytical expression of the JMW current

Now that we have defined suitable equations for the calculation of the relevant Green's functions, we carry on to find an expression for Eq. (3.52) by explicitly determining each quantity in two scenarios where an analytical solution is possible: the **stationary limit** and the **wide-band limit**. The physics relevant to each case is studied in section 4.3. We follow the same procedure as in sections 3.3.1 and 3.3.2.

[3] We can see how this bands and their appearance in the form of Green's functions have spectral weights just as in the analysis of the Hubbard model of section 2.1.1.

4.2.1 Time-independent case: stationary limit

We start by describing all previous quantities in the stationary limit. Once the system responds to an initial perturbation that drives it out of equilibrium and reaches the steady-state situation, expectation values have a trivial time dependence and we proceed similarly to section 3.3.1. The self-energy of the problem is the same as in Eq. (3.60),

$$\Sigma^{r(a)}(\varepsilon) = \sum_{k\alpha} \frac{|V_{k\alpha}|^2}{\varepsilon - \varepsilon_{k\alpha} \pm i\eta}, \quad \text{or} \quad \Sigma^{r(a)}(\varepsilon) = \Lambda(\varepsilon) \mp \frac{i}{2}\Gamma(\varepsilon). \tag{4.33}$$

We also have the energy representation of the bare retarded or advanced propagators given by:

$$\mathcal{G}^{r(a)}_{k\alpha}(\varepsilon) = \frac{1}{\varepsilon - \varepsilon_{k\alpha} \pm i\eta}. \tag{4.34}$$

Similarly, we obtain the lesser component of the self-energy function in the stationary limit as:

$$\Sigma^{<}(\varepsilon) = i\sum_{\alpha} \Gamma^{\alpha}(\varepsilon) f_{\alpha}(\varepsilon). \tag{4.35}$$

The Dyson equations for the QD Green's functions are now products in energy space:

$$\tilde{G}^{r(a)}_{\sigma\sigma,(0)U}(\varepsilon) = \mathcal{G}^{r(a)}_{(0)U}(\varepsilon) + \mathcal{G}^{r(a)}_{(0)U}(\varepsilon)\, \Sigma^{r(a)}(\varepsilon)\, \tilde{G}^{r(a)}_{\sigma\sigma,(0)U}(\varepsilon). \tag{4.36}$$

If we use the energy space definitions above, we can obtain the Hubbard bands propagators as:

$$\tilde{G}^{r(a)}_{\sigma\sigma,(0)}(\varepsilon) = \frac{1}{\varepsilon - \varepsilon_{0(U)} - \Lambda(\varepsilon) \pm \frac{i}{2}\Gamma(\varepsilon)}. \tag{4.37}$$

Going back to Eq. (G.6), we retrieve the retarded and advanced propagators,

$$G^{\mathrm{r(a)}}_{\sigma\sigma}(\omega) = \frac{1 - n_{\bar{\sigma}}}{\omega - \varepsilon_0 - \Lambda(\omega) \pm \frac{\mathrm{i}}{2}\Gamma(\omega)} + \frac{n_{\bar{\sigma}}}{\omega - \varepsilon_0 - U - \Lambda(\omega) \pm \frac{\mathrm{i}}{2}\Gamma(\omega)}. \tag{4.38}$$

From Eq. (G.7) in energy space (time integrals are now products of matrices) and from Eq. (G.9) it follows the solution for the lesser Green's function

$$G^{<}_{\sigma\sigma}(\omega) = \mathrm{i}\sum_{\alpha} \Gamma^{\alpha}(\omega) f_{\alpha}(\omega) \left(\frac{1 - n_{\bar{\sigma}}}{\left[\omega - \varepsilon_0 - \Lambda(\omega)\right]^2 + \left[\Gamma(\omega)/2\right]^2} + \frac{n_{\bar{\sigma}}}{\left[\omega - \varepsilon_0 - U - \Lambda(\omega)\right]^2 + \left[\Gamma(\omega)/2\right]^2} \right). \tag{4.39}$$

Simple algebra for the spectral function $A_{\sigma}(\omega) = \mathrm{i}\left[G^{\mathrm{r}}_{\sigma\sigma}(\omega) - G^{\mathrm{a}}_{\sigma\sigma}(\omega)\right]$ leads to:

$$A_{\sigma}(\omega) = A^{0}_{\sigma}(\omega) + A^{U}_{\sigma}(\omega) = \frac{(1 - n_{\bar{\sigma}})\,\Gamma(\omega)}{\left[\omega - \varepsilon_0 - \Lambda(\omega)\right]^2 + \left[\frac{\Gamma(\omega)}{2}\right]^2} + \frac{n_{\bar{\sigma}}\Gamma(\omega)}{\left[\omega - \varepsilon_0 - U - \Lambda(\omega)\right]^2 + \left[\frac{\Gamma(\omega)}{2}\right]^2}, \tag{4.40}$$

where we can interpret it as a contribution from spectral energies of the Hubbard bands with the independent terms $A^0_\sigma(\varepsilon)$ and $A^U_\sigma(\varepsilon)$. Using Eq. (4.40) and the stationary form of the JMW current in Eq. (3.56), along with the analytical expressions for the Green's functions, it follows that:

$$J_{\mathrm{L(R)}} = -\frac{e}{\hbar}\int \frac{\mathrm{d}\varepsilon}{2\pi}\sum_\sigma A_\sigma(\varepsilon)\frac{\Gamma^{\mathrm{L}}(\varepsilon)\Gamma^{\mathrm{R}}(\varepsilon)}{\Gamma(\varepsilon)}\big[f_{\mathrm{R(L)}}(\varepsilon) - f_{\mathrm{L(R)}}(\varepsilon)\big]. \tag{4.41}$$

The occupancy for an electron with spin σ is the same as the occupation of $\bar\sigma$ electrons as the Green's functions are diagonal in spin, and the leads present no magnetic properties that could produce different contributions of spin currents to the problem. It is possible to see that Eq. (4.39) can be written in terms of the spectral function as $G^<_{\sigma\sigma}(\varepsilon) = i\bar f(\varepsilon)A_\sigma(\varepsilon)$, where it is customary to define $\bar f(\varepsilon) = \frac{\Gamma^{\mathrm{L}}(\varepsilon)f_{\mathrm{L}}(\varepsilon)+\Gamma^{\mathrm{R}}(\varepsilon)f_{\mathrm{R}}(\varepsilon)}{\Gamma(\varepsilon)}$ [72, 76]. With this, it follows that:

$$n_\sigma = \mathrm{Im}\, G^<_{\sigma\sigma}(t,t) = \int \frac{d\varepsilon}{2\pi}\,\mathrm{Im}\, G^<_{\sigma\sigma}(\varepsilon) = \int \frac{\mathrm{d}\varepsilon}{2\pi}\bar f(\varepsilon)A_\sigma(\varepsilon). \tag{4.42}$$

Since $n_\sigma(t) = n_{\bar\sigma}(t)$, we can rewrite Eq. (4.39) in terms of n_σ as $n_\sigma = (1-n_\sigma)\,n^0 + n_\sigma n^U$, where the occupation per magnetic projection is retrieved by,

$$n_\sigma = n_{\bar\sigma} = \frac{n^0}{1+n^0-n^U}, \tag{4.43}$$

with $n^{0(U)}$ given by:

$$n^{0(U)} = \int \frac{\mathrm{d}\varepsilon}{2\pi}\bar f(\varepsilon)\frac{\Gamma(\varepsilon)}{\big[\varepsilon-\varepsilon_{0(U)}-\Lambda(\varepsilon)\big]^2+\big[\Gamma(\varepsilon)/2\big]^2}. \tag{4.44}$$

It is important to mention the connection between the formulas in this section and those in section 3.3.1. By letting $U = 0$ in the expressions of this section, it is immediate to see that we consistently recover the results from the noninteracting case. For example, in Eq. (4.38), if we let $U = 0$, we obtain:

$$G^{\mathrm{r(a)}}_{\sigma\sigma}(\omega) = \frac{1-n_{\bar\sigma}}{\omega-\varepsilon_0-\Lambda(\omega)\pm\frac{\mathrm{i}}{2}\Gamma(\omega)} + \frac{n_{\bar\sigma}}{\omega-\varepsilon_0-\Lambda(\omega)\pm\frac{\mathrm{i}}{2}\Gamma(\omega)} = \frac{1}{\omega-\varepsilon_0-\Lambda(\omega)\pm\frac{\mathrm{i}}{2}\Gamma(\omega)},$$

which reproduces the result of Eq. (4.37).

As mentioned in section 3.3.2, in the WBL approximation we neglect the level-shift function (real part of the retarded self-energy) while its imaginary part is constant. In this way, we can study the WBL in the stationary situation by imposing $\Lambda(\varepsilon) = 0$ and $\Gamma^\alpha(\varepsilon) = \Gamma^\alpha$.

4.2.2 Time-dependent case: WBL approximation

Here, we follow 3.3.2 closely. We neglect the level-shift $\Lambda(\varepsilon)$, and consider energy-independent constant line-width functions such that $\Gamma(t) = \Gamma^L(t) + \Gamma^R(t)$, where $\Gamma_{L/R}(t) = \Gamma^{L/R}\left|u_{L/R}(t)\right|^2$. The self-energy is given by

$$\Sigma^r(t,t') = -\frac{i}{2}\Gamma(t)\delta(t-t'), \tag{4.45}$$

and with this self-energy it is possible to see that

$$\begin{aligned}\tilde{G}^{\mathrm{r}}_{\sigma\sigma,0(U)}(t,t') =& \mathcal{G}^{r,a}_{0(U)}(t,t')\exp\left\{\mp\int_{t'}^{t} dt_1 \frac{1}{2}\Gamma(t_1)\right\},\\ \mathcal{G}^{r,a}_{0(U)}(t,t') =& \mp i\theta(\pm t \mp t')\exp\left[-i\int_{t'}^{t} dt_1 \varepsilon_0(t_1)\right].\end{aligned} \tag{4.46}$$

We find a solution for the lesser Green's function by using Keldysh equation (C.9), whereby defining the useful quantities [72, 76][4]

$$A^{0(U)}_{\alpha}(\varepsilon,t) = \int \mathrm{d}t_1\, u_\alpha(t_1)\, \tilde{G}^{\mathrm{r}}_{\sigma\sigma,0(U)}(t,t_1)\, \mathrm{e}^{\mathrm{i}\varepsilon(t-t_1)}\exp\left(-\mathrm{i}\int_{t}^{t_1} dt_2 \Delta_\alpha(t_2)\right), \tag{4.47}$$

where the lesser Green's functions is shortly rewritten as;

$$G^{<}_{\sigma\sigma}(t,t) = \mathrm{i}\sum_{\alpha}\Gamma^{\alpha}\int\frac{\mathrm{d}\varepsilon}{2\pi} f_\alpha(\varepsilon)\left\{\left[1-n_{\bar{\sigma}}(t)\right]\left|A^0_\alpha(\varepsilon,t)\right|^2 + n_{\bar{\sigma}}(t)\left|A^U_\alpha(\varepsilon,t)\right|^2\right\}. \tag{4.48}$$

Analogous to the interacting stationary limit of the previous section, we can write the magnetic projection occupation by $n_\sigma = (1-n_\sigma)\, n^0 + n_\sigma n^U$, where it follows (similar to Eq. (4.43)) that

$$n_\sigma(t) = n_{\bar{\sigma}}(t) = \frac{n^0(t)}{1+n^0(t)-n^U(t)}, \tag{4.49}$$

where $n^{0(U)}(t)$ is given by:

$$n^{0(U)}(t) = \sum_{\mathrm{L,R}}\Gamma^{\alpha}\int\frac{\mathrm{d}\varepsilon}{2\pi} f_\alpha(\varepsilon)\left|A^{0(U)}_\alpha(\varepsilon,t)\right|^2. \tag{4.50}$$

Then, we write the current as a sum of outgoing and in-going current contributions from the right or left lead to the central region:

$$J_\alpha(t) = J^{\mathrm{out}}_\alpha(t) + J^{\mathrm{in}}_\alpha(t). \tag{4.51}$$

[4] As mentioned in section 3.3, $A^{0(U)}_\alpha(\varepsilon,t)$ is related to the spectral function in certain limits.

The first comes from the lesser Green's function integration over t_1 in Eq. (3.52). From looking at Eq. (4.48):

$$J_\alpha^{out}(t) = -\frac{2e}{\hbar}\Gamma^\alpha u_\alpha^2(t) n_\sigma(t). \tag{4.52}$$

The second contribution comes from the integration over the retarded Green's function of Eq. (3.52). By defining the useful quantities:

$$\begin{aligned} B_\alpha^0(\varepsilon,t) &= \int \mathrm{d}t_1 \left[1 - n_{\bar\sigma}(t_1)\right] u_\alpha(t_1)\, \tilde G^{\mathrm{r}}_{\sigma\sigma,0}(t,t_1)\, \mathrm{e}^{\mathrm{i}\varepsilon(t-t_1)} \exp\left(-\mathrm{i}\int_t^{t_1} dt_2 \Delta_\alpha(t_2)\right), \\ B_\alpha^U(\varepsilon,t) &= \int \mathrm{d}t_1 n_{\bar\sigma}(t_1)\, u_\alpha(t_1)\, \tilde G^{\mathrm{r}}_{\sigma\sigma,U}(t,t_1)\, \mathrm{e}^{\mathrm{i}\varepsilon(t-t_1)} \exp\left(-\mathrm{i}\int_t^{t_1} dt_2 \Delta_\alpha(t_2)\right), \end{aligned} \tag{4.53}$$

it found that this contribution is given by:

$$J_\alpha^{in}(t) = -\frac{e}{\hbar}\Gamma^\alpha u_\alpha(t) \sum_\sigma \int \frac{\mathrm{d}\varepsilon}{\pi} f_\alpha(\varepsilon)\, \mathrm{Im}\left\{B_\alpha^0(\varepsilon,t) + B_\alpha^U(\varepsilon,t)\right\}. \tag{4.54}$$

Finally, the relevant quantity to be studied in the following sections is the total current $J(t) = [J_L(t) - J_R(t)]/2$. The physics of the stationary and WBL approximation in both the noninteracting and interacting cases are studied in the next section. By letting $U = 0$ in the expressions of this section, it is immediate to see that we again consistently recover the results from the noninteracting case of section 3.3.2, just as in section 4.2.1.

4.3 Analysis of the JMW current

The analytical current in Eq. (4.54) would be impossible to fully elucidate without a numerical method to evaluate the one-dimensional integrals appearing in each relevant expression. Hence, we employ Julia programming language [132] to implement Simpson's rule method [133] for numerical integration of all *time-dependent* quantities above. The details of the numerical calculations can be found in Appendix H. The principal objective of this work is the study of time-dependent features of the current. Therefore, we did not numerically reproduce the simple numerical integrals in Eq. (4.41) for the stationary case, but only for the time-dependent one. Even so, we present the results of [76] for this case for further discussion and consistency in section 4.3.1. Our analysis follows the same results for the stationary and time-dependent currents as studied in [72, 76]. The temperature parameter is chosen so that $T > T_K$ where T_K follows from Eq. (2.31)[5]. As such, the relevant cases to consider are:

1. *Time-independent case*: we consider the stationary value obtained by the current due to a **constant applied voltage**, (whose analogous to the *time-dependent* situation is a pulse-like driving voltage of infinite duration) for different configurations and voltages.

[5] We recall from the discussion in chapters 2 and 3 that the HIA does not account for Kondo physics present at higher order correlation effects.

2. *Time-dependent case*: first we consider a **pulse-like driving** voltage of a certain duration, and second, a **harmonic modulation** voltage for different configurations.

In the calculations below, all energy quantities (ε_0, μ_R, μ_L, U, Γ_R, Γ_L, $\Delta_{0(L)(R)}$, Δ) are measured in units of $\Gamma = \Gamma_R + \Gamma_L = 1$. As an example, if ε_0 is given with a numerical value of -5.0, we imply $\varepsilon_0 = -5.0\,\Gamma$. In addition, when we set $T = 0.1$, we mean $k_B T = 0.1\,\Gamma$, $\omega = 0.2$ (frequency in the harmonic driving case of section 4.3.2) implies $\omega = \hbar\omega = 0.2\,\Gamma$. Time is also measured in units of $\hbar/\Gamma$.

4.3.1 Time-independent case: current *VS* voltage curves

We consider the case of a constant voltage in the stationary limit, where the current has reached a stationary value for the applied voltage. Then, a current VS voltage curve is obtained as customary in quantum transport calculations (see section 2.1). Figures 4.1 and 4.2 are the curves obtained in Ref. [76], where the authors solved Eq. (4.41) and use the Hartree-Fock (HF) approximation [75]. In addition, found in the literature is the more sophisticated noncrossing approximation (NCA) [45, 134] for the electronic correlations, employed by the authors as a benchmark method for the approach in the time-independent regime, since the NCA is known to yield better results and encompass a wider range of physics[6].

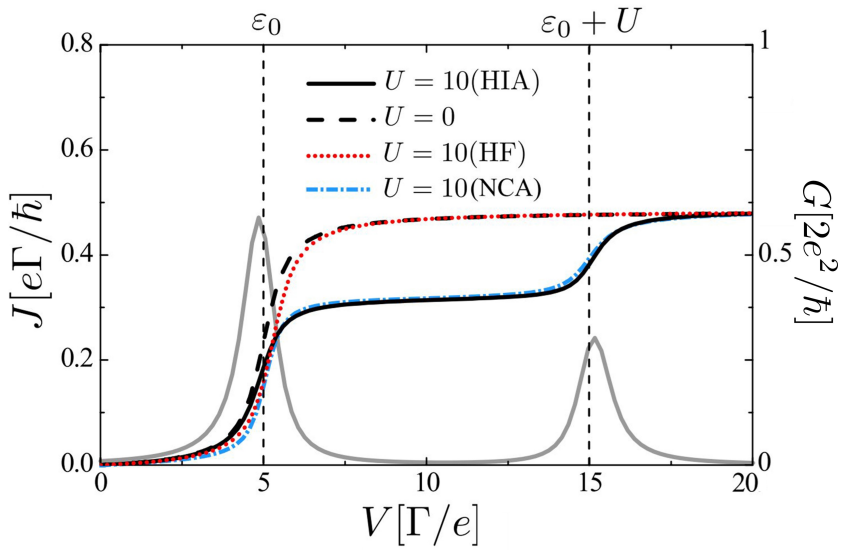

Figure 4.1: Current *VS* voltage for $U = 10$, $\mu_{\rm R} = 0$, $\mu_{\rm L} = V$, $\varepsilon_0 = 5$, $T = 0.1$, $\Gamma_{\rm L} = \Gamma_{\rm R} = 0.5$, in the HIA (black solid line), non-interacting case (black dashed line), Hartree-Fock (red dotted line) and non-crossing approximations (blue dotted line). The conductance is calculated from the formalism employed to obtain Eq. (2.8) (grey curve). (Taken from [76])

[6]Relevant to our work, it suffices to mention that the NCA encompasses Kondo physics and it is, therefore, a better many-body approximation to benchmark the HIA [45].

In general, the applied bias V rises the chemical potential μ_L so that $\mu_L - \mu_R = V$ inducing a nonequilibrium situation in this transport window. The energy of the level and the interacting Coulomb parameter determine the characteristic energies ε_0 and $\varepsilon_0 + U$ of the two transport channels steaming from the Hubbard band splitting in the quantum dot. The current increases as soon as the transport channels are included in the transport window, reaching a resonance closed to $V = \varepsilon_0$. Here, the channel becomes degenerate with the Fermi sea of the left lead and interference improves electron transfer to the device. The same happens at $\varepsilon_0 + U$ with a lower current increase due to the additional cost and two-body effects of the Coulomb repulsion[7]. However, the Coulomb repulsion does not generally lowers the total current with respect to the $U = 0$ case as seen in the left panel of Figure 4.2. For $\varepsilon_0 < V < \varepsilon_0 + U$ the current through the device is constant akin to the conductance quantization phenomena in nanostructures (zero conductance here). For reference, the conductance is computed from the formalism depicted in section 2.2 and we see how it behaves according to Figure 2.7, acquiring resonances at the transport channel energies. For a better comparison, we see how the HF approach yield results very closed to the noninteracting case and completely disagrees in the plateau region transitions as it does not account for the additional transport channel coming from the interacting Coulomb energy. The HIA is bench-marked against the NCA, which is known to contain Kondo physics and usually yields wider Hubbard bands. The difference between these results is more visible in the case $\varepsilon_0 = 0$ (left panel of Figure 4.2) due to the incipient Kondo resonance from the occupied level in resonance with the chemical potentials of the leads for $V = 0$. Double occupancy requires higher bias voltages here, promoting the effect of the spin degree of freedom. Consequently, lower temperatures would increase the disagreement. This is not observed in the case $\varepsilon_0 = -5$, where the double occupancy is reached more quickly with the rise of the bias voltage.

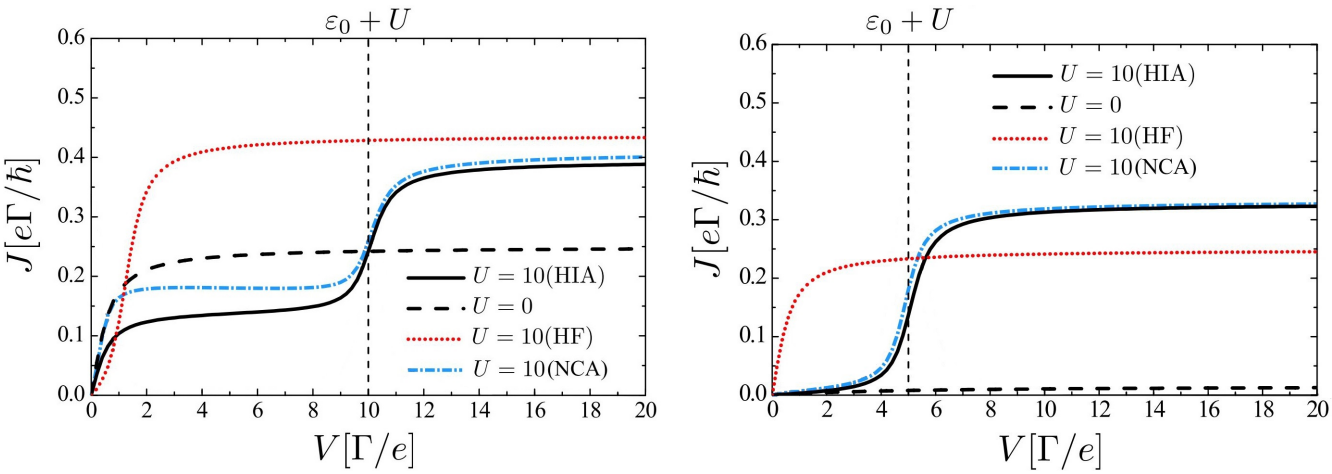

Figure 4.2: Same as figure 4.1, but with $\varepsilon_0 = 0$ (left) and $\varepsilon_0 = -5$ (right). (Taken from [76])

[7]This follows from the spectral weights of each Hubbard bands: $1 - n_{\bar{\sigma}}$ for the energy ε_0 and $n_{\bar{\sigma}}$ for $\varepsilon_0 + U$.

4.3.2 Time-dependent case: pulse-like & harmonic modulation

For the time-dependent case, following Ref. [76] we consider two relevant cases:

1. *Pulse-like driving*: We consider rectangular pulses such that:

$$\Delta_{\mathrm{L/R}}(t) = [\theta(t) - \theta(t-s)]\Delta_{\mathrm{L/R}}, \quad \varepsilon_0(t) = \varepsilon_0 + [\theta(t) - \theta(t-s)]\Delta, \quad u_{\mathrm{L/R}}(t) = 1, \tag{4.55}$$

where s is the time pulse duration, and Δ and $\Delta_{L/R}$ are the amplitudes of the pulse given in units of $(\hbar/\Gamma)$ and (Γ) respectively. In the WBL, this implies $\Gamma^{\mathrm{L/R}}(t) = \frac{1}{2}\Gamma$ and $\Sigma_\sigma(t) = -\frac{\mathrm{i}}{2}\Gamma$.

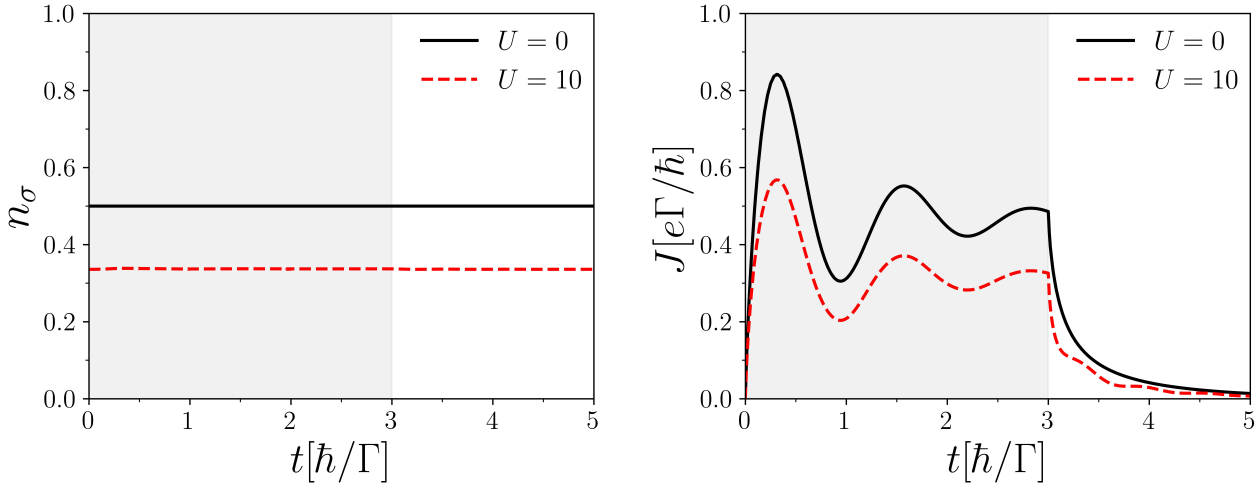

Figure 4.3: Occupancy per spin $n_\sigma(t)$ (left) and time-dependent current $J(t)$ (right) at the dot (top) in the case of pulse modulation with $\Gamma_{\mathrm{L}} = \Gamma_{\mathrm{R}} = 0.5$, $T = 0.1$, $\mu_{\mathrm{L}} = 0$, $\mu_{\mathrm{R}} = 0$, $\varepsilon_0 = 0$, $\Delta_{\mathrm{L}} = 10$, $\Delta_{\mathrm{R}} = 0$, $\Delta = 5$, $s = 3$, for $U = 0$ and $U = 10$. The gray area depicts the pulse duration.

In general, the transport window is determined by $\delta = (\mu_L - \Delta_L) - (\mu_R - \Delta_R)$. The Hubbard bands are centered around the characteristic transport channel energies $E_1 = \varepsilon_0 + \Delta$ and $E_2 = \varepsilon_0 + \Delta + U$. The essence of time-dependent calculations is the controlled shifting of these transport channel energies and the transport window. The spectral weights associated with each channel reflect the spin occupations: $n_\sigma < 1/2$ implies a favorable single electron occupancy $(1 - n_\sigma > 1/2)$, and $n_\sigma > 1/2$ implies a favorable double electron occupancy $(1 - n_\sigma < 1/2)$. In Figure 4.3 above, the dot occupancy for $U = 0$ approaches $1/2$ as E_1 is symmetrically positioned about the transport window, resulting in unchanged occupancy over time $(J_{\mathrm{L}}(t) = -J_{\mathrm{R}}(t))$. Similarly, in the HIA, dot occupancy remains constant at $1/3$, due to the symmetrical position of the lower Hubbard band characteristic energy E_1 with respect to the window ($\delta = 10$ and $\varepsilon_0 = 5$), which, according to Eq. (4.42), implies $n_{\bar{\sigma}} = 1/3$ ($\bar{f}(\varepsilon) = 1/2$ for the n^0 lower Hubbard band). For both finite U and $U = 0$, the current exhibits oscillations with the same period, transiently tending towards an

equilibrium value as electrons bounce between the leads, with a dominant contribution from the left lead due to the value of $\mu_L - \Delta_L$. However, for finite U, the current is smaller as only the E_1 channel contributes to transport within the transport window, whereas for $U = 0$, both do. The results presented here are in complete agreement with the ones presented in Ref. [76], revealing the strictness of the analytical expression retrieved for the current, main objective of this work.

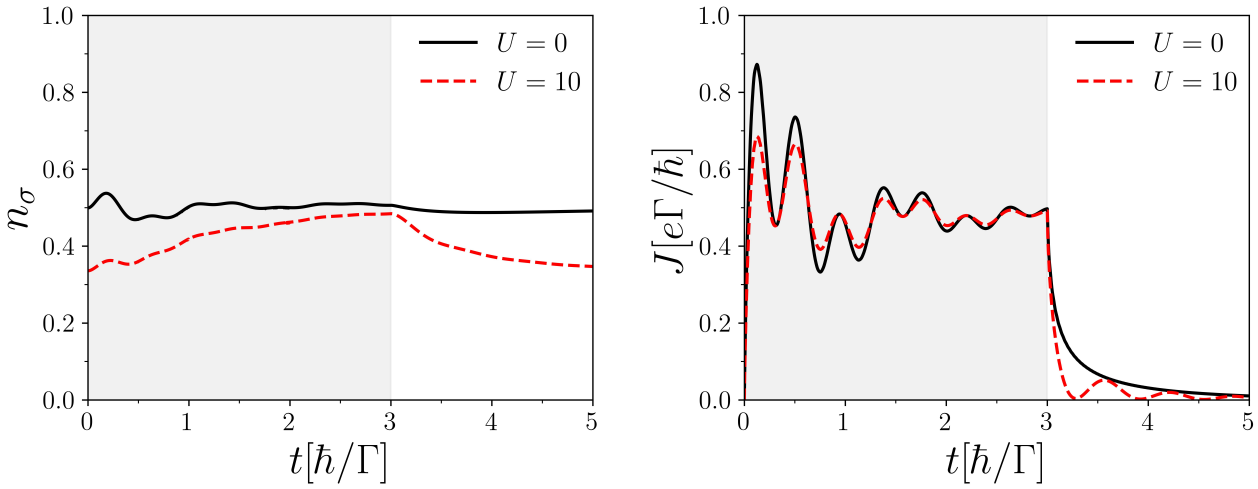

Figure 4.4: Same as Figure 4.3, but for $\Delta_L = 20$, thus ensuring a higher bias window.

When both channels lie in the transport window (Figure 4.4) the current differences are attenuated and the high bias voltage $\Delta_L = 20$ produces a complex time dependence. We recover the same results as in Ref. [76]. We note that E_1 and E_2 have an asymmetric distribution inside the transport windows. From Eq. (4.50), we can see that n^0 and n^U are in general different and the occupancy varies in time while still favoring the single-electron occupancy due to the high cost of E_2 relative to the transport window.

In Figure 4.5, parameters are chosen to illustrate the Coulomb blockade effect. Differing from the parameters chosen in Ref. [76] for the same purpose, we chose $\Delta = 0$ to better differentiate the transport channel energies and transport window. We also calculated the n_σ and $J(t)$ for $U = 0$. At all times, E_1 is below the transport window, making electron occupancy of the energy level very likely. Consequently, for $U = 0$, $n_{\bar{\sigma}} \approx 1$, favoring double occupancy for finite U ($n_{\bar{\sigma}} > 1/2$). For $t > 0$, the current oscillates due to the initial bias onset and quickly reaches zero, indicating no conduction. In the interacting regime, the additional transport channel with characteristic energy E_2 lies inside the transport window for $t > 0$, allowing the quantum dot to conduct electricity. This transition to a conducting regime demonstrates the Coulomb blockade effect.

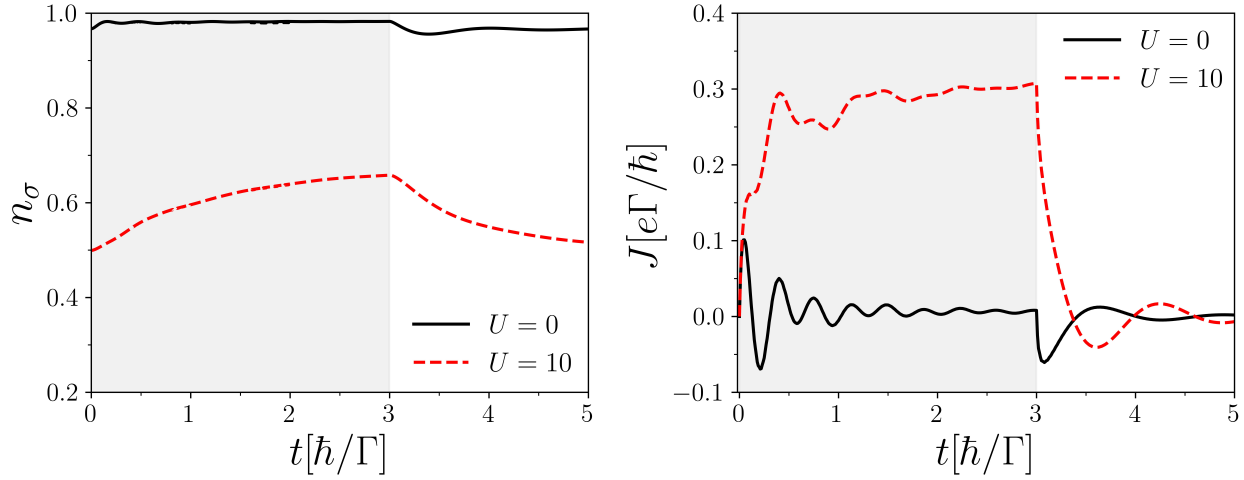

Figure 4.5: Same as Figure 4.3, but for $\varepsilon_0 = -5$ and $\Delta = 0$, thus permitting the visualization of the Coulomb blockade effect.

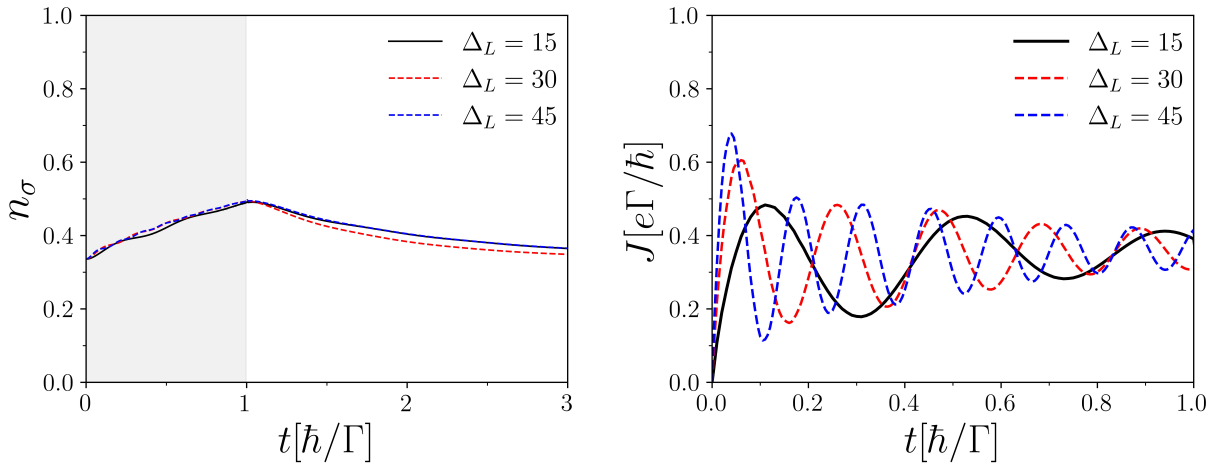

Figure 4.6: Occupancy per spin $n_\sigma(t)$ (left) and current $J(t)$ (right) in the case of step voltage for different values of Δ_L, for $\mu_\mathrm{L} = \mu_\mathrm{R} = 0,\ \varepsilon_0 = 0,\ U = 10,\ T = 0.1,\ \Delta_\mathrm{R} = \Delta = 0,\ s \geq 1$.

The current dependency for different values of Δ_L and temperature k_BT (while keeping other parameters constant) is depicted in Figures 4.6 and 4.7. Once again, the results presented here are in excellent agreement with the results in Ref. [76]. For completeness, we also computed the dot occupancy in these cases (left panel in Figures 4.6 and 4.7). Notably, if all parameters remain unchanged (as in Figure 4.4), we can deduce a simple time dependence for the current. Higher bias increases both the amplitude and period of the oscillations (note the phase factor in Eq. (4.47)) while preserving the steady-state value of the current (E_1 and E_2 remain the same and within δ in

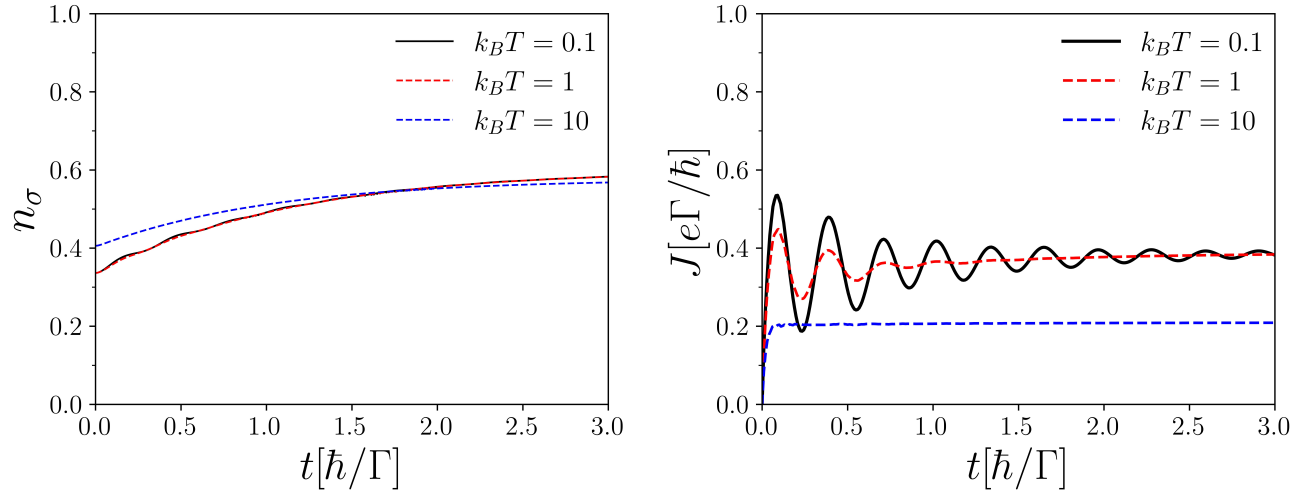

Figure 4.7: Occupancy per spin $n_\sigma(t)$ (left) and current $J(t)$ (right) in the case of step voltage for different temperatures, for $\mu_{\rm L} = \mu_{\rm R} = 0,\ \varepsilon_0 = 0,\ U = 10,\ \Delta_{\rm L} = 20,\ \Delta_{\rm R} = \Delta = 0,\ s \geq 3$.

all cases). As expected, high temperatures are detrimental to current values due to the destruction of interference and high heat fluctuations, forcing the system to reach a steady state in very short time scales, while moderate temperatures could not affect the period. Generally, complex time dependence is attained for small k_BT [76], and dot occupancy is not intricate in both Figures 4.7 and 4.7.

2. *Harmonic modulation*: We consider a harmonic modulation voltage of frequency ω for the left and right leads ("L" and "R") and the quantum dot level ("0"), akin to references [76] and [72]:

$$\Delta_{\rm L/R,0}(t) = \Delta_{\rm L/R,0}\cos(\omega t) \tag{4.56}$$

In Figure 4.8, we observe the time-dependence of dot occupancy and current due to in-phase voltage modulation. We observe an excellent agreement with the results obtained in Ref. [76]. For finite U, the dot occupancy is close to 1/3 but exhibits slight oscillations due to the statistical spectral weights of the Hubbard bands. For $U = 0$, the constant symmetric positioning of the E_1 channel within the transport window explains the constant dot occupancy. For both finite U and $U = 0$, the current becomes periodic in time due to forced periodic modulation, as studied in [72, 135] for $U = 0$. In both cases, the current exhibits the same period, with the HIA showing additional oscillations. A smaller amplitude is observed as the higher Hubbard band, associated with the E_2 channel, moves periodically from 10 to 20 while $\mu_L - \Delta_L$ shifts from 20 to 0, periodically bordering and exiting the transport window $\delta(t)$. The wide-band limit's adiabatic character is evident in the system's rapid response to periodic modulation.

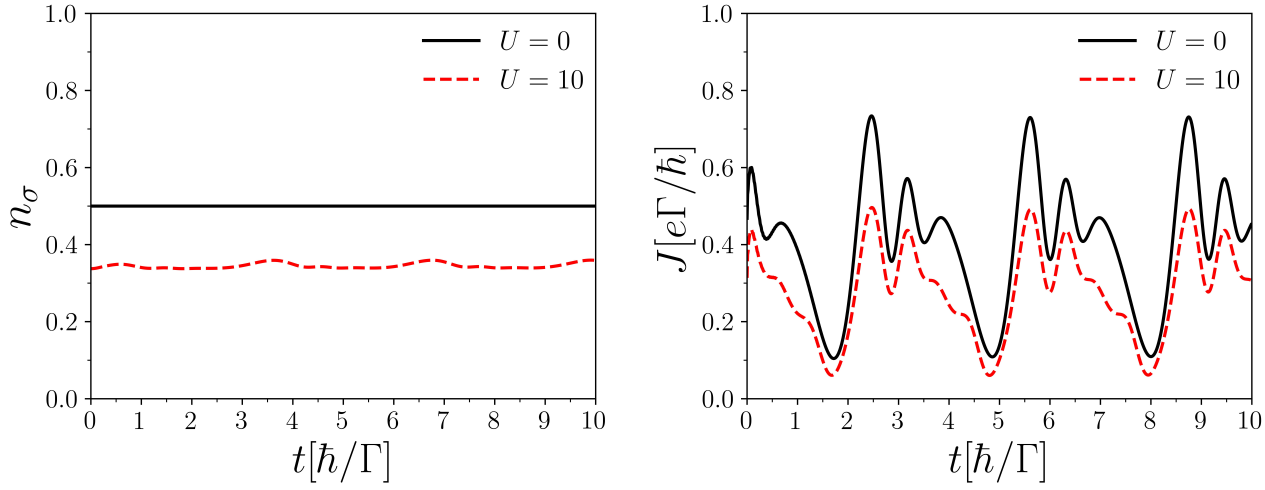

Figure 4.8: Time dependence of current (top) and dot occupancy per spin (bottom) in the case of harmonic modulation, for $\Gamma_{\rm L} = \Gamma_{\rm R} = 0.5$, $T = 0.1$, $\mu_{\rm L} = 10$, $\mu_{\rm R} = 0$, $\varepsilon_0 = 5$, $\Delta_{\rm L} = 10$, $\Delta_{\rm R} = 0$, $\Delta = 5$, $\omega = 2$, $U = 0$ (exact solution) and $U = 10$ (HIA).

With the discussions of the previous results, we have characterized relevant features of the quantum transport properties of the interacting quantum dot systems. Using the NEGF technique, we have obtained the observable characterizing transport in this work, namely the charge current in the JMW formalism. Analytical results were obtained based on the Hubbard band procedure while relying in the HIA for electronic correlations and WBL for the embedding self-energy. In the next chapters, we summarize and highlight the key aspects of this work, and mention some possible avenues towards a more complete understanding of the system on upcoming projects.

5 Conclusions

In this chapter, we present the final remarks and conclusions relevant to this work. We start with an overview of the main points concerning the construction and analysis of quantum transport through the interacting quantum dot system. Finally, we discuss some perspectives and advanced methods to build upon our current understanding of the quantum transport properties.

5.1 Conclusions

In Chapter 2, we explore the primary components necessary for constructing an interacting quantum dot system (IQDS). Initially, we establish the fundamental paradigm of interacting electrons in solids, known as the Hubbard model. We outline its essential assumptions and limitations, discussing significant aspects of its complex physics to elucidate the formation of the quasiparticle band structure, known as Hubbard bands. We then discuss the Anderson and Kondo models, examining the impact of a continuum (represented by a metal as a conducting sea) on the spectrum of an impurity atom. This includes addressing localized magnetic moment formation and the resistance minimum problem explained by the Kondo model. The connection between these models via the Schrieffer-Wolff transformation allows us to focus on the Anderson model, disregarding Kondo physics, as the fundamental model underlying the significant characteristics of interacting systems. Subsequently, we discuss single-electron transport and quantum dots, culminating in constructing the IQDS to simulate the classic two-terminal quantum transport setup. The Coulomb blockade effect in QDs is examined to illustrate how Coulomb repulsion influences single-electron transport.

In Chapter 3, we detail the time-dependent nonequilibrium Green's functions (TDNEGF) approach, the core theoretical method for studying the dynamics of many-body interacting quantum systems. We discuss the physical insights of this approach, including the Schwinger-Keldysh contour, the natural perturbative treatment of interactions, and the equation of motion method. The Hubbard-I approximation (HIA) is proposed as the perturbative approximation employed in this work to describe electronic correlation effects. Our system of interest is defined as a quantum open system, highlighting key concepts of this paradigm. The separation into environment (metallic reservoirs) and system (quantum dot) degrees of freedom allows for defining the embedding self-

energy, representing all environmental effects on the system. We examine the wide-band limit, capturing the essential physics of the lead-central device interaction that facilitates analytical solutions. Finally, we derive and apply the Jauho, Meir, and Wingreen (JMW) formalism for charge current to a noninteracting quantum dot system in both stationary and time-dependent regimes. The charge current is proposed as the fundamental observable, revealing the quantum transport features of the system, setting the stage for applying the method to the system with interactions.

In Chapter 4, we apply the formalism to the interacting problem within the HIA and the wide-band limit. The HIA, which does not account for Kondo physics and has a mean-field character, defines quasiparticle Hubbard bands and their respective Green's functions to obtain closed equations of motion for the propagators. These can be solved analytically to yield a closed expression for the charge current within the JMW formalism in both stationary and time-dependent regimes. A numerical method was developed in Julia for calculating the time-dependent current. Various transport calculations were presented in both stationary and time-dependent regimes, achieving excellent agreement with results previously reported in Ref. [76] for the case of the time-dependent driving, validating the analytical calculations and correct application of the algorithm in Appendix H. Essentially, the bias voltage or time-dependent modulations control and shift the transport channel energies and the system's transport window. The interplay of these quantities determines the current response for given parameter values. Generally, if the transport channel lies within the transport window, the current through the system is enhanced. The interacting situation presents richer physics due to additional transport channels from Hubbard band splitting and the Coulomb blockade effect. In the stationary case, Coulomb repulsion is not always detrimental to the current, and the HIA results showed accuracy when benchmarked against the NCA approximation, except where the incipient Kondo effect is evident. Overall, the HF method is insufficient and inaccurate for studying transport [76].

In the time-dependent regime, pulse-like and harmonic driving voltages were studied to obtain previously reported results. In some cases, the current exhibits periodic transient oscillations, while in other instances, varying parameters lead to a complex time dependence. We also studied the effects of bias voltage and temperature on the current and dot occupations, illustrating the Coulomb blockade-conducting transition. Crucially, temperature reduces both the period and amplitude of current oscillations, while higher biases increase them. Generally, the current reaches a transient state depending only on the transport channel energies and the transport window. Additionally, whenever the higher Hubbard band was favored by the transport window, dot occupancy tended to favor double occupancy ($n_\sigma > \frac{1}{2}$), making transport more intricate.

In Chapter 4 we present key results forming the core of this work, utilizing the developed and applied formalism. The IQDS is a fundamental model system, serving as an indispensable starting point for characterizing complex systems suitable for realistic experimental scenarios. This study provides a comprehensive introduction to the fundamental concepts and analysis of quantum transport in interacting quantum systems. Although the perturbative nature of the method and chosen approximation do not cover all regimes, particularly Kondo physics, it provides analytical solutions for quantities characterizing the system's relevant dynamics.

5.2 Perspectives

The charge current is not the only observable relevant to quantum transport descriptions. A natural extension of this work within the HIA would be the calculation of the time-dependent conductance through the junction and the time-dependent spectral density to elucidate how different modulations affect the system's spectral properties. Calculations could include spin-dependent processes from the effect of magnetic leads with a corrected band structure $\varepsilon_{\mathbf{k}\sigma} \to \varepsilon_{\mathbf{k}\sigma} + \Delta_\sigma(t)$, where different spin contributions to the current equations in (4.54) and (4.52) emerge within the realm of spin transport [136].

The NEGF approach is a powerful and versatile tool for studying open quantum systems and quantum transport phenomena. It excels in treating various regimes, scales, and phenomena uniformly. However, its perturbative nature limits its application to realistic systems with high computational complexity and non-local interactions, where non-perturbative solutions may yield significantly different results compared to finite or infinite summation of diagrams [137]. The scope of this approach extends beyond the methods and results discussed in this work. For instance, the HIA approximation is an initial step beyond the Hartree-Fock treatment but remains a mean-field approximation. Consequently, Kondo physics and other relevant scales are absent from the propagator solutions. As such, the next extension of this work could include calculating the same transport quantities in higher-order approximations, such as the second Born approximation, which can accurately describe Kondo physics and other relevant scales, attaining a more complete characterization of the indispensable interacting quantum dot system. This would make the transition to the double-site quantum dot, or general lattice site systems, more transparent and natural. Additionally, as the reservoirs' spectral properties are increasingly influenced by device dynamics and the lead-device interface becomes more complex, the wide-band limit simplifications can render the open system dynamics description inaccurate.

Solving the propagators on the Schwinger-Keldysh contour is computationally expensive even for short time scales, with costs increasing rapidly with time and system size [138]. Along these lines, moving towards numerically exact approaches offers promising improvements in understanding interacting systems, such as hierarchical equations of motion, tensor network, or dynamical mean field theory approaches [50, 51, 139]. Quantum Monte Carlo, tensor network algorithms, and path integral formulations have been proposed to consider higher-order Feynman diagrams for interactions [140–142]. For a more realistic physical realization of leads, numerical approaches have been proposed to go beyond the wide-band limit, addressing more intricate lead-device interfaces and energy scales associated with strong environment-system effects [143–145]. Pursuing these approaches constitutes a promising direction for future work related to this thesis.

With this final remark, we conclude our work. Our study has illuminated the complex many-body physics and formalism of transport in interacting quantum systems while maintaining an introduction with a pedagogical and accessible narrative. We hope the reader finds this initial exploration both useful and inspiring, encouraging further research into advanced and exciting areas of this field.

6 Appendices

A

Green's function of a degenerated Fermi liquid

Here, we calculate the Green's function of a degenerate Fermi liquid of non-interacting fermions in its ground state. We take the heat bath into account by using a Heisenberg representation where the heat bath's contribution to the energy is subtracted away, so that

$$\hat{H} = \hat{H}_0 - \mu\hat{N} = \sum_{\sigma} \varepsilon_{\mathbf{k}} \hat{c}^{\dagger}_{\mathbf{k}\sigma} \hat{c}_{\mathbf{k}\sigma}, \tag{A.1}$$

is the Hamiltonian of the system and $\varepsilon_{\mathbf{k}} = \frac{\hbar^2 k^2}{2m} - \mu$ the dispersion relation. The ground state for a fluid of fermions is given by

$$|\phi\rangle = \prod_{\sigma|\mathbf{k}|<k_f} \hat{c}^{\dagger}_{\mathbf{k}\sigma}|0\rangle. \tag{A.2}$$

In the Heisenberg representation, $\hat{c}^{\dagger}_{\mathbf{k}\sigma}(t) = e^{i\varepsilon_{\mathbf{k}}t}\hat{c}^{\dagger}_{\mathbf{k}\sigma}$, $\hat{c}_{\mathbf{k}\sigma}(t) = e^{-i\varepsilon_{\mathbf{k}}t}\hat{c}_{\mathbf{k}\sigma}$. For forward-time propagation, it is only possible to add a fermion above the Fermi energy:

$$\begin{aligned} \left\langle \phi \left| \hat{c}_{\mathbf{k}\sigma}(t)\hat{c}^{\dagger}_{\mathbf{k}'\sigma'}(t') \right| \phi \right\rangle &= \delta_{\sigma\sigma'}\delta_{\mathbf{k}\mathbf{k}'} e^{-i\varepsilon_{\mathbf{k}}(t-t')} \left\langle \phi \left| \hat{c}_{\mathbf{k}\sigma}\hat{c}^{\dagger}_{\mathbf{k}\sigma} \right| \phi \right\rangle \\ &= \delta_{\sigma\sigma'}\delta_{\mathbf{k}\mathbf{k}'} \left(1 - n_{\mathbf{k}}\right) e^{-i\varepsilon_{\mathbf{k}}(t-t')}, \end{aligned} \tag{A.3}$$

where $n_{\mathbf{k}} = \theta\left(|k_F| - |\mathbf{k}|\right)$. For backward-time propagation, it is only possible to destroy a fermion, creating a hole, below the Fermi energy (this is the adjoint process):

$$\left\langle \phi \left| \hat{c}^{\dagger}_{\mathbf{k}'\sigma'}(t')\, \hat{c}_{\mathbf{k}\sigma}(t) \right| \phi \right\rangle = \delta_{\sigma\sigma'}\delta_{\mathbf{k}\mathbf{k}'} n_{\mathbf{k}} e^{-i\varepsilon_{\mathbf{k}}(t-t')}, \tag{A.4}$$

so that

$$G(\mathbf{k}, t) = -i\left[\left(1 - n_{\mathbf{k}}\right)\theta(t) - n_{\mathbf{k}}\theta(-t)\right] e^{-i\varepsilon_{\mathbf{k}}t} \tag{A.5}$$

can be expanded as

$$G(\mathbf{k}, t) = \begin{cases} -i\theta_{|\mathbf{k}|-|\mathbf{k}_F|} e^{-i\varepsilon_{\mathbf{k}}t} & (t > 0) \\ i\theta_{|\mathbf{k}_F|-|\mathbf{k}|} e^{-i\varepsilon_{\mathbf{k}}t} & (t < 0). \end{cases} \tag{A.6}$$

The spectral properties due to the time-ordered structure of these functions are what allow us to consider the particle and hole contribution to the SPGF into a single entity. Now, let us calculate the Fourier transform of the Green's function:

$$\begin{aligned} G(\mathbf{k},\omega) &= -i\int_{-\infty}^{\infty} dt e^{i(\omega-\varepsilon_{\mathbf{k}})t} e^{-|t|\delta}\left[\theta_{k-k_F}\theta(t) - \theta_{k_F-k}\theta(-t)\right] \\ &= -i\left[\frac{\theta_{k-k_F}}{\delta - i\left(\omega-\varepsilon_{\mathbf{k}}\right)} - \frac{\theta_{k_F-k}}{\delta + i\left(\omega-\varepsilon_{\mathbf{k}}\right)}\right] = \frac{1}{\omega-\varepsilon_{\mathbf{k}}+i\delta_{\mathbf{k}}}, \end{aligned} \tag{A.7}$$

where $\delta_{\mathbf{k}} = \delta\,\mathrm{sgn}\left(k-k_F\right)$ is defined in the main text. The infinitesimal real number δ is employed as an analytical continuation to the complex plane as a mathematical tool for the evaluation of the integrals in (A.7). Finally:

$$G(\mathbf{k},\omega) = \frac{1}{\omega-\varepsilon_{\mathbf{k}}+i\delta_{\mathbf{k}}}. \tag{A.8}$$

Having obtained the GF of the problem, we can use it to calculate any observable. For example, we can compute the density of particles in a Fermi gas

$$\begin{aligned} \langle\hat{\rho}(x)\rangle &= \sum_{\sigma}\left\langle\psi_{\sigma}^{\dagger}\psi_{\sigma}\right\rangle = -\sum_{\sigma}\left\langle\phi\left|T\psi_{\sigma}\left(x,0^{+}\right)\psi_{\sigma}^{\dagger}(x,0)\right|\phi\right\rangle \\ &= -i(2S+1)G\left(\mathbf{x},0^{+}\right)\big|_{\mathbf{x}=0}, \end{aligned} \tag{A.9}$$

where S is the spin of the fermion, and 0^{+} implies that the second argument approaches zero from the right.

B

Langreth Rules of Analytical Continuation

In this appendix, we describe the procedure to obtain the Langreth rules in the Schwinger-Keldysh contour theory. We need to evaluate the following convolution integral for functions with two arguments lying in the Schwinger-Keldysh contour (denoted with "K"):

$$A(z_1, z_2) = \int_K B(z_1, \tau)\, C(\tau, z_2) \tag{B.1}$$

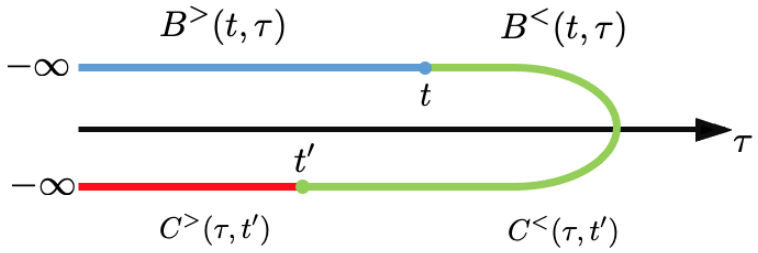

Figure B.1: Function B and C in the Keldysh Contour

Consider arguments $z_1 = t$ and $z_2 = t'$ lying in the contour as shown in Figure B.1. This is equivalent to calculating the lesser component of $A(z_1, z_2)$. The idea is to divide the contour integral (which runs from $-\infty$ to ∞) by parts while considering the arguments in the contour in the following form:

$$\int_{-\infty}^{-\infty} = \int_{-\infty}^{t} + \underbrace{\int_{t}^{t'}}_{1} + \underbrace{\int_{t'}^{-\infty}}_{2} = \int_{-\infty}^{t} \underbrace{- \int_{-\infty}^{t}}_{1} + \int_{-\infty}^{t'} \underbrace{- \int_{-\infty}^{t'}}_{2}. \tag{B.2}$$

The numbers in Eq. (B.2) denote the simple splitting of the given integral (either "1" or "2") after the second equal sign. Let us rewrite the first equal sign above in terms of the given functions $B(t,t')$ and $C(t,t')$. We pay special attention to the order of arguments in the contour for each function in each integral. If the first argument is later(earlier) in the Keldysh contour than the second, we are referring to the greater (lesser) component of the function in question. That is:

$$A^<(t.t') = \int_{-\infty}^{t} d\tau\, B^>(t,\tau)\, C^<(\tau,t') + \int_{t}^{t'} d\tau\, B^<(t,\tau)\, C^<(\tau,t') + \int_{t'}^{\infty} d\tau\, B^<(t,\tau)\, C^>(\tau,t'). \quad \text{(B.3)}$$

Then, we expand the integrals using the second equal in Eq. (B.2), regroup similar integral terms and use the relation between the Keldysh components of the Green's functions [7] to obtain:

$$\begin{aligned} A^<(t,t') &= \int_{-\infty}^{t} \big(B^>(t,\tau) - B^<(t,\tau)\big) C^<(\tau,t') d\tau + \int_{-\infty}^{t'} B^<(t,\tau)\big(C^<(\tau,t') - C^>(\tau,t')\big) d\tau \\ &= \int_{-\infty}^{\infty} \underbrace{\theta(t-\tau)\big(B^>(t,\tau) - B^<(t,\tau)\big)}_{B^R(t,\tau)} C^<(\tau,t') d\tau \\ &+ \int_{-\infty}^{\infty} B^<(t,\tau)\, \underbrace{\theta(t'-\tau)\big(C^<(\tau,t') - C^>(\tau,t')\big)}_{C^A(\tau,t')}\, d\tau. \end{aligned}$$

Finally, we obtain the Langreth rule for $A^<(t,t')$:

$$A^<(t,t') = \int_{-\infty}^{\infty} d\tau \big(B^R(t,\tau)\, C^<(\tau,t') + B^<(t,\tau) C^A(\tau,t')\big). \quad \text{(B.4)}$$

Similarly, we deduce yet another rule with arguments in a different organization:

$$A^>(t,t') = \int_{-\infty}^{\infty} d\tau \big(B^>(t,\tau)\, C^A(\tau,t') + B^R(t,\tau) C^>(\tau,t')\big). \quad \text{(B.5)}$$

C

Details of many-body perturbation theory

In this appendix, we outline the many-body perturbation scheme of quantum theories. Assume a Hamiltonian of the form $\hat{H} = \hat{H}_0 + \hat{H}_{int}$, where the interacting part is a generic simple four product of field operators with a given probability amplitude:

$$\hat{H}_{int} = \frac{1}{2} \int d\mathbf{x} d\mathbf{x}' v\left(\mathbf{x}, \mathbf{x}'\right) \hat{\psi}^{\dagger}(\mathbf{x}) \hat{\psi}^{\dagger}\left(\mathbf{x}'\right) \hat{\psi}\left(\mathbf{x}'\right) \hat{\psi}(\mathbf{x}). \tag{C.1}$$

In this section, we denote $1 = (\mathbf{x}_1, z_1)$. By deriving the SPGF contour-ordered GF $G\left(1, 1'\right) = -\mathrm{i}\left\langle \mathrm{T}_{\gamma}\left[\hat{\psi}_{\mathrm{H}}(1) \hat{\psi}_{\mathrm{H}}^{\dagger}\left(1'\right)\right]\right\rangle$ with respect to one of its time arguments, we obtain an equation of motion (EOM) for the SPGF such that:

$$\left(\mathrm{i}\partial_{z_1} - h(1)\right) G\left(1, 1'\right) = \delta\left(1, 1'\right) + \mathrm{i} \int \mathrm{d}\bar{1} v(1, \bar{1}) G_2\left(1, \bar{1}; 1', \bar{1}^{+}\right), \tag{C.2}$$

where

$$G_2\left(1, 2; 1', 2'\right) = (-\mathrm{i})^2 \left\langle \mathrm{T}_{\gamma}\left[\hat{\psi}_{\mathrm{H}}(1) \hat{\psi}_{\mathrm{H}}(2) \hat{\psi}_{\mathrm{H}}^{\dagger}\left(2'\right) \hat{\psi}_{\mathrm{H}}^{\dagger}\left(1'\right)\right]\right\rangle \tag{C.3}$$

is the two-particle GF. Martin and Schwinger developed a hierarchy for the propagators [64] in analogy to the usual BBGKY hierarchy in classical statistical mechanics [78]. An EOM for G_2 will be in terms of higher order propagators, constituting an infinite hierarchy. Instead of truncating the hierarchy by developing the diagrammatic rules from the application of Wick's theorem [4] to get the perturbative expansion for higher-order propagators, we define the many-body self-energy as a way of decoupling the dynamical evolution of the SPGF from that of the $(N > 1)$-particle GFs:

$$\int \mathrm{d}\bar{1} \Sigma_{\mathrm{MB}}(1, \bar{1}) G\left(\bar{1}, 1'\right) = \mathrm{i} \int \mathrm{d}\bar{1} v(1, \bar{1}) G_2\left(1, \bar{1}; 1', \bar{1}^{+}\right). \tag{C.4}$$

The many-body self-energy is a functional of the SPGF and contains all many-body effects from the interaction part of the theory. The problem at hand becomes that of evaluating the

many-body self-energy that comes from an infinite summation of Feynman diagrams. In this way, we arrive to

$$\left(\mathrm{i}\partial_{z_1} - h(1)\right) G\left(1,1'\right) = \delta\left(1,1'\right) + \int \mathrm{d}\bar{1}\Sigma_{\mathrm{MB}}(1,\bar{1})G\left(\bar{1},1'\right), \tag{C.5}$$

where $h(1)$ is the matrix representation of the quadratic part of the Hamiltonian, once a proper basis (for example an orthonormal spin-orbital basis) is chosen.

By defining a simple EOM for the non-interacting propagator G_0

$$\begin{aligned} \left(\mathrm{i}\partial_{z_1} - h(1)\right) G_0\left(1,1'\right) &= \delta\left(1,1'\right) \\ G_0\left(1,1'\right)\left(-\mathrm{i}\overleftarrow{\partial}_{z_1'} - h\left(1'\right)\right) &= \delta\left(1,1'\right), \end{aligned} \tag{C.6}$$

we can obtain the formal solution to eq. (C.5) which represents the Martin-Schwinger hierarchy. The solution is the Dyson equation:

$$G\left(1,1'\right) = G_0\left(1,1'\right) + \int \mathrm{d}\bar{1}\ \mathrm{d}\bar{2} G_0(1,\bar{1})\Sigma_{\mathrm{MB}}(\bar{1},\bar{2})G\left(\bar{2},1'\right). \tag{C.7}$$

The differential form of the Dyson equation (C.5), when analytically continued to get the $G^{<(>)}$ propagators leads to the quantum kinetic equation [146] or the Kadanoff-Baym equations. This thesis deals with a trivial time-dependence (trivial in the sense that the system Hamiltonian commutes at different times) that renders the integral form (C.7) of the Dyson equation useful. Consequent to the application of Langreth rules to the Dyson integral form, we obtain (in reduced notation):

$$G^{<} = \left(1 + G^{r}\Sigma^{r}\right) G_0^{<} \left(1 + \Sigma^{a}G^{a}\right) + G^{r}\Sigma^{<}G^{a}. \tag{C.8}$$

Equation (C.8) is the so-called Keldysh equation. Note how the self-energy also has different components depending on the position of its time arguments in the Schwinger-Keldysh contour. The quantity $G_0^{<}$ contains information on the initial configuration of the system. This is related to the physical realization of the quantum transport setup, as we see in the next section. In our case, it can be shown that $G_0^{<} = 0$, leading to

$$G^{<}\left(t,t'\right) = \int dt_1 \int dt_2 G^{R}\left(t,t_1\right)\Sigma^{<}\left(t_1,t_2\right)G^{A}\left(t_2,t'\right). \tag{C.9}$$

Systematic construction of the infinite terms in the self-energy functional in terms of Feynman diagrams leads to the regular many-body perturbation theory of quantum field theories [129]. A simple example (among many approximations for the self-energy [74]) is the expansion up to second-order for electron-electron interactions in the many-body self-energy:

$$\begin{aligned} \Sigma_{2B}[G]\left(1,1'\right) =& \Sigma_{\mathrm{HF}}[G]\left(1,1'\right) - \mathrm{i}^2 G\left(1,1'\right)\int \mathrm{d}\bar{1}\ \mathrm{d}\bar{2} v(1,\bar{1})G(\bar{1},\bar{2})G(\bar{2},\bar{1})v\left(1',\bar{2}\right) \\ &+ \mathrm{i}^2 \int \mathrm{d}\bar{1}\ \mathrm{d}\bar{2} v(1,\bar{1})G(1,\bar{2})G(\bar{2},\bar{1})G\left(\bar{2},1'\right) v\left(1',\bar{2}\right), \end{aligned} \tag{C.10}$$

where $\Sigma_{\mathrm{HF}}[G]$ is the Hartree-Fock contribution to the self-energy, given by

$$\Sigma_{\mathrm{HF}}[G]\,(1,1') = -\mathrm{i}\delta\,(1,1') \int \mathrm{d}\bar{1} v(1,\bar{1}) G\left(\bar{1},\bar{1}^{+}\right) + \mathrm{i}G\,(1,1')\,v\left(1^{+},1'\right). \tag{C.11}$$

The Feynman diagram representation of this self-energy approximation can be found in figure C.1.

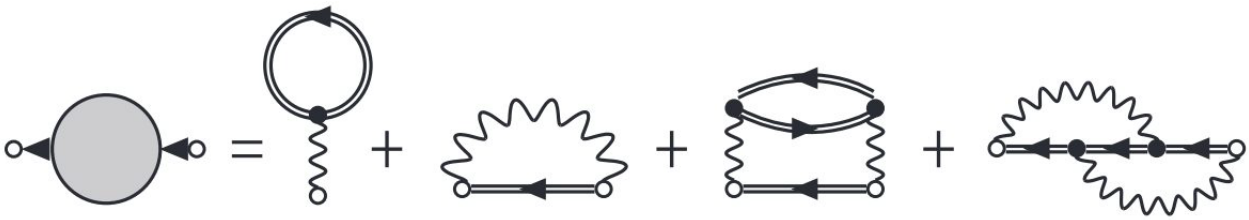

Figure C.1: Diagrammatic representation of the second Born self-energy. Besides the HF terms, it contains the first-order bubble diagram (third term) and the second-order exchange diagram (fourth term). (Figure from Ref. [67])

D

General quantum transport set up

Following the general formulation of Ref. [67], let us consider a very general setup depicted in Figure D.1; an arbitrary number of leads at different temperatures (T_1, T_2...) are coupled to a rather general complex central device D through a tunneling process. The total Hamiltonian in a second quantization spin-orbital orthogonal basis set $\varphi_{i\tau}(\mathbf{x}) = \varphi_i(\mathbf{r})\delta_{\tau\sigma}$ is given by $\hat{H}(z) = \hat{H}_D(z) + \sum_\alpha \hat{H}_\alpha(z) + \hat{H}_{\alpha D}(z)$ (with $\hat{H}_D(z) = \hat{H}_0(z) + \hat{H}_I(z)$), each term given by

$$\begin{aligned}
\hat{H}_0(z) &= \sum_{\mu\nu} h_{\mu\nu}(z)\hat{a}^\dagger_\mu \hat{a}_\nu + \sum_{\bar{\mu}\bar{\nu}} \Omega_{\bar{\mu}\bar{\nu}}(z)\hat{\phi}_{\bar{\mu}}\hat{\phi}_{\bar{\nu}}, \\
\hat{H}_I(z) &= \frac{1}{2}\sum_{ijkl\in D} v_{ijkl}(z)\hat{a}^\dagger_i \hat{a}^\dagger_j \hat{a}_k \hat{a}_l + \sum_{ij}\sum_{\bar{\mu}} \lambda^{\bar{\mu}}_{ij}(z)\hat{a}^\dagger_\mu \hat{a}_\nu \hat{\phi}_{\bar{\mu}}, \\
\hat{H}_\alpha(z) &= \sum_{ij\in\alpha} h_{\alpha ij}(z)\hat{d}^\dagger_i \hat{d}_j, \\
\hat{H}_{\alpha C}(z) &= \sum_{\mu\in C, i\in\alpha} \left(V_{\alpha\mu i}(z)\hat{a}^\dagger_\mu \hat{d}_i + \text{ h.c. } \right),
\end{aligned} \tag{D.1}$$

where the coefficients related to the probability amplitudes and energetic information for each physical process represented by those Hamiltonians are given by:

$$\begin{aligned}
h_{\mu\nu}(z) &= \int \mathrm{d}\mathbf{r}\, \varphi^*_\mu(\mathbf{r}) h(\mathbf{r}, z)\varphi_\nu(\mathbf{r}), \\
h_{\alpha ij}(z) &= \int \mathrm{d}\mathbf{r}\, \varphi^*_i(\mathbf{r}) h_\alpha(\mathbf{r}, z)\varphi_j(\mathbf{r}), \\
V_{\alpha\mu i}(z) &= \int \mathrm{d}\mathbf{r}\, \varphi^*_\mu(\mathbf{r}) V_\alpha(\mathbf{r}, z)\varphi_i(\mathbf{r}), \\
v_{ijkl}(z) &= \int \mathrm{d}\mathbf{r}\mathrm{d}\mathbf{r}' \varphi^*_i(\mathbf{r})\varphi^*_j(\mathbf{r}')\, v(\mathbf{r}, \mathbf{r}', z)\, \varphi_k(\mathbf{r}')\, \varphi_l(\mathbf{r}), \\
\lambda^{\bar{\eta}}_{\mu\nu}(z) &= \int \mathrm{d}\mathbf{r} \varphi^*_\mu(\mathbf{r}) \lambda_{\bar{\eta}}(\mathbf{r}, z)\varphi_\nu(\mathbf{r}).
\end{aligned} \tag{D.2}$$

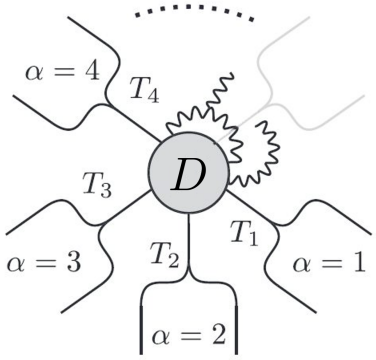

Figure D.1: General quantum transport set up of a complex quantum device D coupled to an arbitrary number of leads at different temperatures T_1, T_2... (Figure from Ref. [67])

Term by term the total Hamiltonian goes as follows: $\hat{H}_0(z)$ is the quadratic part for both bosons and fermions; bosons described by the multi-component $\hat{\phi}$-fields containing the displacement $\hat{\phi}_{\mu,1} = \hat{u}_\mu$ and the momentum operator $\hat{\phi}_{\mu,2} = \hat{p}_\mu$ for the mode μ, where we have introduced a composite index $\bar{\mu} = (\mu, \xi_\mu)$ with $\xi_\mu = 1, 2$, $\hat{H}_I(z)$ contains electron-electron interactions (first term) and electron-boson interactions, $\hat{H}_\alpha$ is the Hamiltonian of the environment part involving the α metallic lead of noninteracting fermions where $h_{\alpha ij}$ also contains a time-dependent external field often referred to as an applied bias voltage, and finally $\hat{H}_{\alpha C}(z)$ is the Hamiltonian connecting the central region and lead α by a tunneling process.

D.1 The embedding approach

Focusing on the SPGF, we can divide its matrix representation by sub-system blocks [67, 75] for each part of the system in the single particle basis chosen before. Once this basis is decided, we employ bold notation from now on for the matrix representation of operators such that $\hat{H}_D \to (\mathbf{H}_D)_{ij} = \langle i, \sigma | \hat{H}_D | j, \sigma \rangle$ For our particular choice of quantum transport setup, we decide for $\alpha = 2$, denoting left (L) and right leads (R) in the usual boundary-driven configuration [109] (Figure 3.3). With this in mind, we write:

$$\mathbf{G} = \begin{bmatrix} \mathbf{G}_{\mathrm{L}} & \mathbf{G}_{\mathrm{LD}} & \mathbf{G}_{\mathrm{LR}} \\ \mathbf{G}_{\mathrm{DL}} & \mathbf{G}_{\mathrm{D}} & \mathbf{G}_{\mathrm{DR}} \\ \mathbf{G}_{\mathrm{RL}} & \mathbf{G}_{\mathrm{RD}} & \mathbf{G}_{\mathrm{R}} \end{bmatrix}, \qquad \mathbf{H} = \begin{bmatrix} \mathbf{H}_{\mathrm{L}} & \mathbf{H}_{\mathrm{LD}} & 0 \\ \mathbf{H}_{\mathrm{DL}} & \mathbf{H}_{\mathrm{D}} & \mathbf{H}_{\mathrm{DR}} \\ 0 & \mathbf{H}_{\mathrm{RD}} & \mathbf{H}_{\mathrm{R}} \end{bmatrix}. \tag{D.3}$$

In this way, we further clarify notation in equation (D.3) by noticing (see (D.1))

$$(\mathbf{H}_\alpha)_{i,j} = (\mathbf{h}_\alpha)_{i,j} = h_{\alpha i,j}, \qquad (\mathbf{H}_{\alpha D})_{\mu,j} = (\mathbf{V}_\alpha)_{\mu,i} = V_{\alpha\mu i}, \qquad (\mathbf{H}_D)_{\mu,\nu} = (\mathbf{h})_{\mu,\nu} = h_{\mu i \nu}.$$

We can now start by projecting the general EOM (3.26) to the central device SPGFs,

$$i\partial_z \mathbf{G}\left(z,z'\right)=\delta\left(z,z'\right)\mathbf{1}+\mathbf{H}(z)\mathbf{G}\left(z,z'\right)+\int d\bar{z}\;\mathbf{\Sigma}_{\mathrm{MB}}(z,\bar{z})\mathbf{G}\left(\bar{z},z'\right), \tag{D.4}$$

and note how the matrix representation for the many-body self-energy $\mathbf{\Sigma}_{MB}$ is actually written as:

$$\mathbf{\Sigma}_{\mathrm{MB}}=\begin{bmatrix}0 & 0 & 0\\ 0 & \mathbf{\Sigma}_{\mathrm{MB,D}}\left[\mathbf{G}_D\right] & 0\\ 0 & 0 & 0\end{bmatrix}. \tag{D.5}$$

The many-body self-energy in Eq. (D.5) has nonvanishing entries only for indices in the region D. This is an immediate consequence of the fact that the diagrammatic expansion of the self-energy starts and ends with an interaction line which in our case is confined in the central region (see the first term in the first equation of Eq. (D.1)). This also implies that $\mathbf{\Sigma}^{MB}\left[\mathbf{G}_D\right]$ is a function of $\mathbf{G}_D$ only.

Now we can write a matrix form for (D.4) as follows:

$$\begin{aligned}i\partial_z\begin{bmatrix}\mathbf{G}_{\mathrm{L}} & \mathbf{G}_{\mathrm{LD}} & \mathbf{G}_{\mathrm{LR}}\\ \mathbf{G}_{\mathrm{DL}} & \mathbf{G}_{\mathrm{D}} & \mathbf{G}_{\mathrm{DR}}\\ \mathbf{G}_{\mathrm{RL}} & \mathbf{G}_{\mathrm{RD}} & \mathbf{G}_{\mathrm{R}}\end{bmatrix}_{(z,z')} &= \delta\left(z,z'\right)\mathbf{1}+\begin{bmatrix}\mathbf{H}_{\mathrm{L}} & \mathbf{H}_{\mathrm{LD}} & 0\\ \mathbf{H}_{\mathrm{DL}} & \mathbf{H}_{\mathrm{D}} & \mathbf{H}_{\mathrm{DR}}\\ 0 & \mathbf{H}_{\mathrm{RD}} & \mathbf{H}_{\mathrm{R}}\end{bmatrix}_{(z)}\begin{bmatrix}\mathbf{G}_{\mathrm{L}} & \mathbf{G}_{\mathrm{LD}} & \mathbf{G}_{\mathrm{LR}}\\ \mathbf{G}_{\mathrm{DL}} & \mathbf{G}_{\mathrm{D}} & \mathbf{G}_{\mathrm{DR}}\\ \mathbf{G}_{\mathrm{RL}} & \mathbf{G}_{\mathrm{RD}} & \mathbf{G}_{\mathrm{R}}\end{bmatrix}_{(z,z')}\\ &\quad+\int d\bar{z}\begin{bmatrix}0 & 0 & 0\\ 0 & \mathbf{\Sigma}_{\mathrm{MB,D}}\left[\mathbf{G}_D\right] & 0\\ 0 & 0 & 0\end{bmatrix}_{(z,\bar{z})}\begin{bmatrix}\mathbf{G}_{\mathrm{L}} & \mathbf{G}_{\mathrm{LD}} & \mathbf{G}_{\mathrm{LR}}\\ \mathbf{G}_{\mathrm{DL}} & \mathbf{G}_{\mathrm{D}} & \mathbf{G}_{\mathrm{DR}}\\ \mathbf{G}_{\mathrm{RL}} & \mathbf{G}_{\mathrm{RD}} & \mathbf{G}_{\mathrm{R}}\end{bmatrix}_{(\bar{z},z')}.\end{aligned}$$

Following the $(2,2)$ component of the set of equations resulting from using (D.3) in (D.4), we have:

$$\begin{aligned}i\partial_z\mathbf{G}_D&=\delta\left(z,z'\right)\mathbf{1}+\mathbf{H}_{DL}\mathbf{G}_{LD}+\mathbf{H}_D\mathbf{G}_D+\mathbf{H}_{DR}\mathbf{G}_{RD}+\int d\bar{z}\;\mathbf{\Sigma}_{\mathrm{MB,D}}(z,\bar{z})\mathbf{G}_D\left(\bar{z},z'\right)\\ &=\delta(z,z')\mathbf{1}+\mathbf{H}_D\mathbf{G}_D+\sum_\alpha\mathbf{H}_{D\alpha}\mathbf{G}_{\alpha D}\left(z,z'\right)+\int d\bar{z}\;\mathbf{\Sigma}_{\mathrm{MB,D}}(z,\bar{z})\mathbf{G}_D(\bar{z},z'),\\ \left[i\partial_z-\mathbf{H}_D(z)\right]\mathbf{G}_D\left(z,z'\right)&=\delta(z,z')\mathbf{1}+\sum_\alpha\mathbf{H}_{D\alpha}\mathbf{G}_{\alpha D}\left(z,z'\right)+\int d\bar{z}\;\mathbf{\Sigma}_{\mathrm{MB,D}}(z,\bar{z})\mathbf{G}_D\left(\bar{z},z'\right).\end{aligned} \tag{D.6}$$

For a projection to the αD components, one sees that:

$$\left[i\partial_z-\mathbf{H}_\alpha(z)\right]\mathbf{G}_{\alpha\mathrm{D}}\left(z,z'\right)=\mathbf{H}_{\alpha\mathrm{D}}\mathbf{G}_{\mathrm{D}}\left(z,z'\right). \tag{D.7}$$

As customary [20, 72], we can define a bare's GFs $\mathcal{G}_\alpha(z,z')$ for the isolated lead α such that:

$$\left[\mathrm{i}\partial_z-\mathbf{H}_\alpha\left(z\right)\right]\mathcal{G}_\alpha\left(z,z'\right)=\delta\left(z,z'\right)\mathbf{1}, \tag{D.8}$$

where the most relevant aspect of our theory is the fact that any time-dependence of the leads must be a trivial one, and we must consider fully non-interacting leads. Otherwise, we wouldn't be able to write

$$\begin{aligned}\int_\gamma \mathrm{d}\bar{z}\; \mathcal{G}_\alpha^{-1}(z,\bar{z})\,\mathcal{G}_\alpha(\bar{z},z') = \delta(z,z')\,\mathbf{1} = \int_\gamma \mathrm{d}\bar{z}\mathcal{G}_\alpha(z,\bar{z})\,\mathcal{G}_\alpha^{-1}(\bar{z},z')\\ \int_\gamma \mathrm{d}\bar{z}\Big[\mathrm{i}\partial_z - \mathbf{H}_\alpha(z)\Big]\delta(z,\bar{z})\,\mathcal{G}_{\alpha\alpha}(\bar{z},z') = \delta(z,z')\,\mathbf{1},\end{aligned} \tag{D.9}$$

so that

$$\Big[\mathrm{i}\partial_z - \mathbf{H}_\alpha(z)\Big]\delta(z,z') = \mathcal{G}_\alpha^{-1}(z,z'), \tag{D.10}$$

to then use Eq.(D.10) to substitute into Eq.(D.7) after multiplying the latter by $\delta(z,z')$ to finally get

$$\mathbf{G}_{\alpha D}(z,z') = \int_\gamma \mathrm{d}\bar{z}\; \mathcal{G}_\alpha(z,\bar{z})\,\mathbf{H}_{\alpha C}(\bar{z})\mathbf{G}_D(\bar{z},z'). \tag{D.11}$$

Equation (D.11) puts any hybrid environment-system propagator in terms of the propagators of each individual part, thus allowing the EOM to be written in terms of $\mathbf{G}_D$ only. Now we use Eq. (D.11) back into (D.6) to get a closed equation for $\mathbf{G}_D$ with its symmetric part also given by:

$$\begin{aligned}\Big[i\partial_z\mathbf{1} - \mathbf{H}_D(z)\Big]\mathbf{G}_D(z,z') = \delta(z,z')\,\mathbf{1} + \int d\bar{z}\; \mathbf{\Sigma}_D(z,\bar{z})\mathbf{G}_D(\bar{z},z'), \text{ and}\\ \mathbf{G}_D(z,z')\Big[-i\overleftarrow{\partial}_{z'}\mathbf{1} - \mathbf{H}_D(z')\Big] = \delta(z,z')\,\mathbf{1} + \int d\bar{z}\; \mathbf{G}_D(z,\bar{z})\mathbf{\Sigma}_D(\bar{z},z'),\end{aligned} \tag{D.12}$$

where we defined $\mathbf{G}_D(z,z')\Big[-i\overleftarrow{\partial}_{z'}\mathbf{1} - \mathbf{H}_D(z')\Big] = -i\partial_{z'}\mathbf{G}_D(z,z') - \mathbf{G}_D(z,z')\,\mathbf{H}_D(z')$ and the device many-body self-enery as $\mathbf{\Sigma}_D = \mathbf{\Sigma}_{\text{em}} + \mathbf{\Sigma}_{\text{MB},D}$, where the *embedding self-energy* is given by:

$$\mathbf{\Sigma}_{\text{em}}(z,z') = \sum_\alpha \mathbf{\Sigma}_{\text{em},\alpha}(z,z') = \sum_\alpha \mathbf{H}_{\text{C}\alpha}\;\mathcal{G}_{\alpha\alpha}(z,z')\,\mathbf{H}_{\alpha\text{C}}. \tag{D.13}$$

This separation of the self-energy allows for the many-body self-energy $\mathbf{\Sigma}_{\text{MB,D}}$ to contain any interactions coming from the device degrees of freedom only. The embedding self-energy $\mathbf{\Sigma}_{\text{em}}$ accounts for the influence of the leads on the device. In this thesis, only electron-electron interactions are considered, as we do not deal with bosonic degrees of freedom in any way.

E

Stationary form of the JMW current

Here, we deduce Eq. (3.56) in detail. We start by rewriting Eq. (3.52) in the following way (we let $\alpha = L, R$):

$$\begin{aligned} J_\alpha(t) = &-\frac{2e}{\hbar}\int\frac{d\varepsilon}{2\pi}\,\mathrm{Tr}\left\{\mathrm{Im}\int_{-\infty}^{t}d\tau\left[e^{-\frac{i}{\hbar}\varepsilon(t-\tau)}\Gamma^\alpha(\varepsilon)G^r(t-\tau)f_\alpha(\varepsilon)\right]\right\} \\ &-\frac{2e}{\hbar}\int\frac{d\varepsilon}{2\pi}\,\mathrm{Tr}\left\{\mathrm{Im}\int_{-\infty}^{t}d\tau\left[e^{-\frac{i}{\hbar}\varepsilon(t-\tau)}\Gamma^\alpha(\varepsilon)G^<(t-\tau)\right]\right\}. \end{aligned} \tag{E.1}$$

Now we define:

$$I_1 = \int_{-\infty}^{t}d\tau\left[e^{-\frac{i}{\hbar}\varepsilon(t-\tau)}\Gamma^\alpha(\varepsilon)G^r(t-\tau)f_\alpha(\varepsilon)\right], \tag{E.2}$$

$$I_2 = \int_{-\infty}^{t}d\tau\left[e^{-\frac{i}{\hbar}\varepsilon(t-\tau)}\Gamma^\alpha(\varepsilon)G^<(t-\tau)\right]. \tag{E.3}$$

We start by solving the integral in (E.3):

$$I_2 = \int_{-\infty}^{t}d\tau\, e^{-\frac{i}{\hbar}\varepsilon(t-\tau)}\Gamma^\alpha(\varepsilon)\int_{-\infty}^{\infty}\frac{d\omega}{2\pi}G^<(\omega)e^{-i\omega(t-\tau)} = \int_{-\infty}^{\infty}\frac{d\omega}{2\pi}\Gamma^\alpha(\varepsilon)G^<(\omega)\int_{-\infty}^{t}d\tau\, e^{\frac{i}{\hbar}(\varepsilon-\hbar\omega)(t-\tau)}.$$

We now analytically continue the previous integral (see reference [147]) to formally solve it:

$$I_2 = \lim_{\eta\to 0}\int_{-\infty}^{\infty}\frac{d\omega}{2\pi}\Gamma^\alpha(\varepsilon)G^<(\omega)\int_{-\infty}^{t}d\tau\, e^{\frac{i}{\hbar}(\varepsilon-\hbar\omega+i\eta)(t-\tau)}.$$

We perform a change in variables such that $t' = t-\tau$ and $dt' = -d\tau$. Limits change such that $-\infty \to \infty$ and $t \to 0$. Then we have:

$$\begin{aligned} I_2 &= \lim_{\eta\to 0}\int_{-\infty}^{\infty}\frac{d\omega}{2\pi}\Gamma^\alpha(\varepsilon)G^<(\omega)\int_{0}^{\infty}dt'\, e^{\frac{i}{\hbar}(\varepsilon-\hbar\omega+i\eta)t'} \\ &= \lim_{\eta\to 0}\int_{-\infty}^{\infty}\frac{d\omega}{2\pi}\Gamma^\alpha(\varepsilon)G^<(\omega)\frac{e^{\frac{i}{\hbar}(\varepsilon-\hbar\omega+i\eta)t'}}{\frac{i}{\hbar}(\varepsilon-\hbar\omega+i\eta)}\bigg|_0^\infty = -i\lim_{\eta\to 0}\int_{-\infty}^{\infty}\frac{d(\hbar\omega)}{2\pi}\Gamma^\alpha(\varepsilon)G^<(\omega)\frac{1}{(\varepsilon-\hbar\omega+i\eta)}. \end{aligned}$$

We now use the formula for Cauchy's principal value:

$$\frac{1}{\varepsilon - \hbar\omega + i\eta} = P\left(\frac{1}{\varepsilon - \hbar\omega}\right) - i\pi\delta(\varepsilon - \hbar\omega), \tag{E.4}$$

to obtain:

$$I_2 = \lim_{\eta\to 0}\int_{-\infty}^{\infty}\frac{d(\hbar\omega)}{2\pi}\Gamma^{\alpha}(\varepsilon)G^{<}(\omega)\left[\frac{-i}{\varepsilon - \hbar\omega} - \pi\delta(\varepsilon - \hbar\omega)\right].$$

Note from Eq. (E.1) that only the imaginary parts of I_1 and I_2 contribute to the integral. By definition, $G^{<}(\omega)$ is imaginary so the first term in the equation above can be neglected. Hence, we only have the delta function part where we straightforwardly obtain:

$$\mathrm{Im}\,(I_2) = -i\,\Gamma^{\alpha}(\varepsilon)G^{<}(\varepsilon). \tag{E.5}$$

Now we solve the integral in (E.2):

$$\begin{aligned} I_1 &= \int_{-\infty}^{t} d\tau\left[e^{-\frac{i}{\hbar}\varepsilon(t-\tau)}\Gamma^{\alpha}(\varepsilon)G^{r}(t-\tau)f_{\alpha}(\varepsilon)\right] \\ &= \Gamma^{\alpha}(\varepsilon)f_{\alpha}(\varepsilon)\int_{-\infty}^{\infty} d\tau\left[e^{-\frac{i}{\hbar}\varepsilon(t-\tau)}G^{r}(t-\tau)\right] = \Gamma^{\alpha}(\varepsilon)f_{\alpha}(\varepsilon)G^{r}(\varepsilon). \end{aligned}$$

Above, we used the fact that $G^{r}(t-\tau)$ is not defined for $t > \tau$ to extend the domain of integration to $+\infty$. Note how we basically have a Fourier transform which leads to the simple result shown above. Next, recall that $\mathrm{Im}\, z = -\frac{i}{2}(z - z^{*})$ for any complex number z. Also, $[G^{r}]^{*} = G^{a}$. Hence:

$$\mathrm{Im}\,(I_1) = -\frac{i}{2}\Gamma^{\alpha}(\varepsilon)f_{\alpha}(\varepsilon)\big[G^{r}(\varepsilon) - G^{a}(\varepsilon)\big]. \tag{E.6}$$

By using equations (E.5) and (E.6) into Eq. (E.1), we recover the result in Eq. (3.56).

F

Detailed calculations of the implementation of TDNEGF and JMW formalism in the quantum dot system

This appendix details all remaining commutators from chapter 4.

1. Calculation of $\left[\hat{H}_S(t), \hat{d}_\sigma(t)\right]$:

   -It is easy to see that:

$$\left[\hat{H}_M, \hat{d}_\sigma\right] = \sum_{k\alpha\sigma} \varepsilon_{k\alpha}(t)\left[\hat{c}^\dagger_{k\alpha\sigma}\hat{c}_{k\alpha\sigma}, \hat{d}_\sigma\right] = 0. \tag{F.1}$$

   This is based on the fact that we always have $\left\{\hat{c}^{(\dagger)}_{k\alpha\sigma}, d^{(\dagger)}_\sigma\right\} = 0$ as they belong to different Hilbert subspaces. For the next term, the device Hamiltonian, we have [1]

$$\left[\hat{H}_D, \hat{d}_\sigma\right] = \varepsilon_0 \sum_\Delta \left[\hat{d}^\dagger_\Delta \hat{d}_\Delta, \hat{d}_\sigma\right] + U\left[\hat{n}_\uparrow \hat{n}_\downarrow, \hat{d}_\sigma\right],$$

$$\left[\hat{d}^\dagger_\Delta \hat{d}_\Delta, \hat{d}_\sigma\right] = \left[\hat{n}_\Delta, \hat{d}_\sigma\right] = \hat{d}^\dagger_\Delta\left\{\hat{d}_\Delta, \hat{d}_\sigma\right\} - \left\{\hat{d}^\dagger_\Delta, \hat{d}_\sigma\right\}\hat{d}_\Delta = -\left\{\hat{d}^\dagger_\Delta, \hat{d}^\dagger_\sigma\right\}\hat{d}_\Delta = -\delta_{\sigma\Delta}\hat{d}_\Delta,$$

$$\left[\hat{n}_\uparrow \hat{n}_\downarrow, \hat{d}_\sigma\right] = \hat{n}_\uparrow\left[\hat{n}_\downarrow, \hat{d}_\sigma\right] + \left[\hat{n}_\uparrow, \hat{d}_\sigma\right]\hat{n}_\downarrow = -\delta_{\downarrow\sigma}\hat{n}_\uparrow\hat{d}_\downarrow - \delta_{\uparrow\sigma}\hat{d}_\uparrow\hat{n}_\downarrow = -\hat{d}_\uparrow\hat{n}_\downarrow.$$

   It follows that

[1] Some useful identities for fermionic operators that are used from now onward [124], where the subscripts "±" refer to the usual anticommutator (+) and commutator (−), are $[\hat{A}\hat{B}, \hat{C}] = \hat{A}[\hat{B}, \hat{C}]_\pm \mp [\hat{A}, \hat{C}]_\pm \hat{B}$ and $[\hat{A}, \hat{B}\hat{C}] = [\hat{A}, \hat{B}]_\pm \hat{C} \mp \hat{B}[\hat{A}, \hat{C}]_\pm$.

$$\left[\hat{n}_\sigma \hat{n}_{\bar{\sigma}}, \hat{d}_\sigma\right] = -\hat{d}_\sigma \hat{n}_{\bar{\sigma}}.$$

Putting it all together, we obtain

$$\left[\hat{H}_D, \hat{d}_\sigma\right] = \varepsilon_0 \sum_\sigma -\delta_{\sigma\Delta}\hat{d}_\sigma - U\hat{d}_\sigma \hat{n}_{\bar{\sigma}} = -\varepsilon_0 \hat{d}_\sigma - U\hat{d}_\sigma \hat{n}_{\bar{\sigma}}. \tag{F.2}$$

Similarly, we develop the tunneling Hamiltonian commutator:

$$\left[\hat{H}_T, \hat{d}_\sigma\right] = \sum_{k\alpha\Delta} V_{k\alpha}\left[\hat{c}^\dagger_{k\alpha\Delta}\hat{d}_\Delta, \hat{d}_\sigma\right] + V^*_{k\alpha}\left[\hat{d}^\dagger_\Delta \hat{c}_{k\alpha\Delta}, \hat{d}_\sigma\right],$$

$$\left[\hat{c}^\dagger_{k\alpha\Delta}\hat{d}_\Delta, \hat{d}_\sigma\right] = \hat{c}^\dagger_{k\alpha\sigma}\left\{\hat{d}_\Delta, \hat{d}_\sigma\right\} - \left\{\hat{c}^\dagger_{k\alpha\Delta}, \hat{d}_\sigma\right\}\hat{d}_\Delta = 0,$$

$$\left[\hat{d}^\dagger_\Delta \hat{c}_{k\alpha\Delta}, \hat{d}_\sigma\right] = \hat{d}^\dagger_\Delta\left\{\hat{c}_{k\alpha\Delta}, \hat{d}_\sigma\right\} - \left\{\hat{d}^\dagger_\Delta, \hat{d}_\sigma\right\}\hat{c}_{k\alpha\sigma} = -\left\{\hat{d}^\dagger_\Delta, \hat{d}_\sigma\right\}\hat{c}_{k\alpha\sigma} = -\delta_{\sigma\Delta}\hat{c}_{k\alpha\sigma}.$$

Then:

$$\left[\hat{H}_T, \hat{d}_\sigma\right] = -\sum_{k\alpha} V^*_{k\alpha}\,\hat{c}_{k\alpha\sigma}. \tag{F.3}$$

If we put together equations (F.1), (F.2) and (F.3), we obtain the first total commutator of this section:

$$\left[\hat{H}_S(t), \hat{d}_\sigma(t)\right] = -\varepsilon_0\hat{d}_\sigma - U\hat{d}_\sigma\hat{n}_{\bar{\sigma}} - \sum_{k\alpha\alpha} V^*_{k\alpha}\hat{c}_{k\alpha\sigma}. \tag{F.4}$$

2. Calculation of $\left[\hat{H}_S(t), \hat{c}_{k\alpha\sigma}(t)\right]$:

   -It's easy to see that $\left[\hat{H}_D, \hat{c}_{k\alpha\sigma}(t)\right] = 0$.

   -Next, we have the commutator for the Hamiltonian of the metals:

$$\begin{aligned}\left[\hat{H}_M, \hat{c}_{k\alpha\sigma}(t)\right] &= \sum_{q\beta\Delta}\varepsilon_{q\beta}\left[\hat{c}^\dagger_{q\beta\Delta}\hat{c}_{q\beta\Delta}, \hat{c}_{k\alpha\sigma}\right] = \sum_{q\beta\Delta}\varepsilon_{q\beta}\left(\hat{c}^\dagger_{q\beta\Delta}\{\hat{c}_{q\beta\Delta}, \hat{c}_{k\alpha\sigma}\} - \{\hat{c}^\dagger_{q\beta\Delta}, \hat{c}_{k\alpha\sigma}\}\hat{c}_{q\beta\Delta}\right)\\ &= -\sum_{q\beta\Delta}\varepsilon_{q\beta}\left\{\hat{c}^\dagger_{q\beta\Delta}, \hat{c}_{k\alpha\sigma}\right\}\hat{c}_{q\beta\Delta} = -\sum_{q\beta\Delta}\varepsilon_{q\beta}\delta_{qk}\delta_{\alpha\beta}\delta_{\sigma\Delta}\hat{c}_{q\beta\Delta}\\ &= -\varepsilon_{k\alpha}\hat{c}_{k\alpha\sigma}.\end{aligned}$$

   -Now the tunneling Hamiltonian:

$$\begin{aligned}
\left[\hat{H}_T, \hat{c}_{k\alpha\sigma}(t)\right] &= \sum_{q\beta\Delta} V_{q\beta}\left[\hat{c}^\dagger_{q\beta\Delta}\hat{d}_\Delta, \hat{c}_{k\alpha\sigma}(t)\right] + V^*_{q\beta}\left[\hat{d}^\dagger_\Delta \hat{c}_{q\beta\Delta}, \hat{c}_{k\alpha\sigma}(t)\right], \\
\left[\hat{c}^\dagger_{q\beta\Delta}\hat{d}_\Delta, \hat{c}_{k\alpha\sigma}(t)\right] &= \hat{c}^\dagger_{q\beta\Delta}\left\{\hat{d}_\Delta, \hat{c}_{k\alpha\sigma}\right\} - \left\{\hat{c}^\dagger_{q\beta\Delta}, \hat{c}_{k\alpha\sigma}\right\}\hat{d}_\Delta = -\left\{\hat{c}^\dagger_{q\beta\Delta}, \hat{c}_{k\alpha\sigma}\right\}\hat{d}_\Delta \\
&= -\delta_{qk}\delta_{\alpha\beta}\delta_{\sigma\Delta}\hat{d}_\Delta, \\
\left[\hat{d}^\dagger_\Delta \hat{c}_{q\beta\Delta}, \hat{c}_{k\alpha\sigma}(t)\right] &= \hat{d}^\dagger_\Delta\left\{\hat{c}_{q\beta\Delta}, \hat{c}_{k\alpha\sigma}\right\} - \left\{\hat{d}^\dagger_\Delta, \hat{c}_{k\alpha\sigma}\right\} = 0.
\end{aligned}$$

-Finally, we have:

$$\left[\hat{H}_T, \hat{c}_{k\alpha\sigma}(t)\right] = \sum_{q\beta\Delta} V_{q\beta}\left[\hat{c}^\dagger_{q\beta\Delta}\hat{d}_\Delta, \hat{c}_{k\alpha\sigma}\right] = -\sum_{q\beta\Delta} V_{q\beta}\delta_{qk}\delta_{\alpha\beta}\delta_{\sigma\Delta}\hat{d}_\Delta = -V_{k\alpha\sigma}\hat{d}_\sigma.$$

-Putting all previous commutators together, we recover Eq. (4.7):

$$\left[\hat{H}_S(t), \hat{c}_{k\alpha\sigma}(t)\right] = -\epsilon_{k\alpha}\hat{c}_{k\alpha\sigma} - V_{k\alpha}\hat{d}_\sigma(t).$$

3. Calculation of the self-energy expression in Eq. (4.12).

-Recall that:

$$\mathcal{G}^r_{k\alpha}(t,t') = -i\theta(t-t')\exp\left[-i\int_{t'}^{t}\varepsilon_{k\alpha}(\tau)d\pi\right]. \tag{F.5}$$

-Recall that $V_{k\alpha}(t) = u_\alpha(t)V_\alpha(\varepsilon^0_k)$. We write the sum in Eq. (4.12) as an integral over energy by letting $\sum_k \to \int d\varepsilon^0_k(t)\rho(\varepsilon^0_k)/2\pi$ and use $\varepsilon_{k\alpha}(t) = \varepsilon^0_k + \Delta_\alpha(t)$. By rewriting ε^0_k as simply ϵ and recognizing the terms in Eq. (4.13) we immediately obtain:

$$\begin{aligned}
\Sigma^r(t,t') &= \sum_{k\alpha} V^*_{k\alpha}(t)\mathcal{G}^r_{k\alpha}(t,t')V_{k\alpha}(t') \\
&= \sum_\alpha -i\theta(t-t')\int\frac{d\varepsilon^0_k}{2\pi}\rho(\varepsilon^0_k)u_\alpha(t)V^*_\alpha(\varepsilon^0_k)\exp\left[-i\varepsilon^0_k(t-t') - i\int_{t'}^{t}\Delta_\alpha(\tau)d\tau\right]u_\alpha(t')V_\alpha(\varepsilon^0_k) \\
&= -i\theta(t-t')\sum_\alpha\int\frac{d\varepsilon}{2\pi}e^{-i\varepsilon(t-t')}\Gamma^\alpha(\varepsilon,t,t').
\end{aligned} \tag{F.6}$$

Following an analogous procedure and employing Eq. (4.10), we obtain Eq. (G.8).

4. Calculating the commutator $\left[\hat{H}_S, \left(\hat{d}_\sigma\hat{n}_{\bar{\sigma}}\right)(t)\right]$. -We need to compute all three terms in:

$$\left[\hat{H}_S, \left(\hat{d}_\sigma\hat{n}_{\bar{\sigma}}\right)(t)\right] = \left[\hat{H}_M, \left(\hat{d}_\sigma\hat{n}_{\bar{\sigma}}\right)(t)\right] + \left[\hat{H}_D, \left(\hat{d}_\sigma\hat{n}_{\bar{\sigma}}\right)(t)\right] + \left[\hat{H}_T, \left(\hat{d}_\sigma\hat{n}_{\bar{\sigma}}\right)(t)\right].$$

-Clearly $\left[\hat{H}_M, \left(\hat{d}_\sigma\hat{n}_{\bar{\sigma}}\right)(t)\right] = 0.$

-Now we calculate the device Hamiltonian commutator:

$$\left[\hat{H}_D, \left(\hat{d}_\sigma \hat{n}_{\bar{\sigma}}\right)(t)\right] = \varepsilon_0(t) \sum_{\Delta} \left[\hat{d}^\dagger_\Delta \hat{d}_\Delta, \hat{d}_\sigma \hat{n}_{\bar{\sigma}}\right] + U\left[\hat{n}_\uparrow \hat{n}_\downarrow, \hat{d}_\sigma \hat{n}_{\bar{\sigma}}\right].$$

-We work on the terms in colors above:

$$\begin{aligned}
\left[\hat{d}^\dagger_\Delta \hat{d}_\Delta, \hat{d}_\sigma \hat{n}_{\bar{\sigma}}\right] &= \left[\hat{n}_\Delta, \hat{d}_\sigma\right] \hat{n}_{\bar{\sigma}} + \hat{d}_\sigma \left[\hat{n}_\Delta, \hat{n}_{\bar{\sigma}}\right] = \left[\hat{n}_\Delta, \hat{d}_\sigma\right] \hat{n}_{\bar{\sigma}} = -\delta_{\Delta\sigma} \hat{d}_\Delta \hat{n}_{\bar{\sigma}}, \\
\left[\hat{n}_\uparrow \hat{n}_\downarrow, \hat{d}_\sigma \hat{n}_{\bar{\sigma}}\right] &= \left[\hat{n}_\uparrow \hat{n}_\downarrow, \hat{n}_{\bar{\sigma}}\right] \hat{d}_\sigma + \left[\hat{n}_\uparrow \hat{n}_\downarrow, \hat{d}_\sigma\right] \hat{n}_{\bar{\sigma}}, \\
\left[\hat{n}_\uparrow \hat{n}_\downarrow, \hat{n}_{\bar{\sigma}}\right] &= \hat{n}_\uparrow \left[\hat{n}_\downarrow, \hat{n}_{\bar{\sigma}}\right] + \left[\hat{n}_\uparrow, \hat{n}_{\bar{\sigma}}\right] \hat{n}_\downarrow = 0, \\
\left[\hat{n}_\uparrow \hat{n}_\downarrow, \hat{d}_\sigma\right] &= \hat{n}_\uparrow \left[\hat{n}_\downarrow, \hat{d}_\sigma\right] + \left[\hat{n}_\uparrow, \hat{d}_\sigma\right] \hat{n}_\downarrow \\
&= -\delta_{\downarrow\sigma} \hat{n}_\uparrow \hat{d}_\downarrow - \delta_{\uparrow\sigma} \hat{d}_\uparrow \hat{n}_\downarrow \\
&= -\hat{d}_\sigma \hat{n}_{\bar{\sigma}}, \\
\left[\hat{n}_\uparrow \hat{n}_\downarrow, \hat{d}_\sigma \hat{n}_{\bar{\sigma}}\right] &= -\hat{d}_\sigma \hat{n}_{\bar{\sigma}}.
\end{aligned}$$

-The above commutators leads to:

$$\begin{aligned}
\left[\hat{H}_D, \left(\hat{d}_\sigma \hat{n}_{\bar{\sigma}}\right)(t)\right] &= \varepsilon_0(t) \sum_{\Delta} -\delta_{\Delta\sigma} \hat{d}_\Delta \hat{n}_{\bar{\sigma}} - U \hat{d}_\sigma \hat{n}_{\bar{\sigma}}, \\
\left[\hat{H}_D, \left(\hat{d}_\sigma \hat{n}_{\bar{\sigma}}\right)(t)\right] &= -\left(\varepsilon_0(t) + U\right) \hat{d}_\sigma \hat{n}_{\bar{\sigma}}.
\end{aligned}$$

-For the tunneling Hamiltonian we have:

$$\left[\hat{H}_T, \left(\hat{d}_\sigma \hat{n}_{\bar{\sigma}}\right)(t)\right] = \sum_{q\beta\Delta} V_{q\beta} \left[\hat{c}^\dagger_{q\beta\Delta} \hat{d}_\Delta, \hat{d}_\sigma \hat{n}_{\bar{\sigma}}\right] + V^*_{q\beta} \left[\hat{d}^\dagger_\Delta \hat{c}_{q\beta\Delta}, \hat{d}_\sigma \hat{n}_{\bar{\sigma}}\right].$$

-Going term by term in the colored terms above:

$$\begin{aligned}
\left[\hat{c}^\dagger_{q\beta\Delta} \hat{d}_\Delta, \hat{d}_\sigma \hat{n}_{\bar{\sigma}}\right] &= \left[\hat{c}^\dagger_{q\beta\Delta} \hat{d}_\Delta, \hat{d}_\sigma\right] \hat{n}_{\bar{\sigma}} + \hat{d}_\sigma \left[\hat{c}^\dagger_{q\beta\Delta} \hat{d}_\Delta, \hat{n}_{\bar{\sigma}}\right] \\
&= \left(\hat{c}^\dagger_{q\beta\Delta} \left\{\hat{d}_\Delta, \hat{d}_\sigma\right\} - \left\{\hat{c}^\dagger_{q\beta\Delta}, \hat{d}_\sigma\right\} \hat{d}_\Delta\right) \hat{n}_{\bar{\sigma}} + \hat{d}_\sigma \left(\hat{c}^\dagger_{q\beta\Delta} \left[\hat{d}_\Delta, \hat{n}_{\bar{\sigma}}\right] + \left[\hat{c}^\dagger_{q\beta\Delta}, \hat{n}_{\bar{\sigma}}\right] \hat{d}_\Delta\right) \\
&= \hat{d}_\sigma \hat{c}^\dagger_{q\beta\Delta} \left[\hat{d}_\Delta, \hat{n}_{\bar{\sigma}}\right] = \delta_{\Delta\bar{\sigma}} \hat{d}_\sigma \hat{c}^\dagger_{q\beta\Delta} d_{\bar{\sigma}} \\
&= -\delta_{\Delta\bar{\sigma}} \hat{c}^\dagger_{q\beta\Delta} \hat{d}_\sigma d_{\bar{\sigma}}.
\end{aligned}$$

$$\begin{aligned}\left[\hat{d}^{\dagger}_{\Delta}\hat{c}_{q\beta\Delta},\hat{d}_{\sigma}\hat{n}_{\bar{\sigma}}\right] &= \left[\hat{d}^{\dagger}_{\Delta}\hat{c}_{q\beta\Delta},\hat{d}_{\sigma}\right]\hat{n}_{\bar{\sigma}}+\hat{d}_{\sigma}\left[\hat{d}^{\dagger}_{\Delta}\hat{c}_{q\beta\Delta},\hat{n}_{\bar{\sigma}}\right]\\ &= \left(\hat{d}^{\dagger}_{\Delta}\left\{\hat{c}_{q\beta\Delta},\hat{d}_{\sigma}\right\}-\left\{\hat{d}^{\dagger}_{\Delta},\hat{d}_{\sigma}\right\}\hat{c}_{q\beta\Delta}\right)\hat{n}_{\bar{\sigma}}+\hat{d}_{\sigma}\left(\hat{d}^{\dagger}_{\Delta}\left[\hat{c}_{q\beta\Delta},\hat{n}_{\bar{\sigma}}\right]+\left[\hat{d}^{\dagger}_{\Delta},\hat{n}_{\bar{\sigma}}\right]\hat{c}_{q\beta\Delta}\right)\\ &= -\left\{\hat{d}^{\dagger}_{\Delta},\hat{d}_{\sigma}\right\}\hat{c}_{q\beta\Delta}\hat{n}_{\sigma}+\hat{d}_{\sigma}\left[\hat{d}^{\dagger}_{\Delta},\hat{n}_{\bar{\sigma}}\right]\hat{c}_{q\beta\Delta}\\ &= -\delta_{\Delta\sigma}\hat{c}_{q\beta\Delta}\hat{n}_{\sigma}+\hat{d}_{\sigma}\left(\left\{\hat{d}^{\dagger}_{\Delta},d^{\dagger}_{\bar{\sigma}}\right\}d_{\bar{\sigma}}-d^{\dagger}_{\bar{\sigma}}\left\{\hat{d}^{\dagger}_{\Delta},d_{\bar{\sigma}}\right\}\hat{c}_{q\beta\Delta}\right)\\ &= -\delta_{\Delta\sigma}\hat{c}_{q\beta\Delta}\hat{n}_{\bar{\sigma}}-\delta_{\Delta\bar{\sigma}}\hat{d}_{\sigma}d^{\dagger}_{\bar{\sigma}}\hat{c}_{q\beta\Delta}.\end{aligned}$$

-With this, we have:

$$\begin{aligned}\left[\hat{H}_T,\left(\hat{d}_{\sigma}\hat{n}_{\bar{\sigma}}\right)(t)\right] &= \sum_{q\beta\Delta}\left(-V_{q\beta}\delta_{\Delta\bar{\sigma}}\hat{c}^{\dagger}_{q\beta\Delta}\hat{d}_{\sigma}d_{\bar{\sigma}}-V^{*}_{q\beta}\delta_{\Delta\sigma}\hat{c}_{q\beta\Delta}\hat{n}_{\bar{\sigma}}-V^{*}_{q\beta}\delta_{\Delta\bar{\sigma}}\hat{d}_{\sigma}d^{\dagger}_{\bar{\sigma}}\hat{c}_{q\beta\Delta}\right)\\ &= \sum_{q\beta}\left(-V_{q\beta}c^{\dagger}_{q\beta\bar{\sigma}}\hat{d}_{\sigma}d_{\bar{\sigma}}-V^{*}_{q\beta}c_{q\beta\sigma}\hat{n}_{\bar{\sigma}}-V^{*}_{q\beta}\hat{d}_{\sigma}d^{\dagger}_{\bar{\sigma}}c_{q\beta\sigma}\right),\\ \left[\hat{H}_T,\left(\hat{d}_{\sigma}\hat{n}_{\bar{\sigma}}\right)(t)\right] &= \sum_{k\alpha}-V_{k\alpha}c^{\dagger}_{k\alpha\bar{\sigma}}\hat{d}_{\sigma}d_{\bar{\sigma}}-V^{*}_{k\alpha}\hat{c}_{k\alpha\sigma}\hat{n}_{\bar{\sigma}}-V^{*}_{k\alpha}\hat{d}_{\sigma}d^{\dagger}_{\bar{\sigma}}c_{k\alpha\bar{\sigma}}.\end{aligned}$$

-Finally, we recover Eq. (4.15):

$$\left[\hat{H}_S,\left(\hat{d}_{\sigma}\hat{n}_{\bar{\sigma}}\right)(t)\right] = -\left(\varepsilon_0(t)+U\right)\left(\hat{d}_{\sigma}\hat{n}_{\bar{\sigma}}\right)(t)-\sum_{k\alpha}V_{k\alpha}(t)c^{\dagger}_{k\alpha\bar{\sigma}}\hat{d}_{\sigma}d_{\bar{\sigma}}+V^{*}_{k\alpha}(t)\hat{c}_{k\alpha\alpha}\hat{n}_{\bar{\sigma}}+V^{*}_{k\alpha}(t)\hat{d}_{\sigma}d^{\dagger}_{\bar{\sigma}}\hat{c}_{k\alpha\sigma}.$$

-Now let's find $\left\langle\left\{\left(\hat{d}_{\sigma}\hat{n}_{\bar{\sigma}}\right)(t),\hat{d}^{\dagger}_{\sigma}(t)\right\}\right\rangle$:

$$\left\langle\left\{\left(\hat{d}_{\sigma}\hat{n}_{\bar{\sigma}}\right)(t),\hat{d}^{\dagger}_{\sigma}(t)\right\}\right\rangle = \left\langle\hat{d}_{\sigma}\left[\hat{n}_{\bar{\sigma}},\hat{d}^{\dagger}_{\sigma}\right]+\left\{\hat{d}_{\sigma},\hat{d}^{\dagger}_{\sigma}\right\}\hat{n}_{\bar{\sigma}}\right\rangle = \left\langle\hat{n}_{\bar{\sigma}}(t)\right\rangle.$$

5. Calculating the hybrid higher-order commutator $\left[\hat{H}_S,\left(\hat{c}_{k\alpha\sigma}\hat{n}_{\sigma}\right)(t)\right]$.

-We need to compute each commutator in:

$$\left[\hat{H}_S,\left(\hat{c}_{k\alpha\sigma}\hat{n}_{\bar{\sigma}}\right)(t)\right] = \left[\hat{H}_M,\left(\hat{c}_{k\alpha\sigma}\hat{n}_{\bar{\sigma}}\right)(t)\right]+\left[\hat{H}_D,\left(\hat{c}_{k\alpha\sigma}\hat{n}_{\bar{\sigma}}\right)(t)\right]+\left[\hat{H}_T,\left(\hat{c}_{k\alpha\sigma}\hat{n}_{\bar{\sigma}}\right)(t)\right].$$

-First the metals Hamiltonian:

$$\left[\hat{H}_M,\left(\hat{c}_{k\alpha\sigma}\hat{n}_{\bar{\sigma}}\right)(t)\right] = \sum_{q\beta\Delta}\varepsilon_{q\beta}\left[\hat{c}^{\dagger}_{q\beta\Delta}\hat{c}_{q\beta\Delta},\hat{c}_{k\alpha\sigma}\hat{n}_{\bar{\sigma}}\right].$$

-We work on the brown term as follows:

$$\begin{aligned}\left[\hat{c}^{\dagger}_{q\beta\Delta}\hat{c}_{q\beta\Delta},\hat{c}_{k\alpha\sigma}\hat{n}_{\bar{\sigma}}\right] &= \left[\hat{c}^{\dagger}_{q\beta\Delta}\hat{c}_{q\beta\Delta},\hat{c}_{k\alpha\sigma}\right]\hat{n}_{\bar{\sigma}} + \hat{c}_{k\alpha\sigma}\left[\hat{c}^{\dagger}_{q\beta\Delta}\hat{c}_{q\beta\Delta},\hat{n}_{\bar{\sigma}}\right] \\ &= \left(\hat{c}^{\dagger}_{q\beta\Delta}\left\{\hat{c}_{q\beta\Delta},\hat{c}_{k\alpha\sigma}\right\} - \left\{\hat{c}^{\dagger}_{q\beta\Delta},\hat{c}_{k\alpha\sigma}\right\}\hat{c}_{q\beta\Delta}\right)\hat{n}_{\bar{\sigma}} \\ &+ \hat{c}_{k\alpha\sigma}\left(\hat{c}^{\dagger}_{q\beta\Delta}\left[\hat{c}_{q\beta\Delta},\hat{n}_{\bar{\sigma}}\right] + \left[\hat{c}^{\dagger}_{q\beta\Delta},\hat{n}_{\bar{\sigma}}\right]\hat{c}_{q\beta\Delta}\right) \\ &= -\left\{\hat{c}^{\dagger}_{q\beta\Delta}\hat{c}_{k\alpha\sigma}\right\}\hat{c}_{q\beta\Delta}\hat{n}_{\bar{\sigma}} = -\delta_{qk}\delta_{\alpha\beta}\delta_{\sigma\Delta}\hat{c}_{q\beta\Delta}\hat{n}_{\bar{\sigma}}.\end{aligned}$$

-Then:

$$\left[\hat{H}_M,\left(\hat{c}_{k\alpha\sigma}\hat{n}_{\bar{\sigma}}\right)(t)\right] = \sum_{q\beta\Delta}\varepsilon_{q\beta}\left(-\delta_{qk}\delta_{\alpha\beta}\delta_{\sigma\Delta}\hat{c}_{q\beta\Delta}\hat{n}_{\bar{\sigma}}\right) = -\varepsilon_{k\alpha}\hat{c}_{k\alpha\sigma}\hat{n}_{\bar{\sigma}}.$$

-Thus, the commutator for the metals is:

$$\left[\hat{H}_M,\left(\hat{c}_{k\alpha\sigma}\hat{n}_{\bar{\sigma}}\right)(t)\right] = -\varepsilon_{k\alpha}\hat{c}_{k\alpha\sigma}\hat{n}_{\bar{\sigma}}.$$

-For the device Hamiltonian, we have:

$$\left[\hat{H}_D,\left(\hat{c}_{k\alpha\sigma}\hat{n}_{\bar{\sigma}}\right)(t)\right] = \varepsilon_0(t)\sum_{\Delta}\left[\hat{d}^{\dagger}_{\Delta}\hat{d}_{\Delta},c_{k\alpha\sigma}\hat{n}_{\bar{\sigma}}\right] + U\left[\hat{n}_{\uparrow}\hat{n}_{\downarrow},c_{k\alpha\sigma}\hat{n}_{\bar{\sigma}}\right].$$

-Working on the colored terms above we have:

$$\left[\hat{d}^{\dagger}_{\Delta}\hat{d}_{\Delta},\hat{c}_{k\alpha\sigma}\hat{n}_{\bar{\sigma}}\right] = \left[\hat{d}^{\dagger}_{\Delta}\hat{d}_{\Delta},\hat{c}_{k\alpha\sigma}\right]\hat{n}_{\bar{\sigma}} + \hat{c}_{k\alpha\sigma}\left[\hat{d}^{\dagger}_{\Delta}\hat{d}_{\Delta},\hat{n}_{\bar{\sigma}}\right] = \hat{c}_{k\alpha\sigma}\left[\hat{d}^{\dagger}_{\Delta}\hat{d}_{\Delta},\hat{n}_{\bar{\sigma}}\right] = 0,$$

$$\left[\hat{n}_{\uparrow}\hat{n}_{\downarrow},\hat{c}_{k\alpha\sigma}\hat{n}_{\bar{\sigma}}\right] = \left[\hat{n}_{\uparrow}\hat{n}_{\downarrow},\hat{c}_{k\alpha\sigma}\right]\hat{n}_{\bar{\sigma}} + \hat{c}_{k\alpha\sigma}\left[\hat{n}_{\uparrow}\hat{n}_{\downarrow},\hat{n}_{\bar{\sigma}}\right] = 0.$$

-We easily see that:

$$\left[\hat{H}_D,\left(\hat{c}_{k\alpha\sigma}\hat{n}_{\sigma}\right)(t)\right] = 0.$$

-For the tunneling Hamiltonian commutator, we have:

$$\left[\hat{H}_T,\left(\hat{c}_{k\alpha\sigma}\hat{n}_{\bar{\sigma}}\right)(t)\right] = \sum_{q\beta\Delta}V_{q\beta}\left[\hat{c}^{\dagger}_{q\beta\Delta}\hat{d}_{\Delta},\hat{c}_{k\alpha\sigma}\hat{n}_{\bar{\sigma}}\right] + V^{*}_{q\beta}\left[\hat{d}^{\dagger}_{\Delta}\hat{c}_{q\beta\Delta},\hat{c}_{k\alpha\sigma}\hat{n}_{\bar{\sigma}}\right].$$

-For the term in purple we have:

$$\begin{aligned}\left[\hat{c}^{\dagger}_{q\beta\Delta}\hat{d}_{\Delta},\hat{c}_{k\alpha\sigma}\hat{n}_{\bar{\sigma}}\right] &= \left[\hat{c}^{\dagger}_{q\beta\Delta}\hat{d}_{\Delta},\hat{c}_{k\alpha\sigma}\right]\hat{n}_{\bar{\sigma}} + \hat{c}_{k\alpha\sigma}\left[\hat{c}^{\dagger}_{q\beta\Delta}\hat{d}_{\Delta},\hat{n}_{\bar{\sigma}}\right]\\ &= \left(\hat{c}^{\dagger}_{q\beta\Delta}\left\{\hat{d}_{\Delta},\hat{c}_{k\alpha\sigma}\right\} - \left\{\hat{c}^{\dagger}_{q\beta\Delta},\hat{c}_{k\alpha\sigma}\right\}\hat{d}_{\Delta}\right)\hat{n}_{\bar{\sigma}} + \hat{c}_{k\alpha\sigma}\left(\hat{c}^{\dagger}_{q\beta\Delta}\left[\hat{d}_{\Delta},\hat{n}_{\bar{\sigma}}\right] + \left[\hat{c}^{\dagger}_{q\beta\Delta},\hat{n}_{\bar{\sigma}}\right]\hat{d}_{\Delta}\right)\\ &= -\left\{\hat{c}^{\dagger}_{q\beta\Delta},\hat{c}_{k\alpha\sigma}\right\}\hat{d}_{\Delta}\hat{n}_{\bar{\sigma}} + \hat{c}_{k\alpha\sigma}\hat{c}^{\dagger}_{q\beta\Delta}\left[\hat{d}_{\Delta},\hat{n}_{\bar{\sigma}}\right]\\ &= -\delta_{kq}\delta_{\alpha\beta}\delta_{\sigma\Delta}\hat{d}_{\Delta}\hat{n}_{\bar{\sigma}} + \delta_{\Delta\bar{\sigma}}\hat{c}_{k\alpha\sigma}\hat{c}^{\dagger}_{q\beta\Delta}d_{\bar{\sigma}}.\end{aligned}$$

-For the term in green we have:

$$\begin{aligned}\left[\hat{d}^{\dagger}_{\Delta}\hat{c}_{q\beta\Delta},\hat{c}_{k\alpha\sigma}\hat{n}_{\bar{\sigma}}\right] &= \left[\hat{d}^{\dagger}_{\Delta}\hat{c}_{q\beta\Delta},\hat{c}_{k\alpha\sigma}\right]\hat{n}_{\bar{\sigma}} + \hat{c}_{k\alpha\sigma}\left[\hat{d}^{\dagger}_{\Delta}\hat{c}_{q\beta\Delta},\hat{n}_{\bar{\sigma}}\right]\\ &= \hat{c}_{k\alpha\sigma}\left[\hat{d}^{\dagger}_{\Delta}\hat{c}_{q\beta\Delta},\hat{n}_{\bar{\sigma}}\right] = \hat{c}_{k\alpha\sigma}\left(\hat{d}^{\dagger}_{\Delta}\left[\hat{c}_{q\beta\Delta},\hat{n}_{\bar{\sigma}}\right] + \left[\hat{d}^{\dagger}_{\Delta},\hat{n}_{\bar{\sigma}}\right]\hat{c}_{qB\Delta}\right)\\ &= \hat{c}_{k\alpha\sigma}\left[\hat{d}^{\dagger}_{\Delta},\hat{n}_{\bar{\sigma}}\right]\hat{c}_{q_{\beta\Delta}} = \hat{c}_{k\alpha\sigma}\left(\left\{\hat{d}^{\dagger}_{\Delta},d^{\dagger}_{\bar{\sigma}}\right\}d_{\bar{\sigma}} - d^{\dagger}_{\bar{\sigma}}\left\{\hat{d}^{\dagger}_{\Delta},d_{\bar{\sigma}}\right\}\right)\hat{c}_{q\beta\Delta}\\ &= -\delta_{\Delta\bar{\sigma}}\hat{c}_{k\alpha\sigma}d^{\dagger}_{\bar{\sigma}}\hat{c}_{q\beta\Delta}.\end{aligned}$$

-Finally, the commutator for the tunneling Hamiltonian is given by:

$$\begin{aligned}\left[\hat{H}_T,\left(\hat{c}_{k\alpha\sigma}\hat{n}_{\bar{\sigma}}\right)(t)\right] &= \sum_{q\beta\Delta}V_{q\beta}\left(-\delta_{kq}\delta_{\alpha\beta}\delta_{\sigma\Delta}\hat{d}_{\Delta}\hat{n}_{\bar{\sigma}} + \delta_{\Delta\bar{\sigma}}\hat{c}_{k\alpha\sigma}\hat{c}^{\dagger}_{q\beta\Delta}d_{\bar{\sigma}}\right) + V^{*}_{q\beta}\left(-\delta_{\Delta\bar{\sigma}}\hat{c}_{k\alpha\sigma}d^{\dagger}_{\bar{\sigma}}\hat{c}_{q\beta\Delta}\right)\\ &= -V_{k\alpha}\hat{d}_{\sigma}\hat{n}_{\bar{\sigma}} + \sum_{q\beta}\hat{c}_{k\alpha\sigma}c^{\dagger}_{q\beta\sigma}d_{\bar{\sigma}} - \sum_{q\beta}V^{*}_{q\beta}\hat{c}_{k\alpha\sigma}d^{\dagger}_{\bar{\sigma}}c_{q\beta\sigma}.\end{aligned}$$

-With the above commutators we recover Eq. (4.18).

-Going back to equation of motion for $G^{r}_{k\alpha\sigma,U}(t,t')$ we obtain:

$$\begin{aligned}i\partial_t G^{r}_{k\alpha\sigma,U}(t,t') =& i\theta(t-t')\left\langle\left\{-\varepsilon_{k\alpha}(t)\left(\hat{c}_{k\alpha\sigma}\hat{n}_{\bar{\sigma}}\right)(t) - V_{k\alpha}(t)\left(\hat{d}_{\sigma}\hat{n}_{\bar{\sigma}}\right)(t),\hat{d}^{\dagger}_{\sigma}(t')\right\}\right\rangle\\ =& \varepsilon_{k\alpha}(t)\left[-i\theta(t-t')\left\langle\left\{\left(\hat{c}_{k\alpha}\hat{n}_{\bar{\sigma}}\right)(t),\hat{d}^{\dagger}_{\sigma}(t')\right\}\right\rangle\right]\\ &+V_{k\alpha}(t)\left[-i\theta(t-t')\left\langle\left\{\left(\hat{c}_{k\alpha}\hat{n}_{\bar{\sigma}}\right)(t),\hat{d}^{\dagger}_{\sigma}(t')\right\}\right\rangle\right]\\ =& \varepsilon_{k\alpha}(t)G^{r}_{k\alpha\sigma,U}(t,t') + V_{k\alpha}(t)G^{r}_{\sigma\sigma,U}(t,t').\end{aligned}$$

6. Third term in Eq. (4.28).

$$\int\mathcal{G}^{r}_{0}(t,\tau)\tilde{\mathcal{G}}^{r}_{U}(\tau,t')\,d\tau = \int\hat{n}_{\bar{\sigma}}(t')\,\mathcal{G}^{r}_{0}(t,\tau)\mathcal{G}^{r}_{0}(\tau,t')\exp\left[-iU(\tau-t')\right]d\tau.$$

-The term in red above can be further developed:

$$\begin{aligned}\mathcal{G}_0^r(t,\tau)\mathcal{G}_0^r(\tau,t') &= -\theta(t-\tau)\theta(\tau-t')\exp\left[-i\int_\tau^t \varepsilon_0(\tau')\,d\tau'\right]\exp\left[-i\int_{t'}^\tau \varepsilon_0(\tau')\,d\tau'\right]\\ &= -\theta(t-\tau)\theta(\tau-t')\exp\left[-i\int_{t'}^t \varepsilon_0(\tau')\,d\tau'\right].\end{aligned}$$

-We can take implicit care of theta functions as their product only delimits the integrals to lie from t' to t as they do. Hence, we ignore them in what follows. Note that:

$$\int_{t'}^t \exp\big[-iU(\tau-t')\big]d\tau = \frac{i}{U}\exp\big[-iU(\tau-t')\big]\Big|_{t'}^t = \frac{i}{U}\big(\exp[-iU(t-t')]-1\big).$$

-Then:

$$\begin{aligned}\int \mathcal{G}_0^r(t,\tau)\tilde{\mathcal{G}}_U^r(\tau,t')\,d\tau &= -n_{\bar\sigma}(t')\exp\left[-i\int_{t'}^t \varepsilon_0(\tau')\,d\tau'\right]\int_{t'}^t \exp\big[-iU(\tau-t')\big]d\tau\\ &= -n_{\bar\sigma}(t')\exp\left[-i\int_{t'}^t \varepsilon_0(\tau')\,d\tau'\right]\frac{i}{U}\big(\exp[-iU(t-t')]-1\big)\\ &= -n_{\bar\sigma}(t')\exp\left[-i\int_{t'}^t \epsilon_0(\tau')\,d\tau'\right]\frac{i}{U}\exp\big[-iU(t-t')\big]\\ &+ n_{\bar\sigma}(t')\exp\left[-i\int_{t'}^t \epsilon_0(\tau')\,d\tau'\right]\frac{i}{U}\\ &= \frac{1}{U}\tilde{\mathcal{G}}_U^r(t,t') - \frac{1}{U}n_{\bar\sigma}(t')\,\mathcal{G}_0^r(t,t').\end{aligned}$$

-We can then write:

$$U\int \mathcal{G}_0^r(t,\tau)\tilde{\mathcal{G}}_U^r(\tau,t')\,d\tau = \tilde{\mathcal{G}}_U^r(t,t') - n_{\bar\sigma}(t')\,\mathcal{G}_0^r(t,t').$$

-Finally:

$$U\int \mathcal{G}_0^r(t,\tau)\mathcal{G}_U^r(\tau,t')\,d\tau = \mathcal{G}_U^r(t,t') - \mathcal{G}_0^r(t,t').$$

G

Hubbard sub-bands procedure

In this appendix, we detail a trick only suitable to the one-level quantum dot for a closed analytical solution of Green's functions of the problem after the application of the so-called wide-band limit [76]. First, we decompose our central region Green's functions as $G^r_{\sigma\sigma}(t,t') = G^r_{\sigma\sigma,0}(t,t') + G^r_{\sigma\sigma,U}(t,t')$ and write $\tilde{\mathcal{G}}^r_0(t,t') = \mathcal{G}^r_0(t,t') - n_{\bar{\sigma}}(t')\,\mathcal{G}^r_0(t,t')$. We start from Eq. (4.29):

$$\begin{aligned}
\rightarrow G^r_{\sigma\sigma,0}(t,t') + G^r_{\sigma\sigma,U}(t,t') &= \tilde{\mathcal{G}}^r_0(t,t') + \tilde{\mathcal{G}}^r_U(t,t') + \int \mathcal{G}^r_0(t,\tau)\,\Sigma^r(\tau,\tau')\big(G^r_{\sigma\sigma,0}(\tau',t') + G^r_{\sigma\sigma,U}(\tau',t')\big)\,d\tau d\tau' \\
&\quad + \int \big(\mathcal{G}^r_U(t,\tau) - \mathcal{G}^r_0(t,\tau)\big)\Sigma^r(\tau,\tau')\,G^r_{\sigma\sigma,U}(\tau',t')\,d\tau d\tau', \\
\rightarrow G^r_{\sigma\sigma,0}(t,t') + G^r_{\sigma\sigma,U}(t,t') &= \tilde{\mathcal{G}}^r_0(t,t') + \tilde{\mathcal{G}}^r_U(t,t') + \int \mathcal{G}^r_0(t,\tau)\,\Sigma^r(\tau,\tau')G^r_{\sigma\sigma,0}(\tau',t')\,d\tau d\tau' \\
&\quad + \int \mathcal{G}^r_U(t,\tau)\Sigma^r(\tau,\tau')\,G^r_{\sigma\sigma,U}(\tau',t')\,d\tau d\tau', \\
\rightarrow G^r_{\sigma\sigma,0}(t,t') + G^r_{\sigma\sigma,U}(t,t') &= \tilde{\mathcal{G}}^r_0(t,t') + \int \mathcal{G}^r_0(t,\tau)\,\Sigma^r(\tau,\tau')G^r_{\sigma\sigma,0}(\tau',t')\,d\tau d\tau' + G^r_{\sigma\sigma,U}(t,t'). \qquad \text{(G.1)}
\end{aligned}$$

From a close inspection of Eq. (G.1) we get an integral equation for $G^r_{\sigma\sigma,0}(t,t')$ similar to Eq. (4.27):

$$G^r_{\sigma\sigma,0}(t,t') = \tilde{\mathcal{G}}^r_0(t,t') + \int \mathcal{G}^r_0(t,\tau)\,\Sigma^r(\tau,\tau')G^r_{\sigma\sigma,0}(\tau',t')\,d\tau d\tau'. \qquad \text{(G.2)}$$

By introducing two new Green's functions

$$\tilde{G}^r_{\sigma\sigma,0}(t,t') = \frac{G^r_{\sigma\sigma,0}(t,t')}{1-n_{\bar{\sigma}}(t')}, \qquad \tilde{G}^r_{\sigma\sigma,U}(t,t') = \frac{G^r_{\sigma\sigma,U}(t,t')}{n_{\bar{\sigma}}(t')}, \qquad \text{(G.3)}$$

we note that equations (4.27) and (G.2) can be written as:

$$\tilde{G}^r_{\sigma\sigma,0}(t,t') = \mathcal{G}^r_0(t,t') + \int \mathcal{G}^r_0(t,t')\,\Sigma^r(t,\tau)\tilde{G}^r_{\sigma\sigma,0}(t,t')\,d\tau d\tau', \qquad \text{(G.4)}$$

$$\tilde{G}^{r}_{\sigma\sigma,U}\left(t,t'\right)=\mathcal{G}^{r}_{U}\left(t,t'\right)+\int\mathcal{G}^{r}_{U}\left(t,t'\right)\Sigma^{r}(t,\tau)\tilde{G}^{r}_{\sigma\sigma,U}\left(t,t'\right)d\tau d\tau'. \tag{G.5}$$

The Green's functions above constitute the **Hubbard bands** or Hubbard excitations discussed in the main text.

By solving equations (G.4) and (G.5), we can obtain $G^{r}_{\sigma\sigma}(t,t')$ after a correct self-consistent obtention of $n_{\bar{\sigma}}(t)$ by noticing that we can re-write Eq. (4.29) as:

$$G^{r}_{\sigma\sigma}\left(t,t'\right)=\big(1-n_{\bar{\sigma}}\left(t'\right)\big)\tilde{G}^{r}_{\sigma\sigma,0}\left(t,t'\right)+n_{\bar{\sigma}}\left(t'\right)\tilde{G}^{r}_{\sigma\sigma,U}\left(t,t'\right). \tag{G.6}$$

Recall that $n_{\sigma}(t)=\operatorname{Im}G^{<}_{\sigma\sigma}(t,t)$. Then an equation for $G^{<}_{\sigma\sigma}(t,t')$ can be easily obtained from the Keldysh equation Eq.(C.9) employed in section 3.1.3. We do this by defining new lesser Green's functions analogous to $\tilde{G}^{r}_{\sigma\sigma,0(U)}(t,t')$:

$$\tilde{G}^{<}_{\sigma\sigma,0(U)}\left(t,t'\right)=\int\tilde{G}^{r}_{\sigma\sigma,0(U)}(t,\tau)\Sigma^{<}(\tau,\tau')\tilde{G}^{a}_{\sigma\sigma,0(U)}\left(\tau',t'\right)d\tau d\tau', \tag{G.7}$$

where $\tilde{G}^{a}_{\sigma\sigma,0(U)}\left(t,t'\right)=\left[\tilde{G}^{r}_{\sigma\sigma,0(U)}(t,\tau)\right]^{*}$, and $\Sigma^{<}\left(t,t'\right)$ is the lesser self-energy given by (see appendix F):

$$\Sigma^{<}\left(t,t'\right)=\sum_{k\alpha}V^{*}_{k\alpha}(t)\mathcal{G}^{<}_{k\alpha}\left(t,t'\right)V_{k\alpha}\left(t'\right)=i\sum_{\alpha}\int\frac{d\varepsilon}{2\pi}e^{-i\varepsilon(t-t')}f_{\alpha}(\varepsilon)\Gamma^{\alpha}\left(\varepsilon,t,t'\right). \tag{G.8}$$

Above, $\Gamma^{\alpha}\left(\varepsilon,t,t'\right)$ is the level-width function given by Eq. (4.13) and $f_{\alpha}(\varepsilon)$ the Fermi function of the $\alpha=L,R$ macroscopic lead given by $f_{\alpha}(\varepsilon)=f\left(\varepsilon-\mu_{\alpha}\right)=1/\big(1+\exp\left[\beta\left(\varepsilon-\mu_{\alpha}\right)\right]\big)$.

Finally, direct application of Eq. (C.9) leads to another equation from which we can obtain $n_{\sigma}(t)$ after solving Eq. (G.7):

$$G^{<}_{\sigma\sigma}\left(t,t'\right)=\big(1-n_{\bar{\sigma}}\left(t'\right)\big)\tilde{G}^{<}_{\sigma\sigma,0}\left(t,t'\right)+n_{\bar{\sigma}}\left(t'\right)\tilde{G}^{<}_{\sigma\sigma,U}\left(t,t'\right). \tag{G.9}$$

H

Numerical Implementation of the time-dependent JMW current

In this appendix, we elucidate the numerical implementation of Eq. (4.51) from which the total current $J(t) = \left[J_L(t) - J_R(t)\right]/2$ follows. We start by rewriting equations (4.47) and (4.53) by splitting the integral over t_1 for $A^{0(U)}_{L/R}(\varepsilon, t)$ and $B^{0(U)}_{L/R}(\varepsilon, t)$ into two parts: $\int_{-\infty}^{t} = \int_{-\infty}^{0} + \int_{0}^{t}$. Notice that the retarded characteristic of $\tilde{G}^{r}_{\sigma\sigma,0(U)}(t, t_1)$ makes zero the integration in the interval $t_1 > t$ (from the theta function $\theta(t - t_1)$ in its definition). The first part is a simple integral of an exponential, where the time dependent arguments are zero for $t < 0$, and clearly $u_{L/R}(t = 0) = 1$. This leads to the following expressions:

$$\begin{aligned} A^{0(U)}_{\alpha}(\varepsilon, t) = {} & \frac{\exp\left[\mathrm{i}\left(\varepsilon - \varepsilon_{0(U)}\right) t\right]}{\varepsilon - \varepsilon_{0(U)} + \frac{\mathrm{i}\Gamma}{2}} \exp\left[-\mathrm{i}\int_0^t \mathrm{d}t_1 \left(\Delta\left(t_1\right) - \Delta_{\alpha}\left(t_1\right) - \frac{\mathrm{i}\Gamma\left(t_1\right)}{2}\right)\right] \\ & - \mathrm{i}\int_0^t \mathrm{d}t_1 \exp\left[\mathrm{i}\varepsilon\left(t - t_1\right)\right] u_{\alpha}\left(t_1\right) \exp\left[-\mathrm{i}\int_{t_1}^t \mathrm{d}t_2 \left(\varepsilon_{0(U)}\left(t_2\right) - \Delta_{\alpha}\left(t_2\right) - i\frac{\Gamma\left(t_2\right)}{2}\right)\right], \end{aligned} \tag{H.1}$$

$$\begin{aligned} B^{0}_{\alpha}(\varepsilon, t) = {} & \frac{\left(1 - n^0_{\bar{\sigma}}\right) \exp\left[\mathrm{i}\left(\varepsilon - \varepsilon_{0(U)}\right) t\right]}{\varepsilon - \varepsilon_{0(U)} + \frac{\mathrm{i}\Gamma}{2}} \exp\left[-\mathrm{i}\int_0^t \mathrm{d}t_1 \left(\Delta\left(t_1\right) - \Delta_{\alpha}\left(t_1\right) - \frac{\mathrm{i}\Gamma\left(t_1\right)}{2}\right)\right] \\ & - \mathrm{i}\int_0^t \mathrm{d}t_1 \left(1 - n_{\bar{\sigma}}(t_1)\right) \exp\left[\mathrm{i}\varepsilon\left(t - t_1\right)\right] u_{\alpha}\left(t_1\right) \\ & \times \exp\left[-\mathrm{i}\int_{t_1}^t \mathrm{d}t_2 \left(\varepsilon_{0(U)}\left(t_2\right) - \Delta_{\alpha}\left(t_2\right) - i\frac{\Gamma\left(t_2\right)}{2}\right)\right], \end{aligned} \tag{H.2}$$

$$\begin{aligned} B^{U}_{\alpha}(\varepsilon, t) = {} & \frac{n^0_{\bar{\sigma}} \exp\left[\mathrm{i}\left(\varepsilon - \varepsilon_{0(U)}\right) t\right]}{\varepsilon - \varepsilon_{0(U)} + \frac{\mathrm{i}\Gamma}{2}} \exp\left[-\mathrm{i}\int_0^t \mathrm{d}t_1 \left(\Delta\left(t_1\right) - \Delta_{\alpha}\left(t_1\right) - \frac{\mathrm{i}\Gamma\left(t_1\right)}{2}\right)\right] \\ & - \mathrm{i}\int_0^t \mathrm{d}t_1 n_{\bar{\sigma}}(t_1) \exp\left[\mathrm{i}\varepsilon\left(t - t_1\right)\right] u_{\alpha}\left(t_1\right) \exp\left[-\mathrm{i}\int_{t_1}^t \mathrm{d}t_2 \left(\varepsilon_{0(U)}\left(t_2\right) - \Delta_{\alpha}\left(t_2\right) - i\frac{\Gamma\left(t_2\right)}{2}\right)\right]. \end{aligned} \tag{H.3}$$

APPENDIX H. NUMERICAL IMPLEMENTATION OF THE TIME-DEPENDENT JMW CURRENT

From here on, a numerical integration method is required to evaluate the integrals above. In this work, we chose Simpson's rule [133] and employed Julia programming language [132] to compute the integrals numerically. It is worth mentioning that we could in principle solve the integrals for the respective pulse modulation of this thesis to get analytical expressions for (4.47) and (4.53). However, we do not consider here such analytical expressions but rather compute the whole integrals using numerical integration methods for the pulses given in equations (4.55)-(4.56).

The algorithm to compute the total current from Eq. (4.51) is determined by 4 steps as shown in the flowchart of figure H.1.

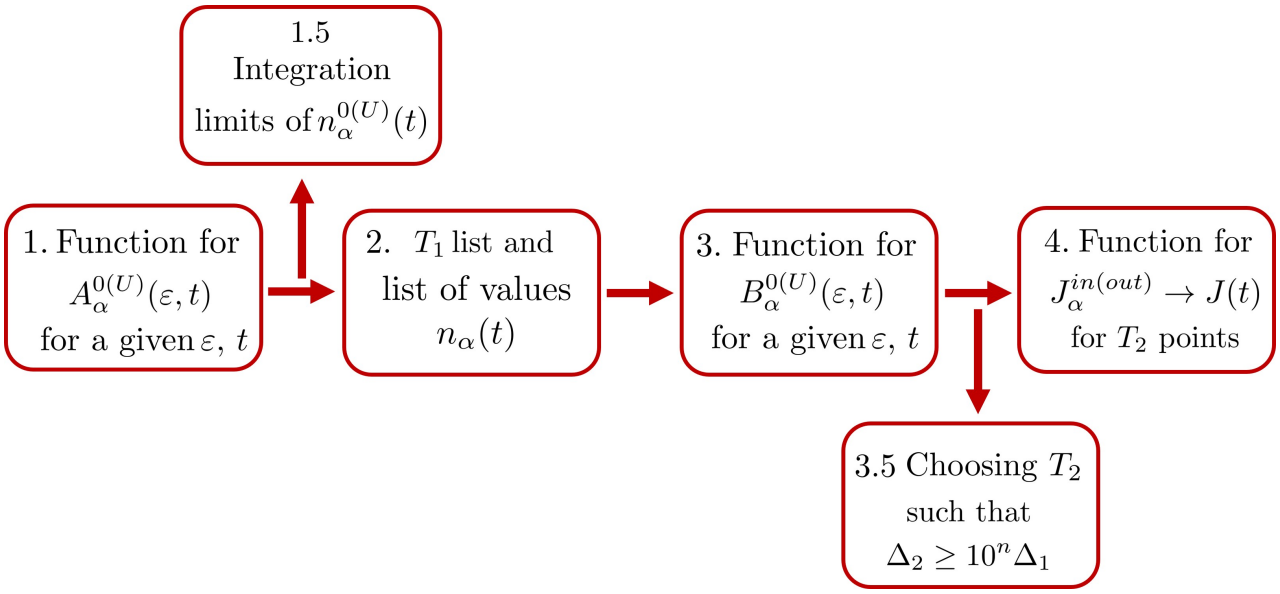

Figure H.1: Flowchart of the numerical algorithm for the time-dependent current $J(t)$.

We can detail this steps as follows:

1. A function is built to compute $A_\alpha^{0(U)}(\varepsilon,t)$ for a given energy ε and at a given time t. The time step dt_1 in Eq. (H.1) is chosen such that the integrand is calculated at 1000 time points, hence ensuring a numerical error of less than 0.1%. From here on, all integrals admit an error of less than 0.1% as a criteria for the resolution of the integrals. However, dt_2 determined only 5 time points for all cases excluding the harmonic simulation (the numerical integral of constants and steps functions required basically no time points), where the same criteria of error determined a number of points greater than 100.

   1.5 Evaluation of $A_\alpha^{0(U)}(\varepsilon,t)$ at different times for different energy values help determining limits of integration of $n_\alpha^{0(U)}(t)$ in Eq. (4.50). In this substep we choose the limits as -200 and 20 to ensure $A_\alpha^{0(U)}(\varepsilon,t) < 10^{-5}$. The number of zeros is doubled as we need the square magnitude of $A_\alpha^{0(U)}(\varepsilon,t)$ times the product with the fermi function, which

tends to zero very quickly for $\varepsilon > \mu_\alpha$ for the usual temperatures of the problem. This reduces the infinite limits of the analytical integral with a correct approximation of zero for $A_\alpha^{0(U)}(\varepsilon, t)$ at 10^{-10}. However, for $\varepsilon < \mu_\alpha$ it tends to one very quickly. This explains the larger lower limit -200. As it turns out, for all cases and parameters, the limits -200 and 20 coincide with this criteria.

2. The energy grid of each energy integral (which is about 1000 points for each case) to be computed for a given number of time points with time step steps Δ_1 defined in a list of times T_1 (whose range is particular to every calculation), is chosen for $n_\sigma^{0(U)}(t)$ by following the same criteria as before and the additional criteria in incise 3.5 below. Hence, in this step we compute $n_\sigma(t)$ at each time point by computing the integrand at each time point using $A_\alpha^{0(U)}(\varepsilon, t)$, a defined function for the fermi function, and Eq. (4.49). This generates a two column list with times in one column and values for n_σ at the other. These values are stored for later use. **This process takes between 7 and 8 hours for all cases considered, with 5000 time points up to 5 seconds.**

3. By using the pre-computed list of $n_\sigma(t)$, in this step we create a function in Julia that computes $B_\alpha^{0(U)}(\varepsilon, t)$ for a certain energy value ε and time t, analogous to the calculation of $A_\alpha^{0(U)}(\varepsilon, t)$ while computing the integrands for the same time points defined in T_1.

   3.5 We note how the resolution of the integrals for $B_\alpha^{0(U)}(\varepsilon, t)$ is directly dependent on time points of list T_1, whose time step should guarantee enough time points for a given t' to accurately compute $B_\alpha^{0(U)}(\varepsilon, t')$ with the desire error of 0.1%. Since the final current is calculated at a determined number of time points described by yet another list T_2, we obtain the criteria that T_2 should have a step Δ_2 such that $\Delta_2 \geq 10^n \Delta_1$, $n \in \mathbb{Z}$, to ensure a correct numerical resolution in the calculation of the $B_\alpha^{0(U)}(\varepsilon, T_2)$ energy integrals, given a list of values for $n_\sigma(t)$ at different times in the T_1 list. For the cases considered we have $n = 2, 3$. This steps calculates the T_2 time list.

4. A list of times with uniform time step Δ_2 defining a time point list T_2 is chosen according to the criteria in 3.5 above for the calculation of each energy integral (with its predetermined energy grid of 1000 points) for $J_\alpha^{in(out)}$. It is immediate to obtain $J(t)$ by using $J(t) = \big[J_L(t) - J_R(t)\big]/2$ and Eq. (4.51). In this step, a function in Julia is created to perform all previous calculations. **This takes between 1 and 2 hours for 500 time points up to 5 seconds**.

Finally, we note that calculating the pairs of curves n_σ vs t and $J(t)$ vs t in the figures of this thesis takes between **9 and 10 hours** in total. Calculations for all pair curves were compiled simultaneously, such that each figure in this thesis takes between **9 and 10 hours** in total. This computation time could be further refined to less than 2 hours per figure by parallelization of the integral calculations and refining memory usage of all quantities in the code.

Bibliography

[1]G. B. Leo. P Kadanoff, *Quantum Statistical Mechanics* (CRC Press, New York, 1962).

[2]A. L. Fetter and J. D. Walecka, *Quantum theory of many-particle systems* (Courier Corporation, 2012).

[3]P. W. Anderson, "More is different," Science **177**, 393–396 (1972).

[4]P. Coleman, *Introduction to Many-Body Physics* (Cambrige University Press, 5, 2015).

[5]G. Stefanucci and R. Van Leeuwen, *Nonequilibrium many-body theory of quantum systems: a modern introduction* (Cambridge University Press, 2013).

[6]J. Fransson, *Non-Equilibrium Nano-Physics. A Many-Body Approach*, Vol. 809 (Springer, Uppssala, 2010).

[7]J. Rammer, *Quantum field theory of non-equilibrium states* (Cambridge University Press, 2007).

[8]A. Kamenev, *Field theory of non-equilibrium systems*, 2nd ed. (Cambridge University Press, 2023).

[9]A. Aviram and M. A. Ratner, "Molecular rectifiers," Chemical physics letters **29**, 277–283 (1974).

[10]G. Cohen and M. Galperin, "Green's function methods for single molecule junctions," The Journal of chemical physics **152** (2020).

[11]M. Thoss and F. Evers, "Perspective: theory of quantum transport in molecular junctions," The Journal of chemical physics **148** (2018).

[12]J. Rammer, *Quantum transport theory* (CRC Press, 2018).

[13]D. Ryndyk, *Theory of quantum transport at nanoscale: an introduction dmitry a. ryndyk: springer, 2016 246 pages,* 129.00(*e – book99.00) isbn 978-3-319-24086-2*, Vol. 42 (Cambridge University Press, 2017), pp. 74–75.

[14]M. R. Hirsbrunner, T. M. Philip, B. Basa, Y. Kim, M. J. Park, and M. J. Gilbert, "A review of modeling interacting transient phenomena with non-equilibrium green functions," Reports on Progress in Physics **82**, 046001 (2019).

[15]M. E. Vance, T. Kuiken, E. P. Vejerano, S. P. McGinnis, M. F. Hochella Jr, D. Rejeski, and M. S. Hull, "Nanotechnology in the real world: redeveloping the nanomaterial consumer products inventory," Beilstein journal of nanotechnology **6**, 1769–1780 (2015).

[16]G. Binnig and H. Rohrer, "Scanning tunneling microscopy—from birth to adolescence," reviews of modern physics **59**, 615 (1987).

[17]G. Binnig, C. F. Quate, and C. Gerber, "Atomic force microscope," Physical review letters **56**, 930 (1986).

[18]T. Boolakee, C. Heide, A. Garzón-Ramírez, H. B. Weber, I. Franco, and P. Hommelhoff, "Light-field control of real and virtual charge carriers," Nature **605**, 251–255 (2022).

[19]S. Datta, *Electronic transport in mesoscopic systems* (Cambridge university press, 1997).

[20]H. Haug, A.-P. Jauho, et al., *Quantum kinetics in transport and optics of semiconductors*, Vol. 2 (Springer, 2008).

[21]E. Lörtscher, "Wiring molecules into circuits," Nature nanotechnology **8**, 381–384 (2013).

[22]L. Farinacci, G. Ahmadi, G. Reecht, M. Ruby, N. Bogdanoff, O. Peters, B. W. Heinrich, F. von Oppen, and K. J. Franke, "Tuning the coupling of an individual magnetic impurity to a superconductor: quantum phase transition and transport," Physical review letters **121**, 196803 (2018).

[23]A. A. Khajetoorians, D. Wegner, A. F. Otte, and I. Swart, "Creating designer quantum states of matter atom-by-atom," Nature Reviews Physics **1**, 703–715 (2019).

[24]J. P. Llinas, A. Fairbrother, G. Borin Barin, W. Shi, K. Lee, S. Wu, B. Yong Choi, R. Braganza, J. Lear, N. Kau, et al., "Short-channel field-effect transistors with 9-atom and 13-atom wide graphene nanoribbons," Nature communications **8**, 633 (2017).

[25]D. J. Rizzo, G. Veber, T. Cao, C. Bronner, T. Chen, F. Zhao, H. Rodriguez, S. G. Louie, M. F. Crommie, and F. R. Fischer, "Topological band engineering of graphene nanoribbons," Nature **560**, 204–208 (2018).

[26]A. C. Hewson, *The kondo problem to heavy fermions*, 2 (Cambridge university press, 1997).

[27]W. De Haas, J. De Boer, and G. Van den Berg, "The electrical resistance of gold, copper and lead at low temperatures," Physica **1**, 1115–1124 (1934).

[28]A. Clogston, B. Matthias, M. Peter, H. Williams, E. Corenzwit, and R. Sherwood, "Local magnetic moment associated with an iron atom dissolved in various transition metal alloys," Physical Review **125**, 541 (1962).

[29]P. W. Anderson, "Localized magnetic states in metals," Physical Review **124**, 41 (1961).

[30]K. G. Wilson, "The renormalization group: critical phenomena and the kondo problem," Reviews of modern physics **47**, 773 (1975).

[31]N. Andrei, "Diagonalization of the kondo hamiltonian," Physical Review Letters **45**, 379 (1980).

[32]N. Andrei, K. Furuya, and J. Lowenstein, "Solution of the kondo problem," Reviews of modern physics **55**, 331 (1983).

[33]P. Vigman, "Exact solution of sd exchange model at t= 0," Soviet Journal of Experimental and Theoretical Physics Letters **31**, 364 (1980).

[34]A. Tsvelick and P. Wiegmann, "Exact results in the theory of magnetic alloys," Advances in Physics **32**, 453–713 (1983).

[35]L. Kouwenhoven and L. Glazman, "Revival of the kondo effect," Physics world **14**, 33 (2001).

[36]J. Elzerman, R. Hanson, J. Greidanus, L. W. Van Beveren, S. De Franceschi, L. Vandersypen, S. Tarucha, and L. Kouwenhoven, "Few-electron quantum dot circuit with integrated charge read out," Physical Review B **67**, 161308 (2003).

[37]J. R. Schrieffer and P. A. Wolff, "Relation between the anderson and kondo hamiltonians," Physical Review **149**, 491 (1966).

[38]G. D. Mahan, *Many-particle physics* (Springer Science & Business Media, 2013).

[39]K. Yu and K. S. Schanze, *Commemorating the nobel prize in chemistry 2023 for the discovery and synthesis of quantum dots*, 2023.

[40]R. Akis, D. K. Ferry, M. J. Gilbert, and S. M. Goodnick, "Quantum transport at nanoscale," in *Handbook of nanoscience, engineering, and technology* (CRC Press, 2018), pp. 68–89.

[41]F. P. García de Arquer, D. V. Talapin, V. I. Klimov, Y. Arakawa, M. Bayer, and E. H. Sargent, "Semiconductor quantum dots: technological progress and future challenges," Science **373**, eaaz8541 (2021).

[42]C. Kloeffel and D. Loss, "Prospects for spin-based quantum computing in quantum dots," Annu. Rev. Condens. Matter Phys. **4**, 51–81 (2013).

[43]P. Seneor, A. Bernand-Mantel, and F. Petroff, "Nanospintronics: when spintronics meets single electron physics," Journal of Physics: Condensed Matter **19**, 165222 (2007).

[44]T. Fujisawa, T. Hayashi, and S. Sasaki, "Time-dependent single-electron transport through quantum dots," Reports on Progress in Physics **69**, 759 (2006).

[45]N. S. Wingreen and Y. Meir, "Anderson model out of equilibrium: noncrossing-approximation approach to transport through a quantum dot," Physical review B **49**, 11040 (1994).

[46]K. Le Hur, "Quantum dots and the kondo effect," Nature **526**, 203–204 (2015).

[47]R. López, R. Aguado, G. Platero, and C. Tejedor, "Kondo effect in ac transport through quantum dots," Physical review letters **81**, 4688 (1998).

[48]U. Schollwöck, "The density-matrix renormalization group," Reviews of modern physics **77**, 259 (2005).

[49]U. Schollwöck, "The density-matrix renormalization group in the age of matrix product states," Annals of physics **326**, 96–192 (2011).

[50]M. Brenes, J. J. Mendoza-Arenas, A. Purkayastha, M. T. Mitchison, S. R. Clark, and J. Goold, "Tensor-network method to simulate strongly interacting quantum thermal machines," Physical Review X **10**, 031040 (2020).

[51]H. Aoki, N. Tsuji, M. Eckstein, M. Kollar, T. Oka, and P. Werner, "Nonequilibrium dynamical mean-field theory and its applications," Reviews of Modern Physics **86**, 779 (2014).

[52]U. Harbola, M. Esposito, and S. Mukamel, "Quantum master equation for electron transport through quantum dots and single molecules," Physical Review B **74**, 235309 (2006).

[53]S. Weiss, J. Eckel, M. Thorwart, and R. Egger, "Iterative real-time path integral approach to nonequilibrium quantum transport," Physical Review B **77**, 195316 (2008).

[54]D. Sexty, T. Gasenzer, and J. Pawlowski, "Real-time effective-action approach to the anderson quantum dot," Physical Review B **83**, 165315 (2011).

[55]L. Magazzù and M. Grifoni, "Feynman-vernon influence functional approach to quantum transport in interacting nanojunctions: an analytical hierarchical study," Physical Review B **105**, 125417 (2022).

[56]S. Kurth, G. Stefanucci, C.-O. Almbladh, A. Rubio, and E. K. Gross, "Time-dependent quantum transport: a practical scheme using density functional theory," Physical Review B **72**, 035308 (2005).

[57]A. Krotz and R. Tempelaar, "A reciprocal-space formulation of surface hopping," The Journal of Chemical Physics **156** (2022).

[58]N. Lenzing, A. I. Lichtenstein, and M. Potthoff, "Emergent non-abelian gauge theory in coupled spin-electron dynamics," Physical Review B **106**, 094433 (2022).

[59]M. ten Brink, S. Gräber, M. Hopjan, D. Jansen, J. Stolpp, F. Heidrich-Meisner, and P. E. Blöchl, "Real-time non-adiabatic dynamics in the one-dimensional holstein model: trajectory-based vs exact methods," The Journal of Chemical Physics **156** (2022).

[60]G. Stefanucci and R. Van Leeuwen, *Nonequilibrium many-body theory of quantum systems: a modern introduction* (Cambridge University Press, 2013).

[61]H. Bruus and K. Flensberg, *Many-body quantum theory in condensed matter physics: an introduction* (OUP Oxford, 2016).

[62]K. Balzer and M. Bonitz, *Nonequilibrium green's functions approach to inhomogeneous systems* (Springer, 2012).

[63]U. Bajpai and B. K. Nikolić, "Time-retarded damping and magnetic inertia in the landau-lifshitz-gilbert equation self-consistently coupled to electronic time-dependent nonequilibrium green functions," Physical Review B **99**, 134409 (2019).

[64]P. C. Martin and J. Schwinger, "Theory of many-particle systems. I," Physical Review **115**, 1342–1373 (1959).

[65]J. Schwinger, "Brownian motion of a quantum oscillator," Journal of Mathematical Physics **2**, 407–432 (1961).

[66]L. V. Keldysh et al., "Diagram technique for nonequilibrium processes," Sov. Phys. JETP **20**, 1018–1026 (1965).

[67]M. Ridley, N. W. Talarico, D. Karlsson, N. L. Gullo, and R. Tuovinen, "A many-body approach to transport in quantum systems: from the transient regime to the stationary state," Journal of Physics A: Mathematical and Theoretical **55**, 273001 (2022).

[68]G. Stefanucci and C.-O. Almbladh, "Time-dependent partition-free approach in resonant tunneling systems," Physical Review B **69**, 195318 (2004).

[69]Y. Zhang, S. Chen, and G. Chen, "First-principles time-dependent quantum transport theory," Physical Review B **87**, 085110 (2013).

[70]M. Ridley, A. MacKinnon, and L. Kantorovich, "Current through a multilead nanojunction in response to an arbitrary time-dependent bias," Physical Review B **91**, 125433 (2015).

[71]B. S. Popescu and A. Croy, "Efficient auxiliary-mode approach for time-dependent nanoelectronics," New Journal of Physics **18**, 093044 (2016).

[72]A. P. Jauho, N. S. Wingreen, and Y. Meir, "Time-dependent transport in interacting and noninteracting resonant-tunneling systems," Physical Review B **50**, 5528–5544 (1994), arXiv:9404027v1 [arXiv:cond-mat].

[73]W. Greiner and J. Reinhardt, *Field quantization* (Springer Science & Business Media, 1996).

[74]N. Schlünzen, S. Hermanns, M. Scharnke, and M. Bonitz, "Ultrafast dynamics of strongly correlated fermions—nonequilibrium green functions and selfenergy approximations," Journal of Physics: Condensed Matter **32**, 103001 (2019).

[75]P. Myöhänen, A. Stan, G. Stefanucci, and R. Van Leeuwen, "Kadanoff-baym approach to quantum transport through interacting nanoscale systems: from the transient to the steady-state regime," Physical Review B **80**, 115107 (2009).

[76]V. Vovchenko, D. Anchishkin, J. Azema, P. Lombardo, R. Hayn, and A. M. Daré, "A new approach to time-dependent transport through an interacting quantum dot within the Keldysh formalism," Journal of Physics Condensed Matter **26**, 10.1088/0953-8984/26/1/015306 (2014), arXiv:1311.4377.

[77]W. Greiner, L. Neise, and H. Stöcker, *Thermodynamics and statistical mechanics* (Springer Science & Business Media, 2012).

[78]M. Kardar, *Statistical physics of particles* (Cambridge University Press, 2007).

[79]G. Grosso and G. P. Parravicini, *Solid state physics* (Academic press, 2013).

[80]Fuxiang Han, *A Modern Course in The Quantum Theory of Solids* (World Scientific, Singapore, 2013).

[81]W. Nolting and A. Ramakanth, *Quantum theory of magnetism* (Springer Science & Business Media, 2009).

[82]G. Stefanucci, R. van Leeuwen, and E. Perfetto, "In and out-of-equilibrium ab initio theory of electrons and phonons," Physical Review X **13**, 031026 (2023).

[83]A. Auerbach, *Interacting electrons and quantum magnetism* (Springer Science & Business Media, 2012).

[84]W. Heisenberg, "Zur theorie des ferromagnetismus.," Z. Physik **49**, 619–636 (1928).

[85]K. Yosida, *Theory of magnetism.: edition en anglais*, Vol. 122 (Springer Science & Business Media, 1996).

[86]H. Fröhlich and F. R. N. Nabarro, "Orientation of nuclear spins in metals," Proceedings of the Royal Society of London. Series A. Mathematical and Physical Sciences **175**, 382–391 (1940).

[87]C. Zener, "Interaction between the d shells in the transition metals," Physical Review **81**, 440 (1951).

[88]M. A. Ruderman and C. Kittel, "Indirect exchange coupling of nuclear magnetic moments by conduction electrons," Physical Review **96**, 99 (1954).

[89]T. Kasuya, "A theory of metallic ferro-and antiferromagnetism on zener's model," Progress of theoretical physics **16**, 45–57 (1956).

[90]K. Yosida, "Magnetic properties of cu-mn alloys," Phys. Rev. **106**, 893–898 (1957).

[91]J. Hubbard, "Electron correlations in narrow energy bands i.," Proceedings of the Royal Society of London. Series A. Mathematical and Physical Sciences **276**, 238–257 (1963).

[92]F. Giustino, "Electron-phonon interactions from first principles," Rev. Mod. Phys. **89**, 015003 (2017).

[93]F. H. Essler, H. Frahm, F. Göhmann, A. Klümper, and V. E. Korepin, *The one-dimensional hubbard model* (Cambridge University Press, 2005).

[94]W. Heitler and F. London, "Wechselwirkung neutraler atome und homöopolare bindung nach der quantenmechanik," Zeitschrift für Physik **44**, 455–472 (1927).

[95]J. Fransson, *Non-Equilibrium Nano-Physics. A Many-Body Approach*, Vol. 809 (Springer, Uppssala, 2010).

[96]A. Altland and B. D. Simons, *Condensed matter field theory* (Cambridge university press, 2010).

[97]A. Blandin and J. Friedel, "Propriétés magnétiques des alliages dilués. interactions magnétiques et antiferromagnétisme dans les alliages du type métal noble-métal de transition," J. phys. radium **20**, 160–168 (1959).

[98]U. Fano, "Effects of configuration interaction on intensities and phase shifts," Physical review **124**, 1866 (1961).

[99]J. Kondo, "G-shift and anomalous hall effect in gadolinium metals," Progress of Theoretical Physics **28**, 846–856 (1962).

[100]F. Haldane, "Scaling theory of the asymmetric anderson model," Physical Review Letters **40**, 416 (1978).

[101]A. Abrikosov, "Electron scattering on magnetic impurities in metals and anomalous resistivity effects," Physics Physique Fizika **2**, 5 (1965).

[102]H. Suhl, "Formation of local magnetic moments in metals," Physical Review Letters **19**, 442 (1967).

[103]A. Ekimov and A. Onushchenko, "Quantum size effect in three-dimensional microscopic semiconductor crystals," SPIE milestone series **180**, 3–5 (2005).

[104]M. Reed, J. Randall, R. Aggarwal, R. Matyi, T. Moore, and A. Wetsel, "Observation of discrete electronic states in a zero-dimensional semiconductor nanostructure," Physical review letters **60**, 535 (1988).

[105]V. Colvin, M. Schlamp, and A. Alivisatos, "Light-emitting diodes made from cadmium selenide nanocrystals and a semiconducting polymer," SPIE milestone series **180**, 396–398 (2005).

[106]W. C. Chan and S. Nie, "Quantum dot bioconjugates for ultrasensitive nonisotopic detection," Science **281**, 2016–2018 (1998).

[107]D. Loss and D. P. DiVincenzo, "Quantum computation with quantum dots," Physical Review A **57**, 120 (1998).

[108]T. A. Fulton and G. J. Dolan, "Observation of single-electron charging effects in small tunnel junctions," Physical review letters **59**, 109 (1987).

[109]G. T. Landi, D. Poletti, and G. Schaller, "Nonequilibrium boundary-driven quantum systems: models, methods, and properties," Rev. Mod. Phys. **94**, 045006 (2022).

[110]R. Landauer, "Spatial variation of currents and fields due to localized scatterers in metallic conduction," IBM Journal of research and development **1**, 223–231 (1957).

[111]Y. V. Nazarov and Y. M. Blanter, *Quantum transport: introduction to nanoscience* (Cambridge university press, 2009).

[112]B. Van Wees, H. Van Houten, C. Beenakker, J. G. Williamson, L. Kouwenhoven, D. Van der Marel, and C. Foxon, "Quantized conductance of point contacts in a two-dimensional electron gas," Physical Review Letters **60**, 848 (1988).

[113]M. A. Kastner, "The single-electron transistor," Reviews of modern physics **64**, 849 (1992).

[114]K. Capelle, "A bird's-eye view of density-functional theory," Brazilian journal of physics **36**, 1318–1343 (2006).

[115]X. Zheng, G. Chen, Y. Mo, S. Koo, H. Tian, C. Yam, and Y. Yan, "Time-dependent density functional theory for quantum transport," The Journal of chemical physics **133** (2010).

[116]Y. Pavlyukh, E. Perfetto, D. Karlsson, R. van Leeuwen, and G. Stefanucci, "Time-linear scaling nonequilibrium green's function methods for real-time simulations of interacting electrons and bosons. i. formalism," Physical Review B **105**, 125134 (2022).

[117]R. Van Leeuwen and G. Stefanucci, "Equilibrium and nonequilibrium many-body perturbation theory: a unified framework based on the martin-schwinger hierarchy," in Journal of physics: conference series, Vol. 427, 1 (IOP Publishing, 2013), p. 012001.

[118]Y. Pavlyukh, E. Perfetto, and G. Stefanucci, "Interacting electrons and bosons in the doubly screened g$\tilde{W}$ approximation: a time-linear scaling method for first-principles simulations," Physical Review B **106**, L201408 (2022).

[119]Y. Pavlyukh, E. Perfetto, D. Karlsson, R. van Leeuwen, and G. Stefanucci, "Time-linear scaling nonequilibrium green's function method for real-time simulations of interacting electrons and bosons. ii. dynamics of polarons and doublons," Physical Review B **105**, 125135 (2022).

[120]E. Perfetto, Y. Pavlyukh, and G. Stefanucci, "Real-time gw: toward an ab initio description of the ultrafast carrier and exciton dynamics in two-dimensional materials," Physical Review Letters **128**, 016801 (2022).

[121]Y. Pavlyukh, E. Perfetto, and G. Stefanucci, "Photoinduced dynamics of organic molecules using nonequilibrium green's functions with second-born, gw, t-matrix, and three-particle correlations," Physical Review B **104**, 035124 (2021).

[122]M. Esposito, M. A. Ochoa, and M. Galperin, "Quantum thermodynamics: a nonequilibrium green's function approach," Physical review letters **114**, 080602 (2015).

[123]M. M. Odashima, B. G. Prado, and E. Vernek, "Pedagogical introduction to equilibrium Green's functions: Condensed-matter examples with numerical implementations," Revista Brasileira de Ensino de Fisica **39**, 1–24 (2017), arXiv:1604.02499.

[124]J. J. Sakurai and J. Napolitano, *Modern quantum mechanics*, 3rd ed. (Cambridge University Press, 2020).

[125]A. M. Zagoskin, *Quantum theory of many-body systems*, Vol. 174 (Springer, 1998).

[126]H. O. John W. Negele, *Quantum Many-Particle Systems* (Advanced Book Classics, 1998).

[127]G. B. Leo. P Kadanoff, *Quantum Statistical Mechanics* (CRC Press, New York, 1962).

[128]D. C. Langreth, "Linear and nonlinear response theory with applications," in *Linear and nonlinear electron transport in solids* (Springer US, Boston, MA, 1976), pp. 3–32.

[129]A. Das, *Quantum Field Theory* (World Scientific, Rochester, 2008).

[130]A. Hewson, "Theory of localized magnetic states in metals," Physical Review **144**, 420 (1966).

[131]U. Weiss, *Quantum dissipative systems* (World Scientific, 2012).

[132]J. Bezanson, S. Karpinski, V. B. Shah, and A. Edelman, "Julia: a fast dynamic language for technical computing," arXiv preprint arXiv:1209.5145 (2012).

[133]R. L. Burden and J. D. Faires, *Numerical analysis* (Brooks Cole, 1997).

[134]N. Bickers, D. Cox, and J. Wilkins, "Self-consistent large-n expansion for normal-state properties of dilute magnetic alloys," Physical Review B **36**, 2036 (1987).

[135]A. Croy and U. Saalmann, "Nonadiabatic rectification and current reversal in electron pumps," Physical Review B **86**, 035330 (2012).

[136]O. Eriksson, A. Bergman, L. Bergqvist, and J. Hellsvik, *Atomistic spin dynamics: foundations and applications* (Oxford university press, 2017).

[137]J. Gukelberger, L. Huang, and P. Werner, "On the dangers of partial diagrammatic summations: benchmarks for the two-dimensional hubbard model in the weak-coupling regime," Physical Review B **91**, 235114 (2015).

[138]M. Schüler, D. Golež, Y. Murakami, N. Bittner, A. Herrmann, H. U. Strand, P. Werner, and M. Eckstein, "Nessi: the non-equilibrium systems simulation package," Computer Physics Communications **257**, 107484 (2020).

[139]L. Magazzù and M. Grifoni, "Feynman-vernon influence functional approach to quantum transport in interacting nanojunctions: an analytical hierarchical study," Physical Review B **105**, 125417 (2022).

[140]C. Bertrand, D. Bauernfeind, P. T. Dumitrescu, M. Maček, X. Waintal, and O. Parcollet, "Quantum quasi monte carlo algorithm for out-of-equilibrium green functions at long times," Physical Review B **103**, 155104 (2021).

[141]Y. Núñez Fernández, M. Jeannin, P. T. Dumitrescu, T. Kloss, J. Kaye, O. Parcollet, and X. Waintal, "Learning feynman diagrams with tensor trains," Physical Review X **12**, 041018 (2022).

[142]J. Berges, *Nonequilibrium quantum fields: from cold atoms to cosmology*, 2015, arXiv:1503.02907 [hep-ph].

[143]J. Varela-Manjarres and B. K. Nikolić, "High-harmonic generation in spin and charge current pumping at ferromagnetic or antiferromagnetic resonance in the presence of spin–orbit coupling," Journal of Physics: Materials **6**, 045001 (2023).

[144]T. Kloss, J. Weston, B. Gaury, B. Rossignol, C. Groth, and X. Waintal, "Tkwant: a software package for time-dependent quantum transport," New Journal of Physics **23**, 023025 (2021).

[145]C. W. Kim and I. Franco, "Theory of dissipation pathways in open quantum systems," The Journal of Chemical Physics **154** (2021).

[146]M. Bonitz, *Quantum kinetic theory*, Vol. 412 (Springer, 2016).

[147]J. D. Vasquez Jaramillo, *Probing magnetism at the atomic scale: non-equilibrium statistical mechanics theoretical treatise*, Vol. 2 (PhD dissertation, Acta Universitatis Upsaliensis, 2018).